

**School of Biomedical Sciences**

**The Self-Association of High Mobility Group Box 1 (HMGB1):  
Implications for Interaction with Receptor for Advanced Glycation End-  
products (RAGE) and DNA**

**Wresti L. Anggayasti**

**This thesis is presented for the Degree of Doctor of Philosophy**

**of**

**Curtin University**

**April, 2015**

## DECLARATION

To the best of my knowledge and belief this thesis contains no material previously published by any other person except where due acknowledgement has been made.

This thesis contains no material which has been accepted for the award of any other degree or diploma in any university.

Signature:

A handwritten signature in black ink, appearing to read 'W. Anggoro'.

Date: 15 April 2015

## ACKNOWLEDGEMENTS

To me, writing a PhD thesis is a journey to a deeper understanding about knowledge, oneself, and life. Translating the knowledge that I have gained into a thesis needs the skill to deliver the message, and not everyone has the opportunity to learn and utilize it for a greater good. During the writing process, I reflect on my four year journey that really developed my character, as a person and scientist. I think that a PhD thesis must be “paripurna” (Bahasa Indonesia: “complete”) but it may not be “sempurna” (“perfect”). A thesis must be thorough and offer a new perspective; hence the “Doctor of Philosophy”. But we must also acknowledge that there are possibilities to expand it, so the thesis is not a finish mark but rather a starting point. Just like the life itself which is a repetitive cycle of completing and restarting, with perfection as the final goal.

I dedicate this thesis to my incredible parents who always inspired me. My Mom provoked my interest to science through art, supported by my Dad who always has scientific answers for all happenings around us. They often said “no” to me, but always said “yes” to anything that would ensure the best education for me, even if that meant pushing their limits to provide for me. My journey would have been heavier if it was not for my best friends for 15-ish years: Arthur, Lyna, Edwina, Dora and Ade; and my cousin Mbak Viviet. Their satirical humour, scoldings and endless support always encouraged me, and I thank them for being my faithful friends. Finishing this project and thesis would have been impossible without my supervisors Prof. Erik Helmerhorst, Prof. Ricardo Mancera and Dr. Steve Bottomley. Erik set an example for me of how a biochemist should be, and I will always be grateful at the vast amount of knowledge that he has passed on to me. Ricardo always offered a critical point of view by asking questions addressing the minute details of my project; something which always refreshed my attitude towards my research. Steve always encouraged me to pay attention to the way I convey my points in this thesis. I am very lucky to have studied under their supervision, and hopefully I can be an amazing scientist like them.

I am grateful for the assistance given by the following people who helped me during my project: Dr. Marcel Heijnen, GE Healthcare’s Biacore expert, for his generous advices and insight on all that is “Biacore”; Dr. Rob Steuart for his support on the ÄKTApurifier; Dr. David Chandler for development of VCC-RAGE and HMGB1 constructs; Dr. Mark Agostino for molecular modelling; Dr. Rashmi Panigrahi (University of Western Australia) for a basic

knowledge on circular dichroism; and Prof. Alice Vrijlink and Caroline Snowball (both from University of Western Australia) for their help with thermal shift assay. Last but not least, I thank Biacore T200 and ÄKTApurifier 100, as they became my “friends” and helped me seven days a week with almost 500 experiments!

# TABLE OF CONTENTS

TABLE OF CONTENTS .....	5
LIST OF FIGURES.....	9
LIST OF TABLES.....	11
LIST OF ABBREVIATIONS.....	12
ABSTRACT.....	15
<b>1 LITERATURE REVIEW.....</b>	<b>17</b>
1.1 High Mobility Group Box 1 (HMGB1) .....	18
1.1.1 Discovery of HMGB1.....	18
1.1.2 Genetic characterization .....	19
1.1.3 Intracellular expression and extracellular localization.....	20
1.1.4 Box A and Box B tandem domains.....	21
1.1.5 Disulfide bond and free cysteine residue.....	23
1.1.6 Acidic C-terminus domain .....	25
1.2 Main receptors of HMGB1.....	27
1.2.1 Receptor of Advanced Glycation End-products (RAGE) .....	27
1.2.2 Toll-Like Receptor (TLR).....	31
1.3 Unravelling the mechanism of HMGB1-receptors interaction.....	33
1.3.1 HMGB1-RAGE: signalling pathway and pathophysiology.....	33
1.3.2 HMGB1-TLR: signalling pathway and pathophysiology.....	36
1.4 Interaction of RAGE and TLRs with their ligands.....	37
1.5 HMGB1 oligomerization .....	38
1.6 The present study.....	40
<b>2 MATERIALS AND METHODS .....</b>	<b>41</b>
2.1 Ethics approval .....	42
2.2 Genetically Modified Organism; Approval and Safety .....	42
2.3 Transformation of competent <i>Escherichia coli</i> and colony isolation .....	42
2.4 Polymerase Chain Reaction (PCR) of the whole competent colony.....	43

2.5	Agarose gel electrophoresis for PCR products .....	44
2.6	Expression of HMGB1 and RAGE constructs .....	44
2.7	Harvesting proteins from bacterial cell culture.....	44
2.8	Acid precipitation of HMGB1.....	45
2.9	Column chromatography.....	45
2.9.1	Heparin column chromatography .....	45
2.9.2	Size exclusion chromatography.....	46
2.10	Polyacrylamide gel electrophoresis (PAGE).....	46
2.11	Western blots .....	47
2.12	Circular dichroism.....	48
2.12.1	The secondary structure of HMGB1 and RAGE .....	48
2.12.2	Reduction and alkylation of HMGB1 .....	48
2.13	Surface Plasmon Resonance (SPR) .....	49
2.13.1	Coupling of HMGB1 to sensor chips.....	50
2.13.2	Binding activity of HMGB1 coupled to sensor chips .....	50
2.13.3	Data modelling and analysis.....	51
2.14	Self-association of HMGB1 .....	52
2.14.1	The effect of ionic strength .....	53
2.14.2	The effect of divalent metal ions.....	53
2.14.3	The combined effect of zinc and ionic strength .....	53
2.14.4	The effect of redox environment .....	54
2.14.5	The effect of pH.....	54
2.15	Thermal Shift Assay .....	55
<b>3</b>	<b>RESULTS .....</b>	<b>57</b>
3.1	Amplification and expression of HMGB1 and VCC-RAGE.....	58
3.2	Purification of HMGB1 and VCC-RAGE constructs .....	58
3.2.1	Purification of HMGB1.....	58
3.2.2	Purification of VCC-RAGE.....	65
3.3	Secondary structure of HMGB1 determined by circular dichroism .....	65
3.3.1	HMGB1 and its cysteine residues .....	65
3.3.2	VCC RAGE secondary structure .....	71

3.4	Optimization of surface plasmon resonance (SPR) .....	71
3.5	Binding activity of purified recombinant HMGB1 .....	75
3.6	The self-association of HMGB1 .....	79
3.6.1	The effect of ionic strength .....	86
3.6.2	Effect of zinc and other divalent metal ions.....	90
3.6.3	Effect of the redox environment.....	94
3.6.4	Effect of pH.....	97
3.7	Thermal shift assay for HMGB1.....	97
<b>4</b>	<b>DISCUSSION.....</b>	<b>103</b>
4.1	Purification of HMGB1.....	104
4.2	Characterization of HMGB1 interactions using SPR.....	106
4.2.1	Immobilization, mass transport and rate constant determination .....	106
4.2.2	Optimization of protein preparation and composition of SPR buffer.....	108
4.2.3	Development of the binding model best fitting SPR sensorgrams .....	109
4.3	Physico-chemical factors affecting the self-association of HMGB1 .....	110
4.3.1	Effect of ionic strength .....	110
4.3.2	Effect of zinc .....	112
4.3.3	Effect of the redox environment.....	113
4.3.4	Effect of pH.....	116
4.4	Molecular models of the self-association of HMGB1.....	117
4.5	Macromolecular crowding and the self-association of HMGB1 in solution .....	119
4.6	Conclusion and future directions .....	120
<b>5</b>	<b>REFERENCES .....</b>	<b>125</b>
<b>6</b>	<b>APPENDICES .....</b>	<b>137</b>
6.1	Appendix A .....	138
6.2	Appendix B.....	139
6.3	Appendix C.....	140

6.4	Appendix D .....	141
6.5	Appendix E.....	143
6.6	Appendix F.....	146



## LIST OF FIGURES

<i>Figure 1.HMGB1 publications by year until 2015. ....</i>	<i>18</i>
<i>Figure 2.Structural representation of HMGB1 domains. ....</i>	<i>22</i>
<i>Figure 3.Schematic representation of NMR-derived structure of HMGB1 Box A....</i>	<i>22</i>
<i>Figure 4.The acidic tail lowers the affinity of HMGB1 towards DNA cellulose. ....</i>	<i>26</i>
<i>Figure 5.The structural domains of RAGE. ....</i>	<i>29</i>
<i>Figure 6.(a) The secondary structure of the V-type domain and (b) the 3D structure with the cationic patch.....</i>	<i>30</i>
<i>Figure 7.Western blot gel membrane assembly. ....</i>	<i>47</i>
<i>Figure 8.Whole-cell PCR amplification of full length HMGB1. ....</i>	<i>59</i>
<i>Figure 9.Whole-cell PCR amplification of VCC-RAGE. ....</i>	<i>60</i>
<i>Figure 10.Induction of the expression of HMGB1 and VCC-RAGE.....</i>	<i>61</i>
<i>Figure 11.(a) SDS-PAGE and (b) Western blot of HMGB1. ....</i>	<i>62</i>
<i>Figure 12.HiTrap Heparin HP purification of HMGB1. ....</i>	<i>63</i>
<i>Figure 13.Superdex 200 10/300 GL chromatography of HMGB1. ....</i>	<i>64</i>
<i>Figure 14.HiTrap Heparin HP purification of VCC-RAGE. ....</i>	<i>66</i>
<i>Figure 15.Superdex 200 10/300 GL chromatography of VCC-RAGE. ....</i>	<i>67</i>
<i>Figure 16.(a) SDS-PAGE and (b) Western blot of VCC-RAGE. ....</i>	<i>68</i>
<i>Figure 17.Circular dichroism profile of HMGB1. ....</i>	<i>69</i>
<i>Figure 18.CD spectra of HMGB1 treated with <math>\beta</math>-mercaptoethanol. ....</i>	<i>70</i>
<i>Figure 19.CD spectra of HMGB1 treated with iodoacetamide.....</i>	<i>72</i>
<i>Figure 20.CD spectrum of VCC-RAGE. ....</i>	<i>73</i>
<i>Figure 21.Optimization of SPR experiments.....</i>	<i>74</i>
<i>Figure 22.Multi cycle kinetics (MCK) of the interaction of HMGB1 with VCC-RAGE. ....</i>	<i>77</i>
<i>Figure 23.Single cycle kinetics (SCK) of the interaction of HMGB1 with pBluescript II SK(-). ....</i>	<i>78</i>
<i>Figure 24.Self-association of HMGB1 analyzed by (a) multi cycle kinetics and (b) steady state affinity. ....</i>	<i>80</i>

<i>Figure 25. The fits of the association phase of sensorgram data using different models.....</i>	<i>81</i>
<i>Figure 26. The fits of the dissociation phases of sensorgram data using different models.....</i>	<i>82</i>
<i>Figure 27. U-values and Chi<sup>2</sup> values of the different kinetic binding models of the self-association of HMGB1.....</i>	<i>83</i>
<i>Figure 28. Comparison of kinetic constants between the 1:1 Langmuir and the dimer/tetramer kinetic binding models of the self-association of HMGB1. ....</i>	<i>85</i>
<i>Figure 29. Effect of ionic strength on the self-association of HMGB1 fitted with dimer/tetramer model. ....</i>	<i>87</i>
<i>Figure 30. Debye-Hückel plots of the self-association of HMGB1.....</i>	<i>88</i>
<i>Figure 31. Stoichiometry of the self-association of 25 nM and 3000 nM HMGB1 at different ionic strengths. ....</i>	<i>89</i>
<i>Figure 32. Influence of divalent metal ions on the self-association of HMGB1. ....</i>	<i>91</i>
<i>Figure 33. Stoichiometry of HMGB1 self-association in the presence of divalent metal ions.....</i>	<i>92</i>
<i>Figure 34. Debye-Hückel plots of the effect of ionic strength on the zinc-dependent self-association of 25 nM HMGB1. ....</i>	<i>93</i>
<i>Figure 35. Stoichiometry of the self-association of 25 nM HMGB1 in the presence of zinc as a function of ionic strength. ....</i>	<i>95</i>
<i>Figure 36. The effect of β-mercaptoethanol on the self-association of HMGB1. ....</i>	<i>96</i>
<i>Figure 37. Effect of pH on the self-association of HMGB1.....</i>	<i>98</i>
<i>Figure 38. Thermal shift plots of LptA and HMGB1 controls. ....</i>	<i>99</i>
<i>Figure 39. Thermal shift plots of HMGB1 with or without ZnCl<sub>2</sub> and β-mercaptoethanol.....</i>	<i>102</i>
<i>Figure 40. Zinc clasp model describing the self-association of HMGB1.....</i>	<i>118</i>
<i>Figure 41. A molecular model of HMGB1 tetramer formation. ....</i>	<i>119</i>

## LIST OF TABLES

<i>Table 1. Forward and reverse primers used to amplify human VCC-RAGE.....</i>	<i>43</i>
<i>Table 2. Forward and reverse primers used to amplify human HMGB1.....</i>	<i>43</i>
<i>Table 3. Specification and parameters of dimer/tetramer model setup. ....</i>	<i>52</i>

## LIST OF ABBREVIATIONS

Abbreviation	Full name
AGE	Advanced Glycation End-products
BSA	Bovine Serum Albumin
CXCR4	CXC chemokine Receptor type 4
CD	Circular Dichroism
DAMP	Damage-associated Molecular Pattern
DIC	Disseminated Intravascular Coagulation
DMF	Dimethylformamide
DTT	Dithiothreitol
EDC	1-ethyl-3-(3-dimethylaminopropyl)carbodiimide
EDTA	Ethylenediaminetetraacetic Acid
ERK	Extracellular signal-regulated Kinase
FRET	Fluorescence Resonance Energy Transfer
GAT	Guerin Ascites Tumour
GFI1	Growth Factor Independence 1
GPX3	Glutathione Peroxidase 3
GST	Glutathione-S-Transferase
GTP	Guanosine-5'-triphosphate
HLA	Human Leucocyte Antigen
HMGB1	High Mobility Group Box 1
HSP	Heat Shock Protein
IL	Interleukin
IFN	Interferon
IPTG	Isopropyl $\beta$ -D-1-thiogalactopyranoside
IRF	Interferon Regulatory Factor
JNK	c-Jun N-terminal Kinase
LDS	Lithium Dodecyl Sulphate

LEF-1	Lymphoid Enhancer Factor 1
LFL	Lactoferrin-like
LPS	Lipopolysaccharide
LptA	Lipopolysaccharide transport A
LRR	Leucine Rich Repeat
MAPK	Mitogen-activated Protein Kinase
MCK	Multi Cycle Kinetics
MD-2	Myeloid Differentiation 2
MDC	Myeloid Dendritic Cell
MHC	Major Histocompatibility Complex
MMP	Matrix Metalloproteinase
MyD88	Myeloid Differentiation primary response gene 88
NCAM	Neural Cell Adhesion Molecule
NHS	N-hydroxysuccinimide
NFκB	Nuclear Factor Kappa (κ) B
NO	Nitric Oxide
NMR	Nuclear Magnetic Resonance
NP	Nitrophorin
NRMSD	Normalized Root Mean Square Deviation
NTA	Nitrilotriacetic Acid
PAMP	Pathogen-associated Molecular Pattern
PBS	Phosphate Buffered Saline
PCA	Perchloric Acid
PCR	Polumerase Chain Reaction
PDC	Plasmacytoid Dendritic Cell
RAGE	Receptor of Advanced Glycation End-products
RU	Resonance Unit
SAPK	Stress-activated Kinase
SCK	Single Cycle Kinetics

SDS-PAGE	Sodium Dodecyl Sulfate - Polyacrylamide Gel Electrophoresis
SIRS	Systemic Inflammatory Response Syndrome
SPR	Surface Plasmon Resonance
SRY	Sex-determining Region Y
SV40	Simian Vacuolating Virus 40
TASK3	TWIK-related Acid Sensitive K(+) 3
TCA	Trichloroacetic Acid
TIR	Toll/IL-1 Receptor
TIRAP	Toll/Interleukin 1 Receptor domain-containing Adaptor Protein
TLR	Toll-Like Receptor
TM456	Thrombomodulin epidermal growth factor-like domains 456
TNF $\alpha$	Tumor Necrosis Factor $\alpha$
TRAM	TRIF-Related Adaptor Molecule
TRIF	TIR domain-containing Adaptor Inducing Interferon
TSP-1	Thrombospondin 1
YAP1	Yeast-Associated Protein 1

## ABSTRACT

High Mobility Group Box 1 (HMGB1), a highly conserved protein, plays key roles in acute sepsis and in chronic inflammatory diseases including cancer, diabetes and Alzheimer's disease. Intracellularly, HMGB1 binds DNA, modifies its structure and assists with the regulation of transcription. Extracellularly, HMGB1 is released either actively or passively from damaged necrotic cells. It thereby promotes inflammatory responses by numerous mechanisms, including by binding to key pattern recognition receptors such as the Receptor of Advanced Glycation End-products (RAGE). In this study, the self-association of HMGB1 is detailed in real-time using Surface Plasmon Resonance. HMGB1 is shown to form dimers, tetramers and higher order oligomers with high affinity in a highly-specific manner. A "dimer/tetramer" fitting model was developed that provided a good fit to the SPR sensorgrams and enabled the kinetics of self association to be evaluated under a variety of physico-chemical conditions. The self-association of HMGB1 was markedly influenced by ionic strength, the presence of zinc ions, the redox environment and the pH.

Dimer formation was independent of ionic strength. However, the formation of HMGB1 tetramers was dramatically influenced by ionic strength; a 0.05 M increase in ionic strength from 0.13 M to 0.18 M decreased the affinity of tetramer formation from dimers by over two orders of magnitude. Given the magnitude of this effect, the role of the acidic tail of HMGB1, which comprises 30 consecutive charged residues, and/or the basic region of HMGB1 may be implicated in tetramer formation.

The effect of zinc on the self association was also dramatic and has never been reported before. Low micromolar zinc influenced both dimer, and in particular, tetramer formation. The affinity and stoichiometry of HMGB1 self-associates increased markedly in the presence of 5  $\mu$ M zinc. At a physiological ionic strength of 0.15 M, dimers seemed to predominate in the absence of zinc, but tetramers predominated in the presence of zinc. Increasing concentrations of zinc promoted higher order oligomers of HMGB1. A preliminary zinc clasp molecular model was developed which can account for the formation of a HMGB1 dimer coordinated by zinc. A model describing tetramer formation was also proposed.

The self association of HMGB1 was also critically dependent on the redox environment. More reduced conditions, as might be found in the intracellular environment and within the nucleus of cells, favoured dimer formation but destabilised tetramers. On the other hand, when the concentration of reducing agent was decreased towards levels that might represent the more oxidised environment of the extracellular environment, the affinity for tetramer formation was markedly increased. Together, these findings suggest that different oligomers of HMGB1 may play different roles in the intracellular and extracellular environments. HMGB1 dimers may preferentially bind DNA, whereas HMGB1 tetramers may promote a more potent inflammatory response when binding to the Receptor for Advanced Glycation End Products (RAGE) and Toll-like Receptor 4 (TLR4).

Thermal shift assays validated the role of zinc and redox conditions in stabilising HMGB1 structure and oligomer formation. In the presence of 5  $\mu$ M zinc and 0.5%  $\beta$ -mercaptoethanol, several melting point transitions of HMGB1 were observed; some at temperatures which might suggest that with more exploration, conditions might be found that are conducive for the crystallisation of HMGB1. This would provide reliable data for more detailed molecular modelling of the self association of HMGB1.

Future studies should now focus on the role of the acidic tail of HMGB1 on its ability to self-associate and on the effect of zinc and redox conditions on the ability of HMGB1 to bind to and activate its target molecules, including DNA, RAGE and TLR4. Efforts to crystallise HMGB1 should be renewed, given the findings in this study. An X-Ray structure of HMGB1 including its acidic tail would greatly advance our understanding of this biologically important molecule. It would also enable a more accurate molecular model describing the self association of HMGB1, which might also in future contribute to the development of a new class of therapeutics targeting chronic inflammatory diseases such as diabetes, cancer and Alzheimer's disease.



## **1 LITERATURE REVIEW**

## 1.1 High Mobility Group Box 1 (HMGB1)

HMGB1 is a highly conserved protein and is abundantly present in the nucleus of almost all eukaryotic cells. HMGB1 has a dual function: the first is an intracellular DNA-binding protein and the second is an extracellular signal of tissue damage (Ito and Maruyama, 2011). It has been confirmed that extracellularly, HMGB1 plays a key role in diseases which are caused by tissue inflammation, such as diabetes, chronic sepsis, Alzheimer's disease and cancer (Zhu et al., 2010). HMGB1 is one of the most prominent ligands of RAGE. HMGB1 itself also interacts with various surface receptors besides RAGE, such as Toll-like receptors (TLRs). The RAGE and TLRs are widely known to mediate pro-inflammatory effects of HMGB1 (Sims et al., 2010). There are a growing number of publications written on the role and importance of HMGB1, as illustrated in Figure 1 from Pubmed.

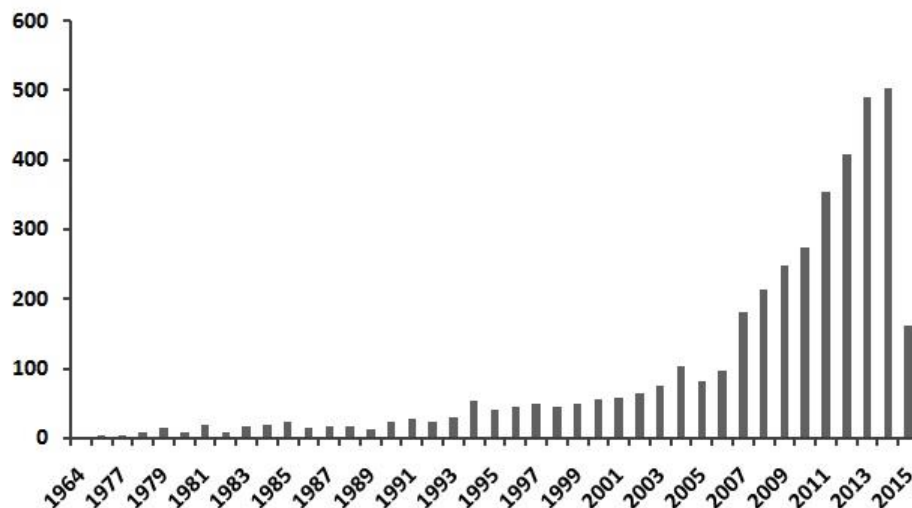


Figure 1. HMGB1 publications by year until 2015.

The data was taken from Pubmed (<http://www.ncbi.nlm.nih.gov/pubmed/?term=hmgbl>).

### 1.1.1 Discovery of HMGB1

Laminin, a glycoprotein with high molecular weight, enhances adhesion and neurite outgrowth in various neuronal cell types. However, the rate of expression of laminin is limited, so it was assumed that other adhesion factors were needed to support neuritic growth in the brain (Rauvala and Pihlaskari, 1987). A 30 kDa protein was isolated from young rat brain and N18 neuroblastoma cells. This protein shares common features with

laminin, such as the ability to bind heparin and its cell-adhesive and neurite-outgrowth promoting properties (Rauvala and Pihlaskari, 1987). Further studies identified this 30 kDa protein as belonging to the High Mobility Group 1 (HMG1) protein family (Parkkinen et al., 1993). Later on, the nomenclature of the HMG proteins was revised, and the 30 kDa protein was then officially renamed as High Mobility Group Box 1 (HMGB1), due to its functional motif which is known as HMG box (Bustin, 2001). HMGB1 was co-purified with other proteins. The HMGB1 cDNA encodes a 30 kDa protein (p30), whereas the co-purified 28 kDa and 29 kDa proteins (p28 and p29) are closely related but have different amino acid sequences. However, recombinant HMGB1 is not accompanied by the p28 and p29 forms (Parkkinen et al., 1993).

An investigation of the expression and localization of HMGB1 in various normal and transformed cells determined that HMGB1 has an extracellular role at the leading edge of migrating cells and is degraded by a plasminogen-dependent mechanism (Parkkinen et al., 1993). This has led to this protein being referred to in different ways. Some studies use the name HMGB1 to specifically refer to the protein as a nuclear protein because it was initially found in the cell nucleus. On the other hand, the name amphoterin refers to the extracellular form of HMGB1, more specifically a protein that binds to the cell surface and plays a role in the migratory responses of cells.

### **1.1.2 Genetic characterization**

HMGB1 is a 30 kDa single chain protein that belongs to the High Mobility Group of highly-expressed, non-histone chromosomal DNA and heparin binding proteins, along with High Mobility Group Box 2 (HMGB2). The HMG box region of the entire HMGB1 is homologous to the HMG boxes of other proteins, such as the testis determining factor (SRY) and lymphoid enhancer factor 1 (LEF-1). The HMG boxes of these two proteins are able to bend DNA *in vitro* and, therefore, this might be a property of HMGB1 as well (Weir et al., 1993). HMGB1 is a highly ubiquitous protein and is highly conserved among different species, with 95% identity between the human, rat and bovine sequences. In fact, the HMGB1 sequences of these species have only two divergent amino acids (Bianchi et al., 1992).

The human HMGB1 gene has been mapped to chromosome 13q12, which contains five exons and four introns. The gene has a very strong TATA-less promoter with an activity rate of more than 18-fold higher than that of the simian vacuolating virus 40 (SV40) promoter (Huttunen, 2002). The gene also has a silencer that can repress the human

HMGB1 gene down to one-sixth of its activity. The silencer contains a binding site for the growth factor independence 1 (GFI1) repressor, which explains the repression effect of the silencer and thus it keeps the expression level of human HMGB1 at the basal level. The first intron of the HMGB1 gene is a G/C rich region that has been claimed to exert an enhancing activity that elevates HMGB1 expression two-three fold (Lum and Lee, 2001).

### **1.1.3 Intracellular expression and extracellular localization**

Earlier findings showed that HMGB1 is expressed in central and peripheral nervous systems during the later phases of embryonic development, while other studies showed that various tumour cells express HMGB1 (Huttunen, 2002, Fages et al., 2000). It was later determined that HMGB1 is expressed in all kinds of tissues and at different developmental stages (Lum and Lee, 2001, Schmidt et al., 2000). Compared to normal cells, HMGB1 is abundantly expressed in transformed cell lines. HMGB1 mRNA localizes at the leading edge of transformed cells grown on laminin. Laminin itself acts as a substrate for glioma migration and invasion through its binding with integrin. This suggests that HMGB1 may be an important factor towards tumour progression and metastasis. HMGB1 is also highly expressed in cells with motile phenotype but it is down-regulated in densely cultured cells (Fages et al., 2000). The secretion of extracellular HMGB1 is also closely connected with the cell motility induced by laminin. The rate of HMGB1 expression in migrating cells is higher than in cells that only bind to the cell matrix (Huttunen, 2002, Fages et al., 2000). Intracellularly, HMGB1 binds DNA and assists with the regulation of transcription (Sims et al., 2010). Both HMGB1 boxes play a significant role in the recognition of DNA and bind DNA without any sequence specificity, which promotes interaction of DNA with transcription factors such as glucocorticoid receptors (Stott et al., 2010).

HMGB1 is secreted by wide range of tissues and cells, such as macrophages, monocytes, endothelial cell, and tumour cells. Extracellular HMGB1 contributes to the migratory responses of various cells, such as neuron and growth cone migration, endothelial and immune cell migration, and the invasive migration of tumour cells (Rauvala and Rouhiainen, 2009). HMGB1 is particularly secreted by macrophages or monocytes in response to stimulation with lipopolysaccharides (LPS) or pro-inflammatory cytokines like the tumour necrosis factor $\alpha$  (TNF $\alpha$ ) and interleukin 1 (IL-1) (Kuniyasu et al., 2005).

HMGB1 lacks a secretion signal peptide and its secretion does not involve the classical secretory pathway within the endoplasmic reticulum and the Golgi apparatus. HMGB1 is reported to be released to the extracellular environment by the non-classical Ca<sup>2+</sup>-

regulated secretory lysosome pathway. Before undergoing vesicle-facilitated exocytosis, nuclear HMGB1 relocates to cytoplasmic organelles, for example endolysosomal compartment (Gardella et al., 2002). The mechanism of secretion of HMGB1 to the extracellular environment is poorly understood. Necrotic and damaged cells can also secrete HMGB1. It has been reported that necrotic cells have a greatly reduced ability to promote inflammation following the release of HMGB1 (Scaffidi et al., 2002).

HMGB1 can be secreted either passively from necrotic cells or actively by inflammatory cells. Upon release to the extracellular environment, HMGB1 acts as a signal of tissue damage. It plays a key role in controlling infection and promoting tissue repair at sites of tissue injury. HMGB1 can act as an immediate trigger of inflammation as well as a late mediator of inflammation (Scaffidi et al., 2002, Rouhiainen et al., 2004). HMGB1 is one of the Damage-associated Molecular Pattern (DAMP) molecules that induce the release of proinflammatory cytokines and chemokines and promote the recruitment of inflammatory cells (Leventhal and Schroppe, 2012). When HMGB1 spreads throughout the systemic circulation, it acts as a lethal mediator and promotes the development of Systemic Inflammatory Response Syndrome (SIRS) and Disseminated Intravascular Coagulation (DIC). It was reported that HMGB1 promotes fibrin deposition in kidneys and increases mortality rate in animal experiments. Treatment with anti-HMGB1 neutralizing antibody rescues the animal from lethal endotoxemia, which suggests that HMGB1 is responsible for endotoxin lethality (Ito and Maruyama, 2011).

#### **1.1.4 Box A and Box B tandem domains**

Structurally, the N-terminal domain of HMGB1 is made up of 185 amino acids, predominantly basic amino acids, and is further divided into two tandem box-like domains, termed Box A and Box B, each being free standing units capable of binding DNA (Figure 2). Each one of these two boxes consists of ~80 amino acids and are ~43% identical to each other (Read et al., 1993, Weir et al., 1993). Both boxes have similar (~56%)  $\alpha$ -helical structure and each box is divided into three amphipathic helices, named helix I, II and III. These helices account for 75% of the total number of residues in each HMG box (Bianchi et al., 1992). Both HMGB1 boxes play a significant role in the recognition of DNA. Interestingly, these boxes bind DNA without any sequence specificity. However, the two boxes are assumed to have different roles in the binding of DNA. Box A preferably binds to distorted DNA, while box B is more effective at bending DNA (Stott et al., 2010).

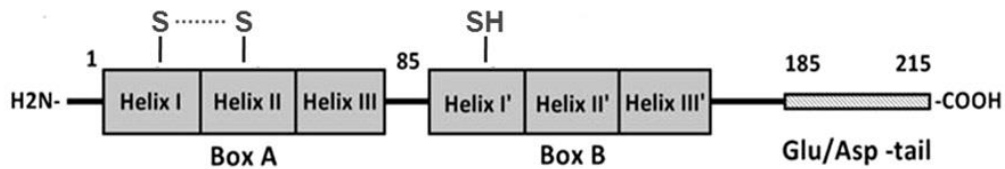


**Figure 2. Structural representation of HMGB1 domains.**

HMGB1 consists of Box A, Box B and the C-terminal acidic tail. Box A has two cysteine residues (Cys23 and Cys45) which forms disulfide bond, and Box B has one free cysteine residue (Cys106).

A unique property of the HMG boxes is a set of conserved aromatic, hydrophobic (particularly valine, isoleucine, alanine, leucine and phenylalanine) and basic amino acid residues. The residues are highly conserved in various organisms, such as rat, pig, trout, *Drosophila melanogaster* and *Saccharomyces cerevisiae*. The regions of similarity consist of amino acids 4-89 in Box A and 90-174 in Box B (Bianchi et al., 1992, Weir et al., 1993).

The tertiary structure of the HMG box has been investigated by constructing a nuclear magnetic resonance (NMR) solution structure of reduced HMG box A (PDB ID: 2YRQ) as shown in Figure 3, reproduced with permission (Wang et al., 2013) (see Appendix A, section 6.1).

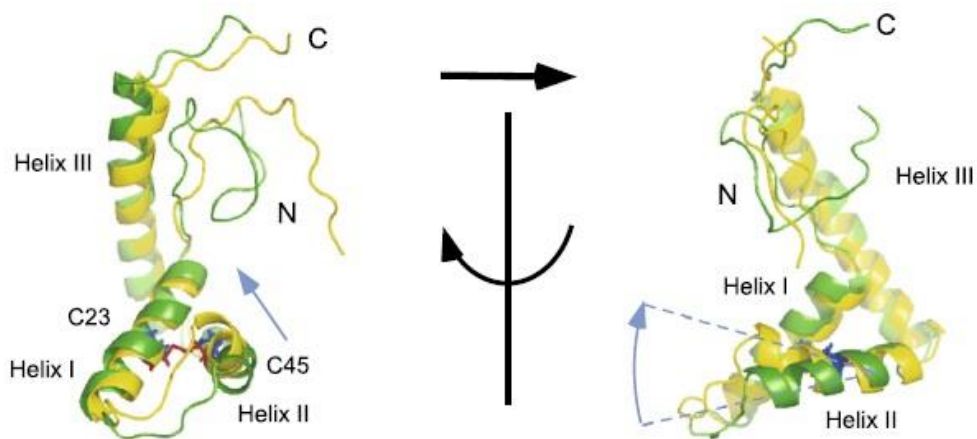


**Figure 3. Schematic representation of NMR-derived structure of HMGB1 Box A.**

The diagrams show the oxidized (yellow) and reduced (green) structure of the Box A of HMGB1, as well as the reduced form (blue) and the oxidized form (red) of the disulfide bond (Cys23-Cys45). The blue arrows represent the apparent change of orientation of the N-terminal part of Helix I. The structure on the right is the 90° rotation of the structure on the left (Wang et al., 2013).

The HMG box was determined to have an unusual L-shape structure consisting of two “arms” with an angle of  $\sim 80^\circ$  between them. The first arm consists of helices I and II while the second arm consists of the extended N-terminal region packed against helix III (Weir et al., 1993). A slightly different model was proposed whereby the angle between the two arms is  $\sim 70^\circ$ . Additionally, the HMG box was described as having a hydrophobic core around which the three helices are arranged (Read et al., 1993).

#### **1.1.5 Disulfide bond and free cysteine residue**

HMGB1 has three cysteine residues, as described in Figure 2. Two of them are in box A: Cys23 and Cys45. These residues can rapidly form intramolecular disulfide bonds in their oxidized state, and the redox reaction is reversible. It suggested that the cellular glutathione (reduced: GSH; oxidized: GSSH) system cannot keep HMGB1 in its reduced state (Sahu et al., 2008). However, the reduction of oxidized HMGB1 by the thioredoxin system is sufficient to keep HMGB1 completely reduced in the cell, which may suggest that there is an equilibrium between the oxidized and reduced forms of HMGB1 (Sahu et al., 2008). The existence of different redox states of HMGB1 has been demonstrated to play a very crucial role towards HMGB1 localization, the change of its intracellular and extracellular activities, and even determining which molecule or receptor that the protein has to interact with (Yang et al., 2013, Yang et al., 2012).

Disulphide bonds are assumed to be important for the structure of proteins. The bonds influence the thermodynamics of protein folding by stabilizing the native conformation of the proteins, and thus maintaining their integrity by protecting them from oxidants and proteolytic enzymes (Hogg, 2003). However, further studies showed that the disulfide bonds also significantly affect protein functions, such as intramolecular disulfide interchange in thrombospondin (TSP)-1, an extracellular glycoprotein which assists growth and tissue differentiation (Hogg, 2003). Different arrangements of disulfide bonds in TSP-1 yields wide varieties of functional roles, such as different abilities in inhibition of neutrophil enzymes, different binding affinities towards  $\text{Ca}^{2+}$  and platelet-derived growth factor, and different Arg-Gly-Asp-dependent cell adhesive activity (Hogg, 2003). Furthermore, a study on transcription factor Yap1 demonstrated that formation of complex intermolecular thiol-disulfide exchange is a crucial part of its function (Delaunay

et al., 2002). The Yap1 which regulates hydroperoxide homeostasis in yeast is closely related to glutathione peroxidase-like enzyme Gpx3. It promotes formation of intramolecular disulfide bond of the Yap1 by acting as a hydroperoxide sensor in Yap1 pathway. Disulfide linkage formation between one of the three cysteine residues of Gpx3 (Cys36) with Cys598 of Yap1 subsequently activates Yap1 and promotes formation of its intramolecular Cys598-Cys303 disulfide bond (Delaunay et al., 2002). These findings further confirmed that the dynamics of cysteine residues in most proteins is not confined to structural role and has important contribution in protein function.

The third cysteine residue of HMGB1, Cys106, is a free residue in box B. This free cysteine residue remains in its reduced state and was reported to aid HMGB1 in binding to its receptors (Yang et al., 2013). HMGB1 interacts with CXC chemokine receptor type 4 (CXCR4) which induces leukocytes recruitment and chemotaxis when all of the cysteine residues are reduced. However, when all cysteines are oxidized or when Cys106 alone is oxidized, there is no Toll-like receptor 4 (TLR4) or CXCR4-dependent signaling. Substitution or modification of any of the cysteine residues prevents TLR4-dependent signalling (Yang et al., 2013). The reduced HMGB1 was reported to specifically mediate autophagy through its interaction with RAGE (Tang et al., 2012). A Surface Plasmon Resonance (SPR) study emphasized that the free cysteine residue is critical for binding of HMGB1 with its receptor, TLR-4 (Yang et al., 2010). Furthermore, the mutation of the Cys106 caused the failure of HMGB1 to stimulate the TNF- $\alpha$  release which suggested that the free cysteine influences immunogenic activity of HMGB1 (Yang et al., 2010). The mutation of Cys106 also shown to promote cytosolic localization of HMGB1 and sustains autophagy, and oxidation of all cysteine residues has been concluded as the main regulator of autophagic flux and HMGB1 translocation (Tang et al., 2010). A further tandem mass-spectrometry study demonstrated that the free Cys106 and the Cys23-Cys45 disulfide bond are essential for stimulation of NF $\kappa$ B translocation and production of TNF- $\alpha$  in macrophages. It is to be noted, however, that the TNF- $\alpha$  stimulating activity requires both reduced free cysteine residue and formation of disulfide-bond, since the Cys106 alone is not enough to trigger cytokine activity of HMGB1 (Yang et al., 2012). Those studies demonstrated that the presence of disulfide bond and/or free cysteine residues in HMGB1 has crucial structure-function relationship.

An earlier study of recombinant eukaryotic and bacterial HMGB1 claimed that reduction of recombinant HMGB1 had no effect at all because the protein preserved its activity (Rouhiainen et al., 2007). A heparin-binding assay utilizing heparin sepharose column



chromatography and either 1 mM dithiothreitol (DTT) or 10 mM  $\beta$ -mercaptoethanol as reducing agents demonstrated that both reduced and non-reduced HMGB1 bind with the same affinity towards the column. It was also proposed that reduction with  $\beta$ -mercaptoethanol did not diminish the ability of recombinant HMGB1 to induce TNF $\alpha$  secretion from mononuclear cells (Rouhiainen et al., 2007). The heparin-binding assay was based on the retention times of reduced and non-reduced HMGB1 in the heparin sepharose column. The bound proteins were eluted with 0.15-1.5 M NaCl gradient, and it was shown that they were eluted with the same concentration of 0.7 M NaCl. The exact magnitude of the affinity of HMGB1 to heparin was not provided, so it is possible that the affinities of reduced and non-reduced HMGB1 to heparin are similar, and therefore it is also possible that they would be eluted from the column at the same point. The observation of unaltered TNF $\alpha$  induction between reduced and non-reduced HMGB1 was not described in detail and, moreover, the effect of reduction and alkylation of HMGB1 on its secondary structure was not elaborated in full. Thus, the conclusions of this study about the effect of reduction on the structure and function of HMGB1 require more detailed investigation.

#### **1.1.6 Acidic C-terminus domain**

The highly acidic C-terminal region of HMGB1 is located behind the two homologous N-terminal HMG boxes, linked by a short basic domain. The tail is unstructured and has low sequence complexity, i.e. it has simple amino acids composition (Stott et al., 2010). This acidic tail is 30 residues long and consists of consecutive glutamic acid and aspartic acid residues (Read et al., 1993). This results in an exceptionally negatively-charged structure, which explains why HMGB1 is “sticky” to various types of surfaces. The highly-charged acidic tail gives HMGB1 its other name, amphoterin. The name amphoterin refers to the dipolar nature of the protein, with a polycationic N-terminal part and a polyanionic acidic tail (Parkkinen et al., 1993, Fages et al., 2000). The adhesive properties of HMGB1 are demonstrated by a wide range of HMGB1 interactions with other molecules, including the Toll-like receptor (TLR) family of cell surface receptors (Rauvala and Pihlaskari, 1987, Huttunen et al., 2002).

The acidic tail is known to reduce the binding affinity of the HMG boxes in HMGB1 to DNA, as shown in Figure 4, reproduced with permission (Lee and Thomas, 2000) (see Appendix B, section 6.2).

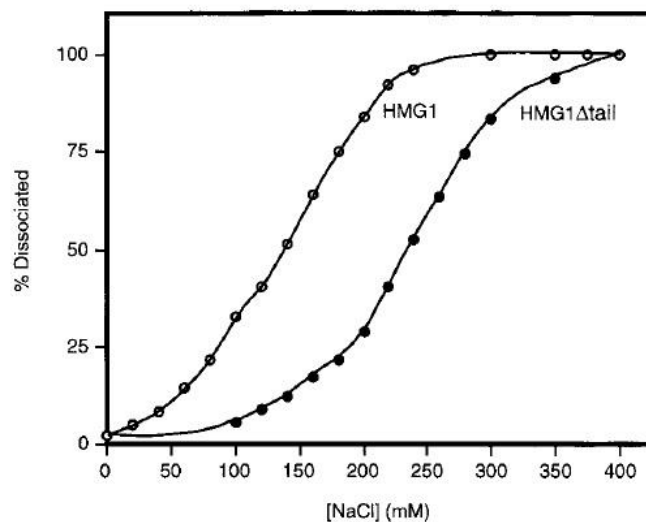


**Figure 4.** The acidic tail lowers the affinity of HMGB1 towards DNA cellulose.

The full length HMGB1 and the HMGB1 without acidic tail were pre-incubated with DNA-cellulose and then eluted with increasing ionic strength. HMGB1 without acidic tail is described to have higher affinity towards DNA cellulose than full length HMGB1 (Lee and Thomas, 2000).

Initially, it was suggested that HMGB1 has lower binding affinity towards four-way DNA junctions and supercoiled DNA compared to other HMG proteins with shorter acidic tail. The acidic C-terminus in HMGB1 differs in length compared to that in HMGB2, which consists of 21 amino acids, with HMGB2 binding to DNA with a higher affinity (Lee and Thomas, 2000). Removal of the tail was shown to reduce selectivity toward distorted DNA structures over linear DNA duplexes (Stott et al., 2010). Thus, the length of the acidic C-terminus appears to determine the ability of HMGB proteins to interact and modify DNA (Lee and Thomas, 2000).

The acidic tail has crucial roles in mediating several protein functions, such as stimulation of transcription, facilitation of chromatin remodelling, and possibly also influencing post-translational modification (Watson et al., 2007). The tail has been shown to interact with the two boxes. The tail makes extensive contacts with linkers and the DNA-binding faces of both HMG boxes, with higher affinity for box B, subsequently facilitating the collapse of HMGB1 (Stott et al., 2010). This explains how the acidic C-terminus of HMGB1 negatively regulates HMGB1-DNA interactions.

## **1.2 Main receptors of HMGB1**

HMGB1 promotes inflammatory responses by numerous mechanisms, including by binding to a diverse array of key pattern recognition receptors such as Mac-1, Syndecan-1 (CD138), phosphacan protein-tyrosine phosphatase- $\zeta/\beta$  and CD24, to name a few (Rauvala and Rouhiainen, 2009, Yang et al., 2010). In some cases, HMGB1 also interacts with its receptors to promote tissue regeneration (Ito and Maruyama, 2011). However, this literature review will focus on two well-studied receptors of HMGB1, namely the Receptor of Advanced Glycation End-products (RAGE) and Toll-Like Receptors (TLRs) (Park et al., 2004).

### **1.2.1 Receptor of Advanced Glycation End-products (RAGE)**

RAGE was initially identified as the receptor for a non-enzymatically glycosylated protein named Advanced Glycation End-product (AGE). A 1990 study observed that AGE accumulates steadily in normal ageing and at an accelerated rate in diabetes, particularly on the surface of endothelial cells, where it promotes the interaction between monocytes and endothelial cells, subsequently triggers pro-inflammatory responses (Kirstein et al., 1990). Subsequent studies successfully isolated two proteins associated with the endothelial cell surface which were claimed to mediate the interaction of AGEs and endothelial cells. Later, these proteins were identified as the Receptor of Advanced Glycation End-products (RAGE) and Lactoferrin-like (LFL) protein (Neeper et al., 1992, Schmidt et al., 1992).

The RAGE gene lies near the junction between Major Histocompatibility Complex (MHC) class III and class II (Sugaya et al., 1994). MHC is known to affect a large number of infectious, auto-immune and inflammatory diseases, such as type I diabetes and rheumatoid arthritis (Neeper et al., 1992, Traherne, 2008). Therefore, it was assumed that RAGE had a strong association with several diseases linked to the MHC. The sequence of RAGE was first reported to have similarity with cell surface glycoprotein MUC 18, a glycoprotein member of the immunoglobulin-like superfamily that serves as a marker of tumour progression in melanoma (Neeper et al., 1992). Subsequently, RAGE was found to share homology with the Neural Cell Adhesion Molecule (NCAM) (Neeper et al., 1992). The C-terminus of RAGE has similarity with the cytoplasmic domain of the B-cell activation marker CD20, which suggests that RAGE might be involved in the immune response system (Neeper et al., 1992). RAGE is a 404 amino acid-long protein with molecular weight of ~55 kDa. After transcription, RAGE pre-mRNA undergoes alternative splicing to modify

the exons and introns of the gene (Koolman and Roehm, 2005). RAGE has approximately 20 isoforms or splice variants which have been identified in a wide range of tissues and cells. The expression level of these splice variants is tissue-specific (Yonekura et al., 2003, Ding and Keller, 2005, Leclerc et al., 2009).

A RAGE polymorphism termed glycine-82-serine (G82S) has a significant impact on inflammatory disease (Xie et al., 2008). It has been found that G82S has linkage disequilibrium with human leucocyte antigen (HLA) DR4, which is strongly associated with diabetes type 1 and rheumatoid arthritis (Ramasamy et al., 2009, Yan et al., 2010, Traherne, 2008). The G82S increases ligand binding affinity of RAGE towards calgranulins (S100 proteins), which leads to adjustment of pro-inflammatory genes and subsequent promotion of the upregulation of intracellular signalling (Hofmann et al., 2002).

RAGE has two N-glycosylation sites, at asparagine residues Asn81 and Asn25, and these may play a role in assisting ligand binding to RAGE since they flank the AGE binding domain (Huttunen, 2002). The G82S polymorphism occurs in one of the N-glycosylation motifs. It has been revealed that RAGE proteins that lack glycosylation or the G82S mutation exhibit three orders of magnitude higher affinity to glycoaldehyde-derived AGE, which is one of the main human AGE fractions (Osawa et al., 2007). High Mobility Group Box 1 protein (HMGB1) has been found to bind to carboxylated N-glycans. Therefore, it appears that the N-glycosylation sites on RAGE assist its interaction with HMGB1. De-glycosylation of RAGE reduced the binding affinity of RAGE for HMGB1 (Srikrishna et al., 2002).

RAGE is classified as a pattern recognition receptor due its ability to recognize multiple structurally diverse, unrelated ligands (Xie et al., 2008, Schmidt et al., 2000). The extracellular domain of RAGE is postulated as the binding site of its ligands and alterations of the sequence of RAGE in that particular domain may have an important effect on ligand binding, which in turn may affect the progression of diseases (Hudson et al., 2008). It has been suggested that the level of expression of soluble RAGE (sRAGE) in human plasma could be used as a biomarker for type I diabetes and other inflammatory conditions (Ramasamy et al., 2009). Various studies have shown that administration of sRAGE could block the interaction between RAGE and its ligands, subsequently slowing down the progression of diseases by preventing the initiation of RAGE-induced signal transduction (Park et al., 1998, Yan et al., 2009, Taguchi et al., 2000).

The RAGE protein consists of three major domains, as shown in Figure 5. The first domain is the extracellular domain, which consists of three immunoglobulin-like domains: one

variable-type (V-type domain) and two constant-type (C-type) domains. The second domain of RAGE is a single hydrophobic transmembrane-spanning helix that anchors the whole protein to the cell surface. The last domain is a highly charged cytoplasmic domain that is important for RAGE signalling (Wilton et al., 2006, Ding and Keller, 2005).

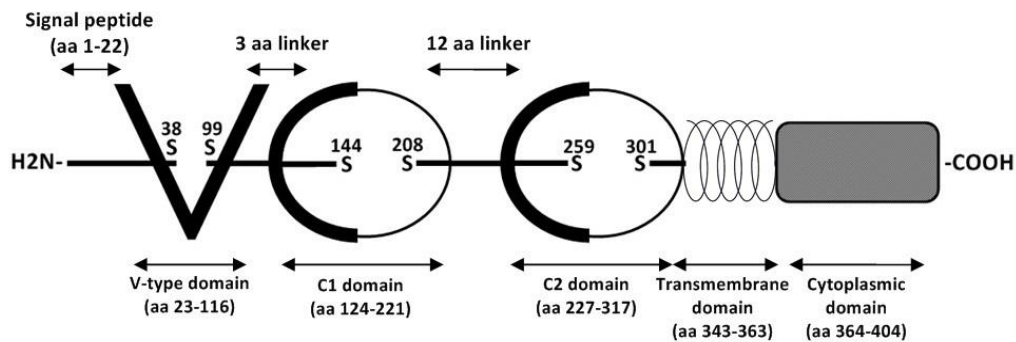


**Figure 5.**The structural domains of RAGE.

The variable type immunoglobulin-like domain (V-type domain) of RAGE is postulated to be the main binding site of multiple RAGE ligands. Previous studies have pointed out that various classes of AGEs bind to the V-type domain. This domain is also suggested to be the binding site for several calgranulins (S100B, S100A1 and S100A12), amyloid oligomers and HMGB1 (Xie et al., 2008, Leclerc et al., 2009). There are some key features of the V-type domain that underlie its binding to various RAGE ligands. As explained previously, the V-type domain possesses two asparagine glycosylation sites in Asn81 and Asn25, which along with G82S polymorphism are believed to contribute to the ligand-binding properties of RAGE (Srikrishna et al., 2002, Osawa et al., 2007).

The NMR three-dimensional structure of the RAGE V-type domain has helped to rationalise its binding mechanism to ligands. The recombinant V-type domain of RAGE spans a region 99 amino acids long between Ala23 and Pro121, with a molecular mass of 11 kDa. The structure has 21 intermolecular hydrogen bonds and one disulfide bond between Cys38 and Cys99. There are seven  $\beta$ -strands connected by six loops which form two  $\beta$ -sheets. These sheets are linked together by the disulfide bond, resulting in a  $\beta$ -sandwich structure. This structure, however, has two features that distinguish it from common V-type immunoglobulin structures, particularly in loop 3 of the structure: the presence of an additional  $\alpha$ -helix and the lack of two  $\beta$ -strands (Matsumoto et al., 2008).

Analysis of the secondary structure of V-type domain shows that there is a high degree of flexibility within the domain structure due to the presence of hydrogen bonds and the dynamic properties of certain residues (Xie et al., 2008). The hydrogen bonded amides which participate in the formation of  $\beta$ -sheets have been shown to have a high exchange rate with deuterium in an assay of hydrogen-deuterium exchange of backbone amide. NMR relaxation studies identified residues that showed dynamic motions on the millisecond to microsecond timescale, located in the middle of the  $\beta$ -strands and within or at the end of the flexible loops (Xie et al., 2008).

The molecular surface of the V-type domain is characterized by a distribution of positively charged residues that cluster in a specific area and form a cationic patch, which gives the V-type domain a net positive charge. The 3D structure with the cationic patch and the secondary structure are shown in Figure 6, reprinted with permission (Matsumoto et al., 2008) (see Appendix C, section 6.3).

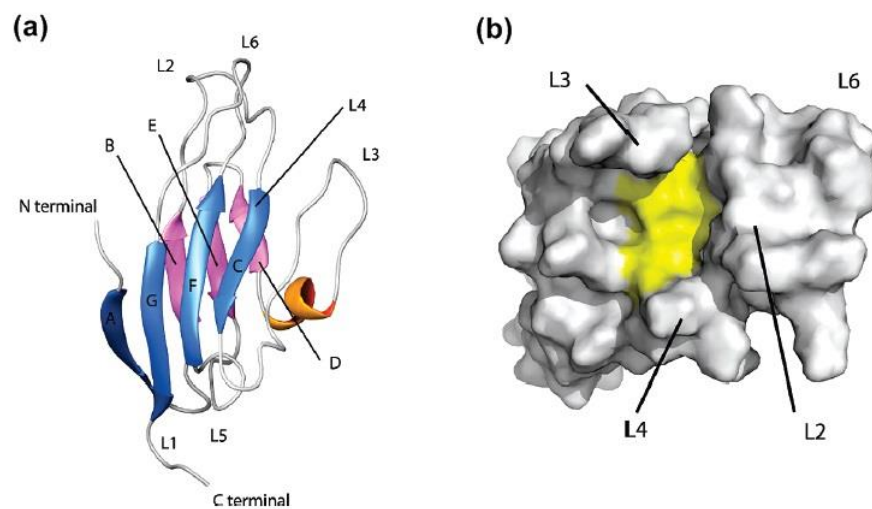


**Figure 6.(a) The secondary structure of the V-type domain and (b) the 3D structure with the cationic patch.**

The secondary structure of the V-type domain (a) consists of seven  $\beta$ -strands, shown on the figure as A, B, C, D, E, F, and G. The cationic patch in the 3D structure is shown on the molecular surface as the yellow part (Matsumoto et al., 2008).

This positively charged patch mediates RAGE binding to negatively charged ligands such as AGE. The involvement of charge in RAGE-ligand binding is also associated with one of the N-glycosylation sites (Asn81). Asn81 contains an anionic glycan which contributes to

the binding properties of the V-type domain (Matsumoto et al., 2008). Some studies have suggested that HMGB1 binds to RAGE through the N-glycosylation sites. HMGB1 has a highly negative charge in its acidic C-terminal tail, so the positively charged patch in the vicinity of Asn81 may bind to this negatively charged region in HMGB1. Studies by Hori et al. and Srikrishna et al. found that rat HMGB1 and bovine lung RAGE interact with an interaction affinity ( $K_D$ ) of approximately 10 nM (Hori et al., 1995, Srikrishna et al., 2002). Interestingly, when RAGE was de-glycosylated, the affinity was determined to decrease to about 20 nM (Srikrishna et al., 2002). A surface plasmon resonance study utilizing commercially manufactured RAGE and HMGB1 reported the interaction affinity to be about 98 nM (Ling et al., 2011).

### **1.2.2 Toll-Like Receptor (TLR)**

Toll-like receptors (TLRs) are a family of transmembrane proteins, highly conserved pattern-recognition receptors which play a key role in conducting an organism's defense against infection (Leventhal and Schroppel, 2012). TLRs are one of the important key factors which activate and regulate the innate immune system and inflammation. After recognizing a specific conserved pathogenic pattern, referred to as Pathogen-associated Molecular Pattern (PAMP), the TLRs are activated and promote a signaling cascade which results in cytokine production and adaptive immune response (Dasu et al., 2010a, Tsan and Gao, 2004). The first discovery of the involvement of TLRs in innate immunity happened in *Drosophila* (Suhir and Etzioni, 2010). Indeed the name "Toll-like receptor" was based on their homology to Toll protein in *Drosophila* which was discovered to play an important role in the defense against fungal infection (Suhir and Etzioni, 2010). Mammals and drosophila use Toll receptor family to detect the invasion of microorganism. The signaling pathway of the Toll receptor identified in *Drosophila* is highly similar to interleukin 1 (IL-1) pathway in mammals which subsequently activates the NF $\kappa$ B. It was concluded that the cytoplasmic domain of Toll receptor in drosophila and IL-1 receptor in mammals are highly conserved and referred to as Toll/IL-1 Receptor (TIR) domain (Takeda et al., 2003).

The structure of TLRs consists of two domains: the extracellular domain, which serves as ligand-binding domain and is characterized by Leucine-Rich Repeat (LRR) motifs, and the intracellular signaling TIR domain (Suhir and Etzioni, 2010). A recent study reported that the TLR family consists of 13 cell surface and intracellular pattern recognition receptors, which detect a diverse array of ligands expressed by potentially invading pathogens

(Leventhal and Schroppe, 2012). Ten TLRs have been identified in human: TLR1, 2, 4, 5, 6 and TLR10 are extracellular, whereas TLR3, 7, 8 and TLR9 are intracellular, possibly related to their ligand-binding function (Suhir and Etzioni, 2010).

TLRs are generally expressed on several cell types. The mRNA for all TLRs, except TLR3, is expressed in monocytes and macrophages, which are predominant cells of the innate immune system and are important in some proinflammatory-based diseases, such as atherosclerosis and diabetes (Dasu et al., 2010a). The expression of TLRs in dendritic cells is divided based on the type of cells. Myeloid Dendritic Cell (MDC) expresses TLR1, 2, 4, 5 and TLR8, and occasionally TLR7. Plasmacytoid Dendritic Cell (PDC) expresses TLR7 and TLR9. The expression of the TLRs also depends on the maturity of the dendritic cells. TLR3 is only expressed in mature dendritic cells. Phagocytes were also reported to show ample expression of all TLRs, whereas several TLRs are expressed exclusively in B cells. Mast cells express TLR2, 4 and TLR8 (Takeda et al., 2003).

Each one of the TLRs has a specific role in recognizing and mediating signals for various pathogenic components. For example, TLR4 was identified as signal transducer for lipopolysaccharides (LPS), which occupy a large portion of the Gram-negative bacterial cell wall. TLR4 also binds to Myeloid Differentiation-2 (MD-2), which helps it to recognize endotoxins (Tsan and Gao, 2004). The mRNA expression level of MD-2 is also known to increase together with TLR6 mRNA expression in Type 2 Diabetic patients (Dasu et al., 2010a). TLR2 is known to bind components of the Gram-positive bacteria. TLR2 has a wide range of ligand recognition specificity as it can form heterodimers with other TLRs and sometimes with CD14 and CD36 (Dasu et al., 2010a). TLR2 recognizes triacyllipopeptides in association with TLR1, and diacyllipopeptides in association with TLR6. TLR2 also identifies lipoproteins and peptidoglycans. TLR3 recognizes double-stranded RNA and TLR7 identifies single-stranded RNA (Tsan and Gao, 2004). Ligands for TLR2 and TLR4, the best-studied members of the TLR family, include Heat Shock Protein 60 (HSP60), HSP70, endotoxin, hyaluronan, Advanced Glycation End-products (AGE), extracellular matrix components and High Mobility Group Box 1 (HMGB1) (Dasu et al., 2010a). The affinity of the interaction between HMGB1 and the TLR4/MD-2 complex has been reported to be 1.5  $\mu$ M, whereas the interaction between Box B of HMGB1 and the same complex has been reported to be 22  $\mu$ M (Yang et al., 2010). TLRs are also expressed in other cell types that are known to contribute to inflammatory responses. In Type 2 Diabetic subjects, the increase of TLR2 and TLR4 expression has been shown in common insulin resistance target



tissues, such as skeletal muscle, adipose tissue and in human monocytes under hyperglycemia conditions (Dasu et al., 2010a).

The TLR-ligand binding promotes self-association of TLR, which form a complex of TLR subunits containing adaptor proteins from the family of the Myeloid Differentiation primary response gene 88 (MyD88). Binding leads to further signal transduction events that activate Mitogen-activated Protein Kinases (MAPKs) and NF $\kappa$ B, which triggers transcription of proinflammatory chemokines such as monocyte chemoattractant protein-1 and cytokines such as IL-1, IL-6, and TNF $\alpha$  (Devaraj et al., 2008). The MyD88-dependent pathway is regulated by MyD88 and Toll/Interleukin 1 Receptor (TIR) domain-containing Adaptor Protein (TIRAP), and this pathway activates proinflammatory cytokine production through NF $\kappa$ B. Other regulators are TIR domain-containing Adaptor Inducing Interferon (TRIF) and TRIF-related adaptor molecule (TRAM), which activate Interferon Regulatory Factor 3 (IRF3) and subsequently produce type I interferon (IFN) (Leventhal and Schroppe, 2012). In addition, a MyD88-independent pathway involving TRIF is essential for TLR3 and TLR4 signaling and induces IFN- $\beta$  (Dasu et al., 2010a). In the case of Type 1 Diabetes, it was demonstrated that deficiency of MyD88 results in reduction in atherosclerotic plaque size, lipid content, expression of proinflammatory genes, and systemic expression of proinflammatory cytokines, such as IL-1 and Tumor Necrosis Factor (TNF) (Devaraj et al., 2008).

LPS, mainly responsible for exaggerated innate immune response in sepsis, are known to interact with TLR4 and CD14, a cell surface glycoprotein. A Fluorescence Resonance Energy Transfer (FRET) study demonstrated that LPS appear to promote interaction between CD14 and TLR4, which leads to nuclear translocation of NF $\kappa$ B. It is also known that LPS stimulation upregulates the expression of CD14 and TLR4 (Jiang et al., 2000).

### **1.3 Unravelling the mechanism of HMGB1-receptors interaction**

#### **1.3.1 HMGB1-RAGE: signalling pathway and pathophysiology**

HMGB1 induces innate immune responses when it forms a complex with DNA, lipids and pro-inflammatory cytokines. These complexes need the cell surface receptors of HMGB1 to induce inflammation. HMGB1 as one of the DAMP molecules induces signaling by interacting with its receptors (Leventhal and Schroppe, 2012). Previous studies pointed out that the RAGE-HMGB1 interaction stimulates the activation of NF $\kappa$ B and has been

implicated in embryonic and cancer cell motility and invasion (Luan et al., 2010). In endothelial cells, neurites and tumour cells, the RAGE-HMGB1 interaction activates multiple signalling pathways, such as Ras/MAPK, the Rho small family of GTPases and NFκB, as well as the activation of several MAP kinases, such as p38, p44/42, and SAPK/JNK (Kokkola et al., 2005). The induction of cell motility by RAGE involves the Rho small family of small GTP-hydrolysing proteins (GTPases) Cdc42 and Rac1. Rac1 mediates membrane ruffling and formation of lamellopodia, whereas Cdc42 regulates the formation of filopodia (Huttunen et al., 1999). Through the activation of the GTPases, RAGE then activates p38 and stress-activated protein kinase (SAPK)/JNK (Taguchi et al., 2000). RAGE is also known to mediate cellular activation through the MAPK signalling pathway. RAGE binds ERK1 and ERK2, members of MAP kinase. The activated ERK1/2 then activates the small GTP-hydrolysing proteins (GTPases) Ras and MMP2/9 (Ishihara et al., 2003, Kuniyasu et al., 2002, Koolman and Roehm, 2005).

The interaction of RAGE with HMGB1 activates a signalling cascade in a cell-specific manner. It was demonstrated that TLR-9 activation stimulates HMGB1 release from the nucleus. HMGB1 subsequently binds RAGE and activates the p38 and ERK1/2-MAPK pathways, which leads to the NFκB pathway and promotes the maturation and migratory capacity of dendritic cells (Kierdorf and Fritz, 2013). In myoblasts and rhabdomyosarcoma, this interaction stimulates the p38 pathway, which results in myogenic differentiation, reduced proliferation and migration and the release of MMP1 and 2 (Sorci et al., 2013). The RAGE-HMGB1 interaction is associated with apoptosis in macrophages through the activation of the SAPK/JNK pathway (Taguchi et al., 2000). Phosphorylation levels of Rac1 and SAPK/JNK increased when macrophage differentiation of a monocytic leukemia cell line was treated with HMGB1 (Kuniyasu et al., 2005). However, the RAGE-HMGB1 interaction also enhances the expression of NFκB, which counters the apoptotic effect caused by Rac1 and SAPK/JNK. Activation of NFκB by the RAGE-HMGB1 interaction possibly mediates anti-inflammatory responses and thus promotes cell survival (Kuniyasu et al., 2005).

In the cell nucleus, HMGB1 serves as a chromatin-binding factor that bends DNA and promotes protein assembly, while in its secreted form HMGB1 binds to RAGE and mediates inflammatory responses (Scaffidi et al., 2002). The RAGE-HMGB1 interaction causes sustained activation of RAGE, which subsequently promotes chronic cellular activation and tissue injury. This contributes to several common diseases that involve chronic inflammation (Rauvala and Rouhiainen, 2009). The RAGE-HMGB1 interaction is

widely considered to be a crucial factor for the growth and invasive migration of tumour cells. The interaction also promotes tumour progression by inducing cell survival (Huttunen et al., 2000). The pathophysiological effects triggered by the RAGE-HMGB1 interaction are assumed to be cell-specific to some extent. The signalling pathway activated by RAGE upon binding to HMGB1 is generally similar, but the outcomes might slightly differ from one type of cell to the other.

HMGB1 acts as a surface for the assembly of fibrinolytic complexes, which leads to the activation of MMPs which regulate tumorigenesis, whereas tumour cells that overexpress RAGE have an increasing activity of MMP-2 and MMP-9. Therefore, RAGE-HMGB1 interaction was suggested to play an important role in tumour cell invasiveness. (Taguchi et al., 2000). HMGB1 by itself is secreted by mononuclear cells after induction and mediates the trans-endothelial migration of monocytes. The small GTPases (Cdc42 and Rac1) are essential mediators of monocyte invasion through the endothelium. HMGB1 has been shown to be specifically adhesive for monocytes, which triggers the extensive spreading of cells (Rouhiainen et al., 2004). In cancer cells, RAGE has been reported to be distributed exclusively on invasive primary tumors and metastatic regions in lymph nodes, whereas HMGB1 is expressed in all cell types and stages of disease progression (Kuniyasu et al., 2002). RAGE is closely associated with cell growth and invasion through MAP kinase induction in glioma cells (Taguchi et al., 2000, Kuniyasu et al., 2002).

HMGB1 binds firmly to chromatin in apoptotic cells, whereas in necrotic cells it rapidly dissociates from chromatin and is leaked to the extracellular environment. The release of HMGB1 immediately triggers inflammatory responses by the production of tumour necrosis factor- $\alpha$  (TNF- $\alpha$ ), the regulator and amplifier of inflammation. This establishes HMGB1 as one of the signals of cell necrosis (Scaffidi et al., 2002, Luan et al., 2010, Kokkola et al., 2005). Recently it has been reported that apoptotic cells are also capable of releasing HMGB1; however, the secreted HMGB1 has a more tolerogenic nature rather than pro-inflammatory (Sims et al., 2010).

Besides its pro-inflammatory effects, the interaction of RAGE with HMGB1 has multiple beneficial outcomes. Their interaction stimulates upregulation of the expression of the mRNA of Chromogranin B (Fages et al., 2000), which is a heparin-binding protein that is responsible for the enhancement of neurite outgrowth (Rouhiainen et al., 2004). It is also believed that HMGB1 induces anti-apoptotic responses by inducing the expression of the anti-apoptotic protein Bcl-2 in neuronal cells. Activation of RAGE by HMGB1 triggers the

activation of NF $\kappa$ B and the upregulation of Bcl-2, which results in cell survival (Huttunen et al., 1999, Huttunen et al., 2000). The RAGE-HMGB1 interaction also induces the gene expression of a novel transmembrane protein termed amphoterin-induced gene and ORF (AMIGO), which is highly expressed in the nervous system. AMIGO promotes cell-cell interaction in fibre tracts of the nervous system (Kuja-Panula et al., 2003). The HMGB1-activated RAGE signalling was reported to promote neurogenesis and cardiac muscle regeneration. In myoblasts, HMGB1 that is released by injured myofibers sequentially stimulates RAGE, which triggers expansion of myoblast population and myogenic differentiation (Sorci et al., 2013).

### **1.3.2 HMGB1-TLR: signalling pathway and pathophysiology**

HMGB1 interacts in particular with TLR2 and TLR4 (Leventhal and Schroppe, 2012). Other than that, HMGB1 also interacts with TLR7 and TLR9 (Sims et al., 2010). HMGB1 is described to be upregulated after ischemia-reperfusion injury (Leventhal and Schroppe, 2012). Blocking HMGB1 before the injury occurs decreases tubular damage, but applying recombinant HMGB1 aggravates the injury. The ischemia-reperfusion state is not altered when TLR4 is not present, regardless of the presence of recombinant HMGB1 or the blockade of HMGB1. Together with TLR4, HMGB1 was also claimed to increase adhesion molecules in microvascular endothelial cells (Leventhal and Schroppe, 2012). Furthermore, allograft injury also shows the increase of HMGB1 expression, together with TLR2 and TLR4. The release of hypoxia-induced HMGB1 is promoted by the production of TLR4-dependent reactive oxygen species (Leventhal and Schroppe, 2012). A Fluorescence Resonance Energy Transfer (FRET) study investigated the interaction of Toll-like receptor 2 (TLR2) and TLR4 with HMGB1 in macrophages, showing that HMGB1, TLR2 and TLR4 interact on the cell surface at the early stages of cell stimulation (Park et al., 2006).

The binding of TLR4 to HMGB1 needs Cys23 and Cys45 to form a disulfide bond and Cys106 to stay free. A Surface Plasmon Resonance (SPR) study concluded that the free cysteine residue is critical for binding of HMGB1 with TLR4. The mutation of the Cys106 caused the failure of HMGB1 to stimulate TNF $\alpha$  release, which suggested that the free cysteine influences the immunogenic activity of HMGB1 (Yang et al., 2010). Several ligands of TLR, such as the Class A Cytosine-Guanine-rich (CpG-A)-DNA and LPS, are known to form complexes with HMGB1, which subsequently triggers stronger inflammatory responses (Ibrahim et al., 2013).

A study on Type 2 Diabetes reported that patients have high circulating levels of HMGB1, Heat Shock Protein 60 (HSP60), HSP70, and hyaluronan, which subsequently trigger and activate TLR2, leading to a proinflammatory state. Further coimmunoprecipitation studies suggested the existence of an association between TLR2, TLR4, HMGB1, and HSP60 (Dasu et al., 2010a).

#### **1.4 Interaction of RAGE and TLRs with their ligands**

Most of interactions between proteins are determined by the capability of the individual protein to oligomerize (Ali and Imperiali, 2005). It has been suggested that oligomeric proteins comprise roughly a third of cellular proteins. The prevalent oligomeric state of cellular proteins is tetrameric, and it has been implied that this oligomeric form is favoured due to a number of functional advantages, such as higher activity due to the possible increasing number of active sites, higher level of control, and more resistancy to degradation (Ali and Imperiali, 2005).

In case of RAGE, its association with AGE promotes the oligomerization of the receptor (Matsumoto et al., 2008). Bacterially expressed sRAGE was reported to be monomeric but once RAGE interacts with AGE, it forms oligomers. Thus, RAGE oligomerization is assumed to be a ligand-dependent event. Furthermore, it is believed that oligomerization triggers the activation of the signal transduction pathway of RAGE (Dattilo et al., 2007). It has been reported that the V-type domain is the mediator of RAGE oligomerization following the binding of RAGE to AGE. Oligomerization of RAGE also increases the binding affinity of RAGE to its ligands presumably because it triggers interaction of multiple V-type domains of RAGE with each other and, therefore, increases the likelihood of ligand binding to RAGE because more binding sites become available (Xie et al., 2008). A co-immunoprecipitation assay also showed that the RAGE protein with the V-type domain deleted is not capable of interacting with other RAGE molecules (Zong et al., 2010). However, Zong et al. did not elaborate the impact of the deletion of other RAGE domains towards RAGE oligomerization. There was also no indication as to whether the isolated V-type domains formed oligomers in solution.

Another RAGE ligand, S100B, has been shown to induce multimerization of the receptor, which is mediated by salt bridges, hydrogen bonds and Zn<sup>2+</sup> ion. The ligand-induced oligomerization of RAGE initiates the signal cascades required for receptor activation

(Koch, 2010). An analytical ultracentrifugation study of S100B showed that its tetrameric form binds two RAGE molecules with higher affinity compared to its dimeric form (Ostendorp et al., 2007). Other studies have suggested that the conformation of the ligands can actually affect the oligomerization of RAGE. In a study of the interaction between RAGE and S100C, the latter undergoes a conformational change in the presence of  $\text{Ca}^{2+}$ . It subsequently forms a hexamer and promotes oligomerization of RAGE upon their interaction. Bacterially-expressed sRAGE was discovered to become a tight tetramer and the  $\text{C}_1$  domain serves as the oligomerization site (Xie et al., 2007).

Similarly, TLRs have also been reported to undergo oligomerization upon binding to their ligands as a key event in their functional activation and cytokine production. It has been confirmed that dimerization is a crucial event for the functional activation of TLRs, leading to the production of cytokines (Dasu et al., 2010b). Either homodimerization or heterodimerization is important for the function of TLRs. Heterodimerization of TLR2 with TLR1 or TLR6 has been shown to be necessary for the recognition of ligands by TLR2. The heterodimer could involve TLR1 and TLR2, or TLR2 and TLR6. Besides heterodimerization, other biochemical studies pointed out that TLRs also form homodimers, such as TLR3 and TLR4 (Tsan and Gao, 2004). Factors such as the presence of high levels of glucose induce heterodimerization between TLR2 and TLR6, which leads to the production of cytokines and the activation of NF $\kappa$ B (Dasu et al., 2010a). These heterodimerizations and homodimerizations are known to trigger the interaction between cytoplasmic TLR and the IL1 receptor domain, which activate intracellular signalling. However, it seems that the mechanism of formation of these homodimers and heterodimers is generally unknown. A study on ischemic reperfusion injury, which occurs during transplantation, speculated that the differences in the level of tissue damage in connection with the relative importance of MyD88-dependent and -independent signaling may reflect an unknown ability of TLRs to affect each other through dimerization (Leventhal and Schroppe, 2012). This may occur because the absence of both TLR2 and TLR4 or each individual TLR actually reduce the level of ischemic reperfusion injury (Leventhal and Schroppe, 2012).

### **1.5 HMGB1 oligomerization**

The oligomerization of HMGB1 was first observed by Duguet and de Recondo, who described a 25 kDa DNA-binding protein that formed tetramers in equilibrium with monomers at low ionic strength ( $\mu = 0.05 \text{ M}$ ) (Duguet and de Recondo, 1978). HMGB1

forms beads when bound to DNA. Visualization by electron microscopy required fixation of HMGB1-DNA complex with glutaraldehyde (Mathis et al., 1980). These HMGB1 beads consist of about 20 HMGB1 monomers (Bonne et al., 1980). The beads are apparently quite unstable, as  $Mg^{2+}$  and  $Ca^{2+}$  destabilise the bead structure (Mathis et al., 1980, Stros et al., 1994).

The method of HMGB1 isolation and purification may influence its ability to oligomerise (Marekov et al., 1984). Extensive treatment with high concentrations of perchloric acid and trichloroacetic acid (5-25%) precipitation over long time (2 hours) does appear to promote the formation of HMGB1 oligomers (Marekov et al., 1984, Wagner et al., 1995). This extensive acid treatment may have influence the properties of HMGB1 in these studies. However, most studies use 2% trichloroacetic acid (TCA) with a precipitation time of less than 30 minutes to purify HMGB1 (Rabbani et al., 1978, Goodwin et al., 1975). It is of interest to note that HMGB1 isolated from *Xenopus laevis* mitochondria in non-denaturing condition binds DNA with high affinity. This HMGB1 still self-associates to form beaded structure in an ionic strength-dependent manner (Mignotte and Barat, 1986).

Post-translational acetylation of HMGB1 appears to promote the oligomerization of HMGB1 isolated from GAT tumour cells (Alexandrova and Beltchev, 1987). However, other post-translational modification such as phosphorylation, methylation, glycosylation or disulphide bonds formation and poly(ADP)-ribosylation may also contribute to HMGB1 oligomer formation (Alexandrova and Beltchev, 1987).

While many studies have reported the oligomerization of HMGB1 and the formation of beads upon interacting with DNA, there are controversies regarding the oligomerization or self-association of HMGB1 in the absence of DNA. Bianchi et al. concluded that both A and B boxes of HMGB1 can form dimers in the presence or absence of DNA (Bianchi et al., 1992), whereas the monomeric boxes did not bind DNA (Bianchi et al., 1992). Dimeric structures are not unusual among the DNA-binding proteins, and is often essential for their DNA-binding properties, such as leucine zipper proteins and helix-loop-helix protein family (Bianchi et al., 1992). However, Teo et al. concluded that box B, and not box A of HMGB1, oligomerizes extensively on supercoiled DNA, but not linear DNA (Teo et al., 1995), and that no significant cross-linking products were observed in the absence of DNA (Teo et al., 1995). These conclusions were supported by Grasser et al. (Grasser et al., 1998). More recently, an analytical ultracentrifugation study by Ranatunga et al. concluded that HMGB1 exists mainly as monomer in solution. There was little evidence of

dimer formation (Ranatunga et al., 1999). Interestingly, the HMGB1 used in their study actually eluted as a 55 kDa protein from gel permeation chromatography, while theoretically, HMGB1 is a 25 kDa protein. The study could not explain this anomaly (Ranatunga et al., 1999). Unfortunately, no further studies have evaluated the self-association properties of HMGB1.

## **1.6 The present study**

The forgoing literature review details how HMGB1 modifies the structure of chromatin by its interaction with DNA and how it promotes inflammation, sepsis, tumour growth, and other diseases upon interaction with receptors such as RAGE and TLRs. The somewhat controversial literature describing the self-association of HMGB1 is also described. The varied reports regarding HMGB1 self-association could be due to the widely varied conditions between studies as well as the purity and source of proteins used in these studies. I set-out to study the self-association of HMGB1 under a variety of physicochemical conditions. I postulate that this approach will be pivotal to understanding the biological mode of HMGB1 action. As detailed in the literature review, it is notable that: 1) HMGB1 forms large oligomeric beads with DNA and 2) RAGE and some of its associated ligands, such as the S100 proteins, also function by forming oligomeric complexes.

The HMGB1 and RAGE proteins used in this study were purified using procedures recently developed by Dr. David Chandler (Chandler, 2015). In his study, a common vector and *Escherichia coli* expression system capable of the high level (mg) cytosolic expression of RAGE and HMGB1 proteins was developed. The purification procedures enabling the purification of these proteins to homogeneity were also developed. Surface plasmon resonance (SPR), a label-free biosensor technique that enables a comprehensive kinetic analysis of molecular interactions in real-time was selected as the method of choice for this study. The technique is elaborated in Appendix E of this thesis.

Using SPR, this thesis reports the first detailed study of the self-association of HMGB1. The influence of a number of key physicochemical parameters on the self-association of HMGB1 is comprehensively investigated. In particular, the influence of ionic strength, metal cations, redox environment and pH on the self-association of HMGB1 was investigated. A model best describing HMGB1 oligomer formation in this study is then proposed. The physiological implication of the properties self-association of HMGB1 is also discussed. In particular, the role of the self-association of HMGB1 on its interaction with DNA, RAGE and other receptors is discussed.



## **2 MATERIALS AND METHODS**

## **2.1 Ethics approval**

Animal or Human ethics approval were not required at any stage of this project.

## **2.2 Genetically Modified Organism; Approval and Safety**

This project utilized commercially available expression systems developed by Invitrogen™. These systems are classified as exempt dealings under parts 1 & 2 of Schedule 2 of the Gene Technology Regulations 2001 (Commonwealth Government of Australia) due to the well-defined nature of the vectors. Notice of the use of these vectors and the associated genes to be expressed is registered with the Curtin University Institutional Biosafety Committee.

## **2.3 Transformation of competent *Escherichia coli* and colony isolation**

Chemically competent T7 Shuffle K (New England BioLabs) *Escherichia coli* (*E. coli*) were transformed with the ampicillin resistance pGS-21a vector containing the full-length HMGB1 gene. An aliquot of 50 µl chemically competent *E. coli* was thawed on ice and 50-100 ng of plasmid (HMGB1-opt-subcloning in pGS-21a, 40 ng/µl, GenScript) was added. The mixture was incubated on ice for 30 minutes before being heat-shocked for 30 seconds in a 42°C water bath. The mixture was immediately placed back on ice, and 950 µl of room temperature SOC media (Invitrogen) or lysogeny broth (LB) media was added. The mixture was then incubated at 37°C for 1 hour at 250 rpm.

A single cell colony was isolated by firstly growing the bacterial suspension on an agar plate. An LB agar plate with 1.5% agarose (w/v) and 100 µg/µl ampicillin was used for selection pressure. An aliquot of 50-100 µl bacterial suspension was transferred to the middle of the plate. The suspension was spread evenly to the whole surface of the agar plate with a “hockey stick”-shaped cell spreader prepared from a glass Pasteur pipette. The colonies were grown by incubating the plate overnight at 37°C.

PCR was used to verify that the colony contained the correct plasmid insert (section 2.4). Following confirmation by PCR, the colony of the transformed *E. coli* was grown in 2-3 ml LB media with shaking at 200 rpm, 37°C, until an OD<sub>600</sub> of 0.8 was reached. The bacterial suspension was frozen at -80°C in 1 ml aliquots after addition of 15% (v/v) glycerol.

## 2.4 Polymerase Chain Reaction (PCR) of the whole competent colony

Two PCR master mixes were prepared: one contained 0.25  $\mu$ M each of the forward and reverse primers for VCC-RAGE (Table 1, done in collaboration with Dr. David Chandler). The other contained 0.25  $\mu$ M each of the forward and reverse primers for HMGB1 (Table 2, 100  $\mu$ M, GeneWorks). Each master mix consisted of 1x PCR buffer (TAQ-Ti DNA POLYMERASE 10x Reaction buffer, Fisher), 0.2 mM dNTPs (dNTP mix 10 mM, Fisher), 2.5 mM MgCl<sub>2</sub> (MgCl<sub>2</sub> 25 mM, Fisher), and 1U of Taq Polymerase (TAQ-Ti DNA POLYMERASE 250 Units 5U/ $\mu$ l, Fisher).

A total volume of 15  $\mu$ l master mix per reaction was kept in a sterile 0.2 ml microcentrifuge tube on ice. Single colonies were picked with a sterile pipette tip from the LB agar plate containing ampicillin with positive colony forming units (refer to the procedure in section 2.3) and transferred to one master mix aliquot. The tubes were placed in a Veriti 96 well thermalcycler (Applied Biosystems) and the insert DNA was amplified using the following procedure: initialization for 5 minutes at 94°C to activate Taq polymerase and lyse cells; 32 cycles of denaturation (0.5 minute at 94°C), annealing (0.5 minute at 56°C) and elongation (1 minute at 72°C). The cycles were completed with a hold cycle ( $\infty$  at 10°C). At the end of the program, reaction mixtures were stored at -20°C until needed.

**Table 1. Forward and reverse primers used to amplify human VCC-RAGE.**

Primer	Sequence	T <sub>m</sub> (°C)
Prok-Forward-RAGE (pF1)	ATGGCCCAAACATTACCGCT	61
Prok-ReverseVC1C2 (pR3)	CAGACCGCTGCCACCAA	59

**Table 2. Forward and reverse primers used to amplify human HMGB1.**

Primer	Sequence	T <sub>m</sub> (°C)
Forward-HMGB1-optimized	5'-CGTCCAGACCTGCCGTGAAGA	62
Reverse-HMGB1-optimized	5'-GCATCCGGTTTACCTTTCGCG	59

## **2.5 Agarose gel electrophoresis for PCR products**

A 2% agarose gel was made by dissolving 2 gram of agarose powder into 100 ml of 1x TAE buffer (40 mM Tris, pH 8.0 containing 20 mM acetic acid, 1 mM ethylenediaminetetraacetic acid (EDTA)). The molten agar mixture was poured into a mold containing the combs and left for about 10 mins to solidify. The sample was prepared by mixing 2  $\mu$ l of 6x loading buffer (GeneWorks) with 10  $\mu$ l of sample. A 10  $\mu$ l aliquot of the sample was loaded into each lane, and 10  $\mu$ l of 100 bp standard (GeneWorks) was used as a marker for DNA size determination. The DNA in the sample was separated based on size by running the gel at 80 V for 50 mins. After DNA separation was completed, the gel was stained with 30  $\mu$ l of GelRed stain (GelRed Nucleic Acid Gel Stain, 10,000x in water, Biotium) dissolved in 100 ml of 1x TAE buffer for 30 minutes with slow shaking. A picture of the gel was taken and analyzed with the program Quantum-Capt integrated with QUANTUM ST5 Gel Documentation System (Fisher Biotech).

## **2.6 Expression of HMGB1 and RAGE**

A competent colony, expressing HMGB1 or VCC-RAGE, was inoculated into a 1 L of LB broth containing 100 mg/L ampicillin and grown at 37°C with overnight shaking at 180 rpm, until the turbidity reached an OD<sub>600</sub> of about 0.8-1. The inoculated culture was then induced with 1 mM isopropyl  $\beta$ -D-1-thiogalactopyranoside (IPTG) and incubated further with shaking at 180 rpm, 37°C, for 2.5-3 hours (HMGB1) or 5 hours (VCC-RAGE). The cells were pelleted by centrifugation at 9720 x *g* with Sorvall RC 5B Plus centrifuge for 30 minutes. The pellets were stored at -20°C or immediately used.

## **2.7 Harvesting proteins from bacterial cell culture**

The pellets from 1L of bacterial culture (see section 2.6) were resuspended with 20 ml sonication buffer (10 mM NaH<sub>2</sub>PO<sub>4</sub>, pH 7.4 containing 0.1 mM DTT with 1 tablet of complete Mini EDTA-free protease inhibitor cocktail (Roche) per 10 ml of buffer. The total suspension was divided into 5 ml fractions in 10 ml centrifuge tubes, which were placed in an ice slurry bath to reduce sample heating during sonication. A microtip probe of

Misonix S-4000 was used. The amplitude was set to 80 with 10 pulses. The intermittent burst was set to 30 seconds sonication and 1 minute cooling to prevent sample heating. The crude protein lysate was obtained by collecting the supernatant from centrifugation at 5370 x g with Avanti JE centrifuge (Beckman Coulter) for 30 minutes.

## **2.8 Acid precipitation of HMGB1**

The soluble fraction of HMGB1 from sonication (see section 2.7) was treated with trichloroacetic acid (TCA) to remove other contaminant proteins. The purity of the HMGB1 fraction was checked with SDS-PAGE (see section 2.10). A volume of 40% TCA was added to the lysate to the final concentration of 2% TCA. The lysate was then centrifuged at 5370 x g with an Avanti JE centrifuge (Beckman Coulter) for 30 minutes to obtain the soluble HMGB1. The pH of the soluble fraction was immediately brought back to 7.4 by adding 2M NaOH.

## **2.9 Column chromatography**

All fractionation procedures were carried out with an ÄKTApurifier 100 (GE Healthcare). The protocols were written and the results were analyzed with Unicorn software version 5.20.

### **2.9.1 Heparin column chromatography**

As the first step of protein purification, the HMGB1 and RAGE crude extracts were passed through a heparin column. A heparin column was selected because HMGB1 and RAGE were shown to specifically bind heparin (Ling et al., 2011). The crude extract was filtered with a Minisart 0.2 µm filter (Sartorius stedim biotech) and purified with the HiTrap Heparin HP column (1 or 5 ml, GE Healthcare). Firstly, the column was equilibrated with 2 column volumes of wash buffer (for HMGB1: 10 mM NaH<sub>2</sub>PO<sub>4</sub>, pH 7.4 containing 0.1 mM DTT; for RAGE: 10 mM NaH<sub>2</sub>PO<sub>4</sub>, pH 7.4 containing 0.1 mM DTT and 3 mM EDTA). The filtered protein sample was injected onto the sample loop, and the sample was held in the sample loop during the column wash step. After the wash step with 2-5 column volumes of wash buffer, the sample was injected from the sample loop to the column by flowing 2x sample volume of wash buffer to the sample loop. The HMGB1 was eluted from

the column with 15 column volume of linear gradient elution to the final concentration of 100% elution buffer (10 mM NaH<sub>2</sub>PO<sub>4</sub>, pH 7.4 containing 0.1 mM DTT and 1M NaCl). RAGE was eluted with 10 column volumes linear gradient elution to the concentration of 50% elution buffer (10 mM NaH<sub>2</sub>PO<sub>4</sub>, pH 7.4 containing 0.1 mM DTT, 3 mM EDTA and 2M NaCl), followed by 5 column volume of 50% elution buffer, and finally 10 column volume of isocratic gradient to the final concentration of 100% elution buffer. All steps were done with the flow rate of 0.5 ml/minute for a 1 ml column and 1 ml/minute for a 5 ml column.

### **2.9.2 Size exclusion chromatography**

A Superdex 200 10/300 GL (GE Healthcare) column was equilibrated with 1.5 column volumes of 10 mM HEPES buffer pH 7.4) containing 150 mM NaCl, 3 mM EDTA, 0.05% (v/v) Tween 20 and 0.5 mM β-mercaptoethanol. The sample was injected from the sample loop to the column by flowing 2x sample volume of buffer to the sample loop. Finally, the protein was eluted from the column with 1.5 column volume of buffer. The concentration of the obtained protein was then determined by infra-red spectrometry on a Direct Detect spectrometer (Millipore) and subsequently the total volume of the obtained protein was aliquoted in smaller volumes of 50-100 μl with addition of 5% (v/v) glycerol and stored in -80°C.

### **2.10 Polyacrylamide gel electrophoresis (PAGE)**

A protein sample with a volume of up to 13 μl was mixed with 5 μl of NuPAGE LDS Sample Buffer 4x (Invitrogen) and 2 μl β-mercaptoethanol (Sigma-Aldrich), to make a final volume of 20 μl. If the sample volume was less than 13 μl, the aliquot was topped up with dH<sub>2</sub>O to 20 μl. The mixture was then boiled at 95°C for 5 minutes to further denature the protein before loading the sample to the PAGE gel. The NuPAGE 4-12% Bis-Tris Gel 1.0mm x 12 well (Invitrogen) were used. For protein size determination, 8 μl of Novex Sharp Protein Standard (Invitrogen) was added to the gel. Proteins in the sample were separated based on their electrophoretic mobility by running the system in NuPAGE MOPS SDS Running Buffer (Invitrogen) at 200 V for 45 minutes. After protein separation was completed, the gel was used for Western Blotting (see section 2.11) or stained with PageBlue protein staining solution (ThermoFisher) for 1 hour and subsequently destained with dH<sub>2</sub>O to visualize the protein band.

## 2.11 Western blots

Proteins from the SDS-PAGE gel (section 2.10) were transferred to a Hybond ECL Nitrocellulose membrane (Amersham) to make proteins accessible for specific antibody detection. The layering of the membrane and gel was done as shown in Figure 7.

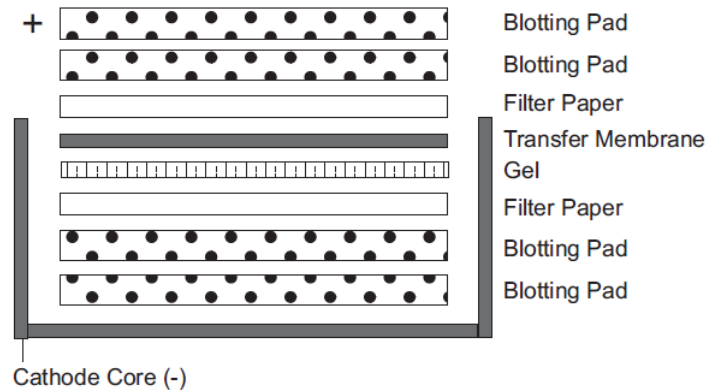


**Figure 7. Western blot gel membrane assembly.**

Figure taken from X Cell Blot Module available online from [https://tools.lifetechnologies.com/content/sfs/manuals/blotmod\\_pro.pdf](https://tools.lifetechnologies.com/content/sfs/manuals/blotmod_pro.pdf) (Catalog no. EI9051, Invitrogen).

This gel-membrane stack was placed in X Cell II Blot module tank (Invitrogen) filled with transfer buffer (25 mM Tris-HCl, pH 7.6 containing 192 mM glycine, 10% methanol and 0.03% SDS). The proteins were transferred to the nitrocellulose membrane at 30 V for 60 minutes. After transfer, the membrane was rinsed briefly with wash buffer (phosphate buffered saline (PBS) containing 0.05% Tween 20) and blocked overnight in gentle agitation at 4°C with blocking buffer (PBS containing 1% BSA). The membrane was then incubated in gentle agitation for 2 hours at room temperature with primary antibody for HMGB1 (Mouse  $\alpha$ -HMGB1 (Abnova) with a final concentration of 1  $\mu$ g/ml in blocking buffer). The membrane was washed 3 times with wash buffer, 5 minutes per wash. Subsequently, the membrane was incubated in gentle agitation for 2 hours at room temperature with secondary antibody for HMGB1 (Goat  $\alpha$ -mouse, Alkaline Phosphatase conjugated (Jackson), with a final concentration of 0.25  $\mu$ g/ml in blocking buffer). The membrane was washed 3 times with wash buffer, 5 minutes per wash, followed by staining for 5-10 minutes with 10 ml of staining solution. The staining solution consist of

AP color development buffer (100 mM Tris-HCl, pH 9.5 containing 9.8 mM MgCl<sub>2</sub>), mixed with 1% AP color reagent A (MgCl<sub>2</sub> with nitroblue tetrazolium in aqueous dimethylformamide (DMF)) and 1% AP color reagent B (5-bromo-4-chloro-3-indolyl phosphate in DMF). The buffer and its reagents were supplied by Bio-Rad. Once the protein band was visible (8-10 s) the reaction was stopped by adding dH<sub>2</sub>O. The membrane was then dried by leaving it overnight at room temperature.

The procedure was also used for VCC-RAGE, using different primary antibody (Goat  $\alpha$ -mRAGE (R&D Systems) with a final concentration of 0.1  $\mu$ g/ml in blocking buffer) and secondary antibody (Rabbit  $\alpha$ -goat, Alkaline Phosphatase conjugated (Millipore), diluted 1:4000 in blocking buffer).

## **2.12 Circular dichroism**

Prior to all CD experiments in this study, all protein constructs were dialyzed into 10 mM KH<sub>2</sub>PO<sub>4</sub> buffer, pH 7.4, to remove interfering additives. This study used a JASCO J-815 spectropolarimeter and all programs were written with Spectrum Manager software. All runs were performed with standard sensitivity (100 mdeg), data pitch of 1 nm, continuous scanning mode with speed of 100 nm/min, response of 1s and band width of 1 nm. Absorbance was monitored over the range of 260-185 nm. A 1.0 mm pathlength rectangular Spectrosil Quartz cuvette (Starna) was blanked over 5 accumulated scans using 400  $\mu$ l of 10 mM KH<sub>2</sub>PO<sub>4</sub> buffer, pH 7.4. CD measurement of proteins was conducted using the buffer as the diluent, and the CD absorption spectrum was accumulated over 5 scans. The obtained CD profiles were analysed in DichroWeb using reference set 6 which optimized the wavelength range of 185-240 nm and fitted with CONTIN.

### **2.12.1 The secondary structure of HMGB1 and RAGE**

Secondary structure analysis was performed using 2 and 20  $\mu$ M HMGB1 or 28  $\mu$ M RAGE. These concentrations were used to reduce noise and the experiment was performed according to the guidelines detailed above (section 2.12).

### **2.12.2 Reduction and alkylation of HMGB1**

The effect of reducing the disulfide bond with the reducing agent  $\beta$ -mercaptoethanol and of alkylating the free thiol group with iodoacetamide on the HMGB1 construct was determined by observing changes to the secondary structure change of the proteins. For the  $\beta$ -mercaptoethanol assay, three aliquots of proteins were prepared and different



concentrations of  $\beta$ -mercaptoethanol were added to each aliquot. The final working concentrations of  $\beta$ -mercaptoethanol used were 1 mM, 5 mM and 10 mM, respectively. The samples were incubated for 1 hour on ice before measurements in the spectropolarimeter. The CD spectra obtained for each concentration was then blank-subtracted. The blank consist of 10 mM  $\text{KH}_2\text{PO}_4$ , pH 7.4 with the respective  $\beta$ -mercaptoethanol concentration. The similar treatment, including the blank-subtraction, was also performed for samples treated with different concentrations of iodoacetamide. The final working concentrations for the iodoacetamide assay were 0.5 mM, 1 mM and 5 mM.

### **2.13 Surface Plasmon Resonance (SPR)**

All experiments were carried out at 25°C using flow rate of 30  $\mu\text{l}/\text{min}$ , an association time of 120s, a dissociation time of 200s, with multi cycle kinetics unless otherwise stated. Regeneration of the chip was carried out by injection of 10 mM NaOH for 30s with a flow rate of 30  $\mu\text{l}/\text{min}$ . The results were analyzed in Biacore T200 analysis software with a steady state affinity approach, a 1:1 Langmuir kinetic binding model, or a dimer/tetramer model (as outlined in section 2.13.3) to obtain all binding constants and measurements of the quality of the fit. The goodness of fit of the models can be determined by several ways. First way is by visual inspection of the fittings. Ideally, the experimental sensorgram should overlay with the fitting model, instead of overlapping. Second way is by looking at the residuals, i.e. the differences between experimental values and fitted values for each data points in the sensorgrams. A perfect fit will have residuals which scatter around 0 RU. A residual which shows a systematic deviations from the axis of 0 RU indicates that a fitting model may not be suitable for a particular experimental sensorgram. A deviation within +/- 10 RU is still considered to be acceptable (Healthcare, 2010). The third way is the inspection of the  $\text{Chi}^2$  value which is measured as percentage of the maximal response ( $R_{\text{max}}$ ) of each sensorgram, which is related to the residual value. The value of the  $\text{Chi}^2$  should preferably fall within a percent or so of  $R_{\text{max}}$  (Healthcare, 2010). The fourth is inspection of the U-value which estimates the uniqueness of the rate constants  $k_a$ ,  $k_d$  and  $R_{\text{max}}$ . The rate constants can not be uniquely determined when there is a significant correlation between the pairs of the parameters. The parameters are said to be correlated when it is possible to determine a value from a combined function of more than two parameters without being able to determine unique values for individual parameters. The

significant correlation between parameters is indicated by the U-value of above 25 (Healthcare, 2010). Choosing an appropriate fitting model to determine the binding constants of an interaction is important because mismatch between the experimental data and the fitted model will lead to difficulties in determining the binding affinity constants and/or significant errors in their estimation.

### **2.13.1 Coupling of HMGB1 to sensor chips**

The dextran matrix of the CM5 sensor chip (GE Healthcare) was activated with 0.05 M N-hydroxysuccinimide (NHS) and 0.2 M 1-ethyl-3-(3-dimethylaminopropyl)carbodiimide (EDC), which form NHS-esters, prior to the immobilization of HMGB1 to the sensor chip. Upon contact with the ligands, in this case HMGB1, the NHS-esters react with the amine groups on the ligand (Healthcare, 2008b). HMGB1 was diluted to a final concentration of 50 nM in 10 mM sodium acetate buffer, pH 4.5. It was then coupled to the dextran matrix of the gold surface of a flow cell on the sensor chip by flowing the 50 nM HMGB1 with a flow buffer that consists of 10 mM HEPES, pH 7.4 containing 150 mM NaCl, 3 mM EDTA, 0.05% (v/v) Tween 20, 0.5 mM  $\beta$ -mercaptoethanol and 0.1% (w/v) BSA. The rest of the dextran matrix which did not bind HMGB1 was deactivated with 1M ethanolamine, pH 8.5 (Healthcare, 2008b). The amount of HMGB1 immobilized was determined to be 180 Resonance Units (RU). A control surface was prepared by activating the dextran matrix over a second flow cell with NHS and EDC and subsequently deactivating it with ethanolamine. Correction of all binding curves was done by applying double-referencing, in which the data obtained was first subtracted from the control surface followed by subtraction from the flowing buffer injection cycle.

### **2.13.2 Binding activity of HMGB1 coupled to sensor chips**

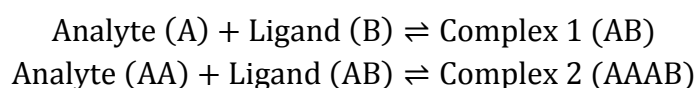
The aliquot of VCC-RAGE was diluted to concentrations of 32 nM, 16 nM, 8 nM, 4 nM and 2 nM with 10 mM HEPES buffer, pH 7.4 containing 133 mM NaCl, 3 mM EDTA, 0.05% (v/v) Tween 20, 0.5 mM  $\beta$ -mercaptoethanol and 0.1% (w/v) BSA, and passed through the 180 RU of immobilized HMGB1.

An aliquot of 100 nM vector pBluescript II SK(-) was mixed with 6 U of topoisomerase I for every 0.6 pmol of the vector. The aliquot was incubated at 37°C for 1 hour in flow buffer 50 mM HEPES, pH 7.4 containing 50 mM KCl, 10 mM MgCl<sub>2</sub>, 0.1 mM EDTA, 0.5 mM DTT and 30  $\mu$ g/ml BSA. Topoisomerase I was used to relax the strand of the pBluescript vector, which may increase the chance of the vector to interact with HMGB1. The DNA aliquot

was then diluted to concentrations of 32 nM, 16 nM, 8 nM, 4 nM and 2 nM with the same buffer so that the flow buffer and the sample buffer were identical, thus minimizing the occurrence of bulk refractive index differences between sample buffer and the flowing buffer. The DNA dilution series were passed through the immobilized HMGB1.

### 2.13.3 Data modelling and analysis

The sensorgrams of the self-association of HMGB1 was fitted with the built-in fitting models in Biacore T200 system. The 1:1 Langmuir model is a recommended default fit for most rate data, as it is the simplest model that defines many molecular interactions by assuming that one ligand molecule couples with one analyte molecule (Healthcare, 2010). Bivalent analyte model simulates one analyte molecule binds one ligand molecule and the resulting complex binds to another ligand (Healthcare, 2010). Heterogenous ligand model describes the interaction between one analyte and two separate ligands. This type of interaction is commonly caused by different attachment orientation of the ligands to the sensor chip surface, and it subsequently enables one analyte molecule to bind two ligand molecules at the same time (Healthcare, 2010). The last model is the two state reactions model which is developed from 1:1 Langmuir model. The first stage of the model algorithm represents formation of an analyte-ligand complex consists of two molecules. The first stage is followed by a second stage which represents the possibility of conformational changes which stabilizes the complex (Healthcare, 2010). In this study, the dimer/tetramer kinetic binding model was developed to better characterize the self-association of HMGB1. It was written using Biacore T200 analysis software. The following equation was used:



The kinetics of the first reaction between Analyte (A) and Ligand (B) were represented by kinetic constants  $k_{a1}$  and  $k_{d1}$  and describes dimer formation. Ideally, the equation should be written as  $A + A = AA$  for dimer formation, and  $AA + AA = AAAA$  for tetramer formation. However, because the command input in the Biacore T200 Analysis Software itself did not enable this type of format, the common symbols, A and B, were used. The second reaction between Analyte AA and Ligand AB represents tetramer formation and the kinetic

constants are  $k_{a2}$  and  $k_{d2}$ . **Table 3** describes the reactants and their specifications as inputted to the software, as well as the details the parameters used to develop the model.

**Table 3. Specification and parameters of dimer/tetramer model setup.**

		Specification		
Reactant	Category	Other specifications/Commands		
A	Analyte	Concentration (Conc), Mass transfer ( $tc \cdot f^{(1/3)}$ )		
B	Ligand	Binding capacity (RMax)		
AA	Analyte	Concentration (Conc), Mass transfer ( $tc \cdot f^{(1/3)}$ )		
AB	Complex	Generate response		
AAAB	Complex	Generate response		
		Parameters		
Name	Value	Type	Initial value/Attach to	Description
$k_{a1}$ (1/Ms)	$k_{a1}$	Fit global	1e5	
$k_{d1}$ (1/s)	$k_{d1}$	Fit global	1e-3	
Rmax (RU)	Rmax	Fit global	YMax	
Conc (M)	Conc	Constant	Concentration (M)	Allow negative value
tc	tc	Fit global	1e8	
Flow ( $\mu$ l/min)	f	Constant	Flow ( $\mu$ l/min)	Allow negative value
RI (RU)	RI	Fit local	YMax/5	Allow negative value
$k_{a2}$ (1/Ms)	$k_{a2}$	Fit global	1e5	
$k_{d2}$ (1/s)	$k_{d2}$	Fit global	1e-3	

#### 2.14 Self-association of HMGB1

To characterise the self-association of HMGB1, a series of concentrations of 8000 nM, 4000 nM, 2000 nM, 1000 nM, 500 nM, 250 nM and 125 nM of analyte HMGB1 were passed through the flow cell with immobilized HMGB1. The buffer used was 10 mM HEPES, pH 7.4 containing 133 mM NaCl, 3 mM EDTA, 0.05% (v/v) Tween 20, 0.5 mM  $\beta$ -

mercaptoethanol and 0.1% (w/v) BSA, which gives a total ionic strength ( $\mu$ ) of 150 mM. The total ionic strength of this buffer matches the physiological ionic strength.

#### **2.14.1 The effect of ionic strength**

The effect of ionic strength on affinity constant for self-interaction of HMGB1 was determined at six different ionic strength concentrations. The flow buffers were made of 10 mM HEPES, pH 7.4 containing 3 mM EDTA, 0.05% (v/v) Tween 20, 0.5 mM  $\beta$ -mercaptoethanol and 0.1% (w/v) BSA with NaCl concentrations of 113 mM, 123 mM, 133 mM, 143 mM, 153 mM or 163 mM. Those NaCl concentrations made total ionic strengths of 130 mM, 140 mM, 150 mM, 160 mM, 170 mM or 180 mM. The total ionic strength was determined by the ionic strength of each components of the buffer, i.e. HEPES, EDTA and NaCl. The analyte HMGB1 were made to final concentration of 25 nM and 3000 nM in each different buffer and ran as triplicates. The stoichiometry was calculated by using this equation: (experimental RMax / immobilized RU) + 1; with the immobilized RU of 180.

#### **2.14.2 The effect of divalent metal ions**

Different physiological metal ion concentrations were used to investigate their effects on self-association properties of HMGB1. Magnesium and calcium were chosen because they are related with the formation of HMGB1 beads in the concentration of 1 mM and 3 mM, respectively (Mathis et al., 1980). The rationale of choosing zinc will be explored in section 4.3.2 of the Discussion chapter. All flow buffers were made without EDTA and with total ionic strength ( $\mu$ ) of 150 mM. The ZnCl<sub>2</sub> buffer was 10 mM HEPES, pH 7.4 containing 5  $\mu$ M ZnCl<sub>2</sub>, 135 mM NaCl, 0.05% (v/v) Tween 20, 0.5 mM  $\beta$ -mercaptoethanol and 0.1% (w/v) BSA. The CaCl<sub>2</sub> buffer was 10 mM HEPES, pH 7.4 containing 2 mM CaCl<sub>2</sub>, 129 mM NaCl, 0.05% (v/v) Tween 20, 0.5 mM  $\beta$ -mercaptoethanol and 0.1% (w/v) BSA. The MgCl<sub>2</sub> buffer was 10 mM HEPES, pH 7.4 containing 1 mM MgCl<sub>2</sub>, 132 mM NaCl, 0.05% (v/v) Tween 20, 0.5 mM  $\beta$ -mercaptoethanol and 0.1% (w/v) BSA. A concentration series of 200 nM, 150 nM, 100 nM, 50 nM and 10 nM of analyte HMGB1 were used in this assay.

#### **2.14.3 The combined effect of zinc and ionic strength**

As a follow up of the ionic strength effect on the HMGB1 self-association, the impact of zinc ions and six different ionic strengths on self-association between the immobilized HMGB1 and a triplicate of 25 nM analyte HMGB1 will be observed. The flow buffers were made of 10 mM HEPES, pH 7.4 containing of 5  $\mu$ M ZnCl<sub>2</sub>, 0.05% (v/v) Tween 20, 0.5 mM

$\beta$ -mercaptoethanol and 0.1% (w/v) Bovine Serum Albumin. This buffer was prepared with NaCl concentrations of 115 mM, 125 mM, 135 mM, 145 mM, 155 mM or 165 mM. The total ionic strength of each of these buffers was 130 mM, 140 mM, 150 mM, 160 mM, 170 mM or 180 mM respectively. The HMGB1 was incubated first in each of these buffers for 1 hour in room temperature.

To investigate whether the zinc effect was real, a series of buffers of different ionic strengths containing both 5  $\mu$ M ZnCl<sub>2</sub> and 3 mM EDTA was prepared. The NaCl concentrations used were 113 mM, 123 mM, 133 mM, 143 mM, 153 mM or 163 mM which made total ionic strengths of 130 mM, 140 mM, 150 mM, 160 mM, 170 mM or 180 mM. These buffers also made of 10 mM HEPES, pH 7.4 containing 0.05% (v/v) Tween 20, 0.5 mM  $\beta$ -mercaptoethanol and 0.1% (w/v) Bovine Serum Albumin.

#### **2.14.4 The effect of redox environment**

To observe if there was any effect of reducing the disulfide bond of the 25 nM analyte HMGB1 on its self-association, five flowing buffers with different  $\beta$ -mercaptoethanol concentrations were used. They were made of 10 mM HEPES, pH 7.4 containing 133 mM NaCl, 3 mM EDTA, 0.05% (v/v) Tween 20 and 0.1% (w/v) BSA with  $\beta$ -mercaptoethanol concentrations of 0 mM, 0.5 mM, 1 mM, 5 mM and 10 mM. HMGB1 was pre-incubated for 1 hour with each buffer to ensure reduction of the disulfide bond.

#### **2.14.5 The effect of pH**

The effect of pH was determined with a triplicate of 25 nM HMGB1 at four different pH values. The ionic strengths of the flow buffers are adjusted to 150 mM in account of the effect of the pH and pKa values. The buffers for pH 4.0, 4.8 and 5.7 were each made of 50 mM sodium acetate containing 3 mM EDTA, 0.05% (v/v) Tween 20, 0.5 mM  $\beta$ -mercaptoethanol and 0.1% BSA, with 139 mM, 119 mM and 102 mM NaCl, respectively. The buffer for pH 7.4 was made of of 10 mM HEPES containing 144 mM NaCl, 3 mM EDTA, 0.05% (v/v) Tween 20, 0.5 mM  $\beta$ -mercaptoethanol and 0.1% BSA.

## 2.15 Thermal Shift Assay

A thermal shift assay was conducted to see whether HMGB1 had the potential to be crystallized<sup>1</sup>. Crystallization of a protein is a complex procedure which is strongly influenced by environmental factors such as pH, ionic strength, additives, protein concentration and temperature. The biochemical and biophysical properties of the protein itself, for example the homogeneity, stability and solubility, are also crucial for crystallization (Ericsson et al., 2006). The more stable a protein is, the more amenable it is for crystallization. The thermal shift assay can be performed in common qPCR machines, and the result curves can be used to determine the melting temperature ( $T_m$ ) of a protein. When certain conditions or components increase the melting temperature, it is also said to stabilize the protein (Phillips and de la Pena, 2011). This assay utilized the SYPRO Orange protein gel stain dye (Invitrogen), which binds to hydrophobic surfaces of the protein. The basis of this method is that the denaturation of a protein can be observed through its exposure to a hydrophobic fluorophore. As the protein starts to denature and unfold due to increasing temperature, the fluorescence signal of the dye increases in response to the exposure of hydrophobic surfaces to the aqueous environment. As such, a real-time detection of the fluorescence emission can be plotted as a function of temperature (Ericsson et al., 2006).

The experiment was carried out with Bio-Rad C1000 Thermal Cycler (Bio-Rad) and the software Bio-Rad CFX Manager version 2.0 was used to write the experimental setup and analyse the result. The 5000x concentrated SYPRO Orange dye was diluted 1:1000 in dH<sub>2</sub>O. The 20  $\mu$ l reaction mixture consisted of 14.5  $\mu$ l test buffer, 0.5  $\mu$ l of 3.6 mg/ml HMGB1 in 10 mM HEPES, pH 7.4 containing 133 mM NaCl, 3 mM EDTA and 5  $\mu$ l of the diluted SYPRO Orange. The dye was always be added immediately before the mixture was loaded on the instrument. Four types of control mixtures were also used in the technique. The first control mixture was a buffer control, which contained 15  $\mu$ l of buffer (10 mM HEPES, pH 7.4 containing 135 mM NaCl, 5  $\mu$ M ZnCl<sub>2</sub> and 0.5 mM  $\beta$ -mercaptoethanol) and 5  $\mu$ l of dye, to confirm whether there was any background noise caused by the additives in the buffer, particularly the zinc ions and  $\beta$ -mercaptoethanol. The second control

---

<sup>1</sup> Thermal shift assays were done in collaboration with Caroline Snowball and Prof. Alice Vriejlink (University of Western Australia).

mixture was a protein control, containing 0.5  $\mu$ l of HMGB1 and 19.5  $\mu$ l of buffer (10 mM HEPES, pH 7.4 containing 135 mM NaCl, 5  $\mu$ M ZnCl<sub>2</sub> and 0.5 mM  $\beta$ -mercaptoethanol) to check whether HMGB1 with buffer generated a signal without the fluorescence dye. The third control mixture consisted of 0.5  $\mu$ l of HMGB1 with the 10 mM HEPES, pH 7.4 containing 133 mM NaCl and 3 mM EDTA, to ascertain if the combination of the HMGB1 and the dye without zinc and  $\beta$ -mercaptoethanol would give a fluorescence signal. The fourth control mixture was a positive control, which contained 19.5  $\mu$ l buffer and 0.5  $\mu$ l of protein LptA, to determine if the protein gave signal with the dye. The protein LptA generally works in the thermal shift assay as positive control. All reactions were mixed in PCR microtubes.

There were four buffers used in this experiment which would allow comparison of results in the presence or absence of ZnCl<sub>2</sub> and/or  $\beta$ -mercaptoethanol. The first buffer was 10 mM HEPES, pH 7.4 containing 133 mM NaCl, 3 mM EDTA and 0.5 mM  $\beta$ -mercaptoethanol. The second buffer was 10 mM HEPES, pH 7.4 containing 135 mM NaCl, 5  $\mu$ M ZnCl<sub>2</sub> and 0.5 mM  $\beta$ -mercaptoethanol. The third buffer was 10 mM HEPES, pH 7.4 containing 133 mM NaCl and 3 mM EDTA, and the fourth buffer was 10 mM HEPES, pH 7.4 containing 135 mM NaCl and 5  $\mu$ M ZnCl<sub>2</sub>. The experiment setup started with initial cycle of 5°C for 30s, then continued with temperature increases from 5°C to 95°C in 0.5 degree increments over 30s and this gave a total cycle time of about 90 minutes. The last cycle was 95°C for 30s. The fluorescence signal was detected with five different emission wavelengths, but the HEX dye wavelength (535-556 nm) provided the most fitting detection in this study.



### **3 RESULTS**

### **3.1 Amplification and expression of HMGB1 and VCC-RAGE**

A synthetic human HMGB1 construct was sub-cloned into a pGS-21a vector, which was then used to transform chemically competent T7 Shuffle K *E.coli* cells. Colonies containing the synthetic human HMGB1 gene insert were then indentified by PCR. A single band with the expected size of about 470 bp was observed for each of the four transformed colonies (Figure 8). The human VCC-RAGE domain construct, which does not contain the transmembrane domain, was also sub-cloned into a pGS-21a vector and then used to transform chemically competent TOP10 *E.coli* cells. Colonies containing the synthetic VCC-RAGE gene insert were then indentified by PCR. A single band with the expected size of about 1150 bp was obtained for four out of five transformed colonies (Figure 9). A 30 kDa band, correlating with the expected size of full length HMGB1, was observed on SDS-PAGE following induction of the *E.coli* cells (Figure 10). Similarly, a band of about 40 kDa correlating with the expected size of full length VCC-RAGE was observed on SDS-PAGE following induction of the *E.coli* cells (Figure 10).

### **3.2 Purification of HMGB1 and VCC-RAGE**

#### **3.2.1 Purification of HMGB1**

Prior to column chromatography, the soluble fraction of *E.coli* cells was treated with trichloroacetic acid according to section 2.8 in the Methods chapter, which appeared to remove most of the contaminant proteins, as indicated in Figure 11a. The result of heparin purification for recombinant HMGB1 is shown in Figure 12. HMGB1 was eluted as one peak at the end of the linear gradient, indicating that 1 M NaCl was needed to elute HMGB1 from the heparin column. SDS-PAGE was used to determine the fractions containing HMGB1. These fractions were pooled and analysed by size exclusion chromatography, as shown in Figure 13. The recombinant HMGB1 was eluted as a single peak, which indicated that the protein was monocomponent. To verify the size of the HMGB1 protein and whether its purity was sufficient for further studies, a fraction from each purification step was collected and loaded into a SDS-PAGE gel and stained with Coomassie stain, as outlined in section 2.10 in the Methods chapter. HMGB1 was expressed in its correct size and reached a level of purity of 95 %, i.e. the target protein constitutes approximately 95% of the total protein yield, with a concentration of about 0.8-1 mg/ml (Figure 11).

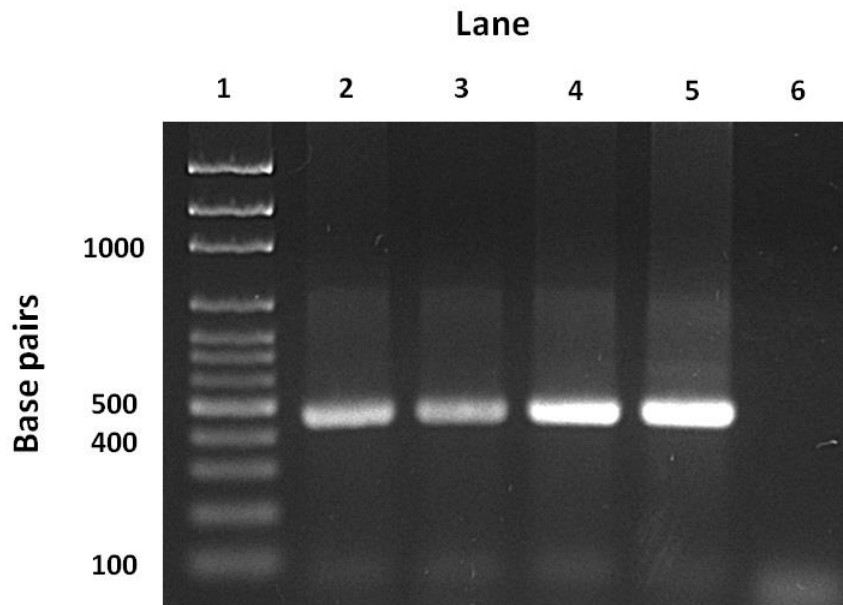


**Figure 8. Whole-cell PCR amplification of full length HMGB1.**

The HMGB1 insert gene was amplified with PCR and visualised as outlined in Methods chapter 2, section 2.4 and section 2.5, respectively. PCR products from reaction mixtures with pGS-21a-HMGB1 as template were loaded into lanes 2, 3, 4, and 5. A negative control sample was loaded into lane 6. A 100 bp ladder was loaded into lane 1.

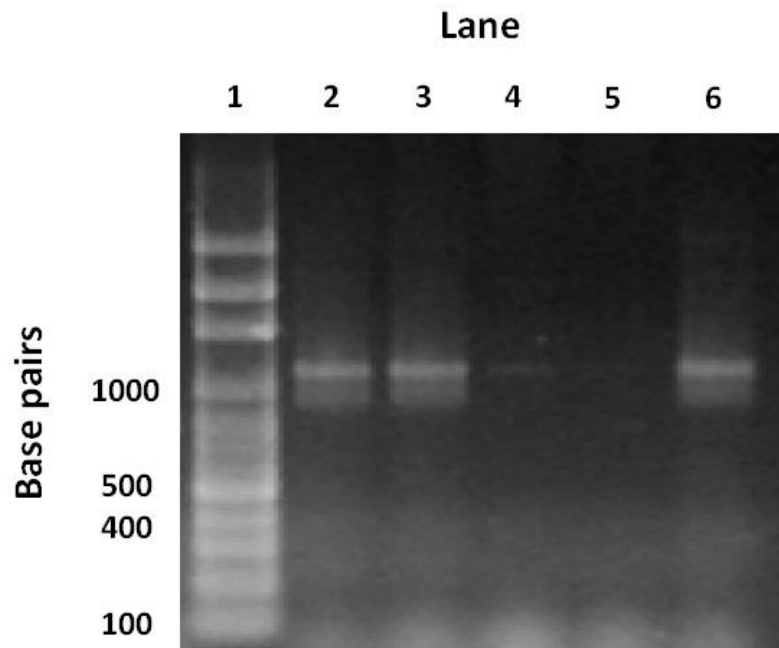


**Figure 9. Whole-cell PCR amplification of VCC-RAGE.**

The VCC-RAGE insert gene was amplified with PCR and visualised as outlined in Methods chapter 2, section 2.4 and section 2.5, respectively. PCR products from reaction mixtures with pGS-21a-VCC RAGE as template were loaded into lanes 2, 3, 4, 5, and 6. A broad range ladder marker was loaded into lane 1 (done in collaboration with Dr. David Chandler).

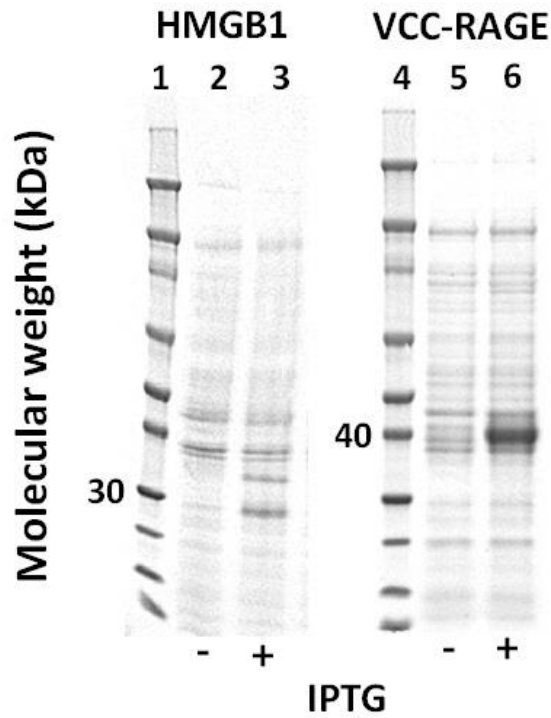


**Figure 10. Induction of the expression of HMGB1 and VCC-RAGE.**

Protein constructs expressed in *E.coli*, after induction by isopropyl  $\beta$ -D-1-thiogalactopyranoside (IPTG) as described in the Methods chapter (section 2.6), were run on a SDS-PAGE gel stained with Coomassie (section 2.10). The lanes with (+) sign correspond to the induced proteins and the lanes with the (-) sign correspond to the uninduced proteins. Protein molecular weight markers are shown in lanes 1 and 4.

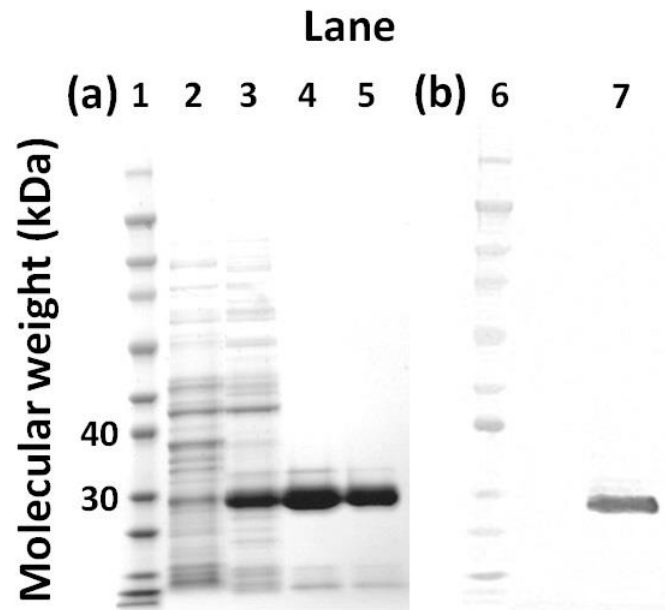


**Figure 11.(a) SDS-PAGE and (b) Western blot of HMGB1.**

In SDS-PAGE (a), lanes 1 and 6 contained protein molecular weight markers. Lane 2 contained the soluble crude fraction after sonication. Lane 3 contained HMGB1 after trichloroacetic acid precipitation. Lane 4 contained pooled HMGB1 fractions from heparin chromatography purification. Lane 5 contained the HMGB1 fractions from size exclusion chromatography. In the Western Blot (b), lane 7 shows the total HMGB1 obtained after size exclusion chromatography, which was identified by a specific antibody against HMGB1 (section 2.11).

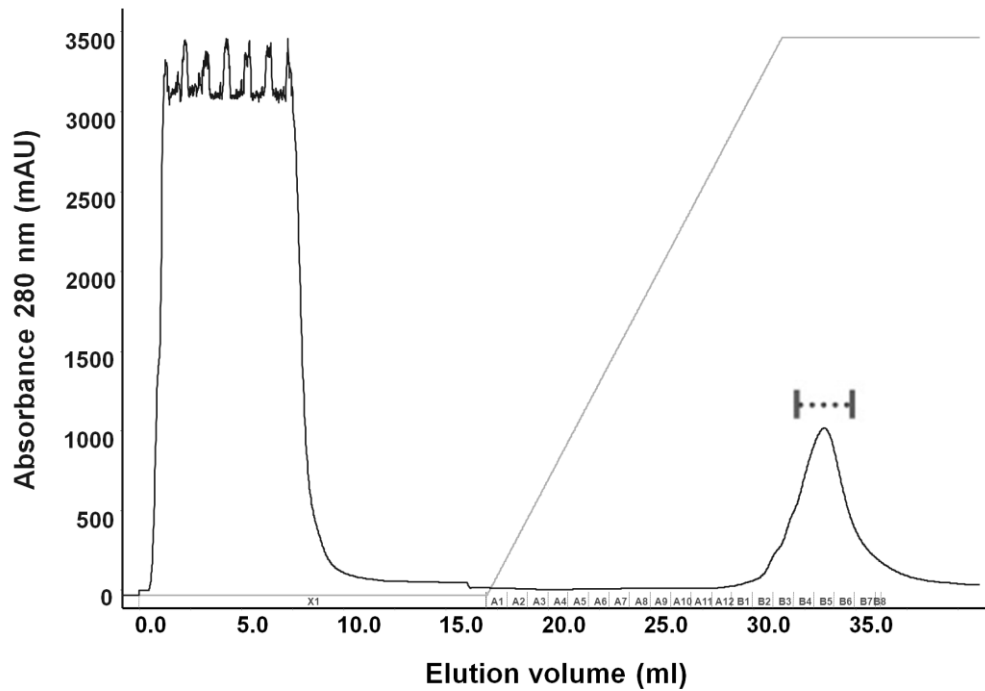


**Figure 12. HiTrap Heparin HP purification of HMGB1.**

The soluble fraction of HMGB1 was obtained by sonicating the *E.coli* cells and subsequently treating them with 2% trichloroacetic acid (Methods chapter, sections 2.7 and 2.8), followed by elution through a HiTrap Heparin HP column (GE Healthcare), as outlined in section 2.9.1. The HMGB1 fractions, marked by the dashed line, were confirmed by SDS-PAGE and subsequently analysed by size exclusion chromatography.

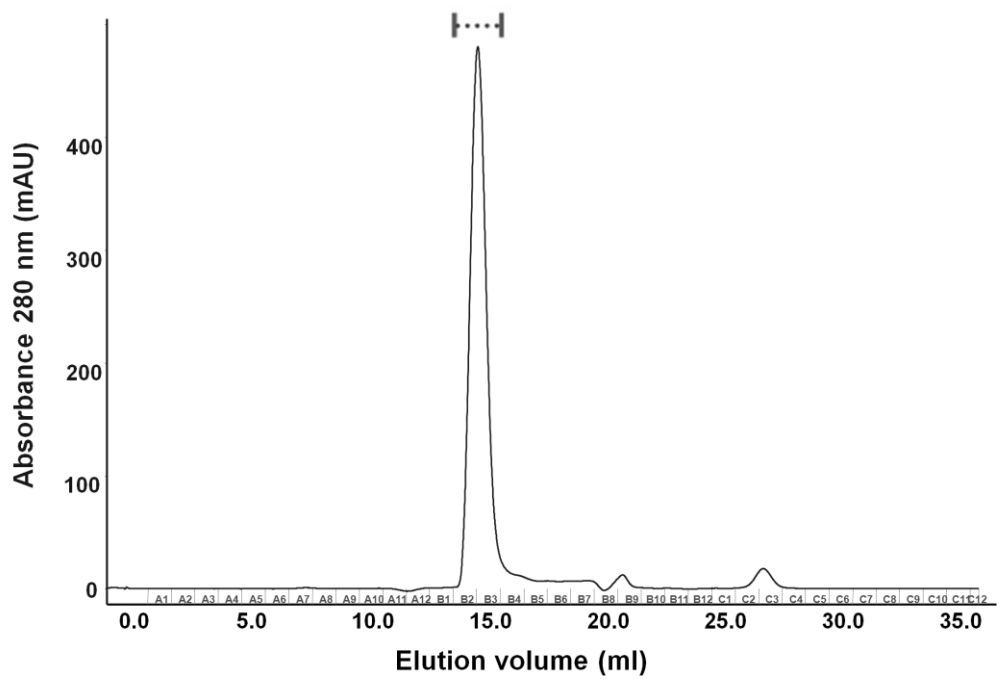


**Figure 13.** Superdex 200 10/300 GL chromatography of HMGB1.

The chromatography procedure is detailed in the Methods chapter, section 2.9.2. HMGB1 was eluted as a single peak. SDS-PAGE and Western blot confirmed that the fractions indicated by the dashed line contained HMGB1. These fractions were subsequently taken for final confirmation by Western Blot.



### **3.2.2 Purification of VCC-RAGE**

The VCC-RAGE was purified by heparin chromatography (Figure 14) and mainly eluted in the second peak during the isocratic gradient comprising 1 M NaCl. The pooled fractions containing VCC-RAGE was then purified by size exclusion chromatography. The elution profile is shown in Figure 15. The protein was eluted as a single peak with few minor peaks, which indicates that the protein was monocomponent. To verify whether the VCC-RAGE protein had the correct size with sufficient purity, a fraction from each purification step was loaded into Coomassie stained SDS-PAGE gel. Figure 16 shows that VCC-RAGE in both SDS-PAGE and Western Blot was expressed in the correct size with 90% purity, and an approximate concentration of 0.3-0.5 mg/ml, measured with Direct Detect (Millipore).

### **3.3 Secondary structure of HMGB1 determined by circular dichroism**

#### **3.3.1 HMGB1 and its cysteine residues**

The structure of HMGB1 represents a complex arrangement of two box-like domains and a highly unstructured acidic tail. The circular dichroism (CD) spectrum of purified recombinant HMGB1 is shown in Figure 17. Estimation of the secondary structure content showed that purified HMGB1 was dominated by  $\alpha$ -helical structure (37%), followed by 29% unordered structure, 19% turns and 16%  $\beta$ -sheet. The associated normalized root-mean-square deviation (NRMSD) value of 0.075 indicates that the error in fitting the experimental spectrum was fairly small. As indicated in Appendix D, section 6.4, an NRMSD value of 0 indicates a perfect fit whilst a value above 0.25 indicates error. Reduction of the disulfide bond with increasing concentration of  $\beta$ -mercaptoethanol was shown to affect the secondary structure of HMGB1 (Figure 18). Addition of 1 mM  $\beta$ -mercaptoethanol caused only a slight change of the secondary structure, but addition of 5 and 10 mM  $\beta$ -mercaptoethanol caused a large change in secondary structure.

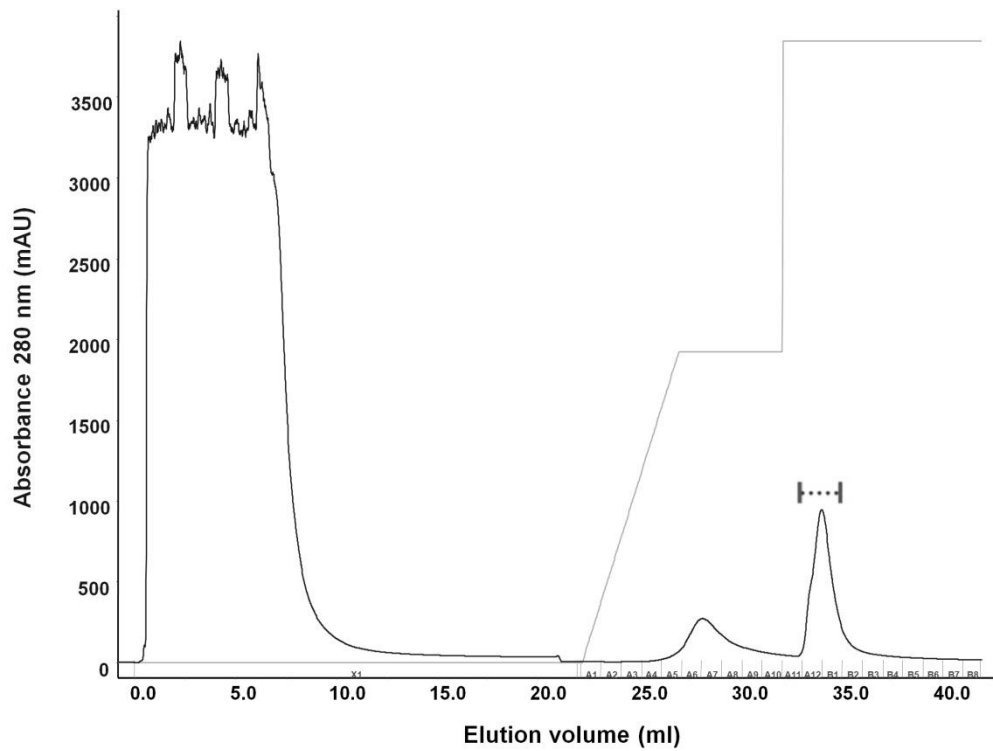


**Figure 14. HiTrap Heparin HP purification of VCC-RAGE.**

The soluble fraction of VCC-RAGE was passed through a HiTrap Heparin HP column (GE Healthcare). The VCC-RAGE fractions marked by the dashed lines were confirmed to contain VCC-RAGE by SDS-PAGE.

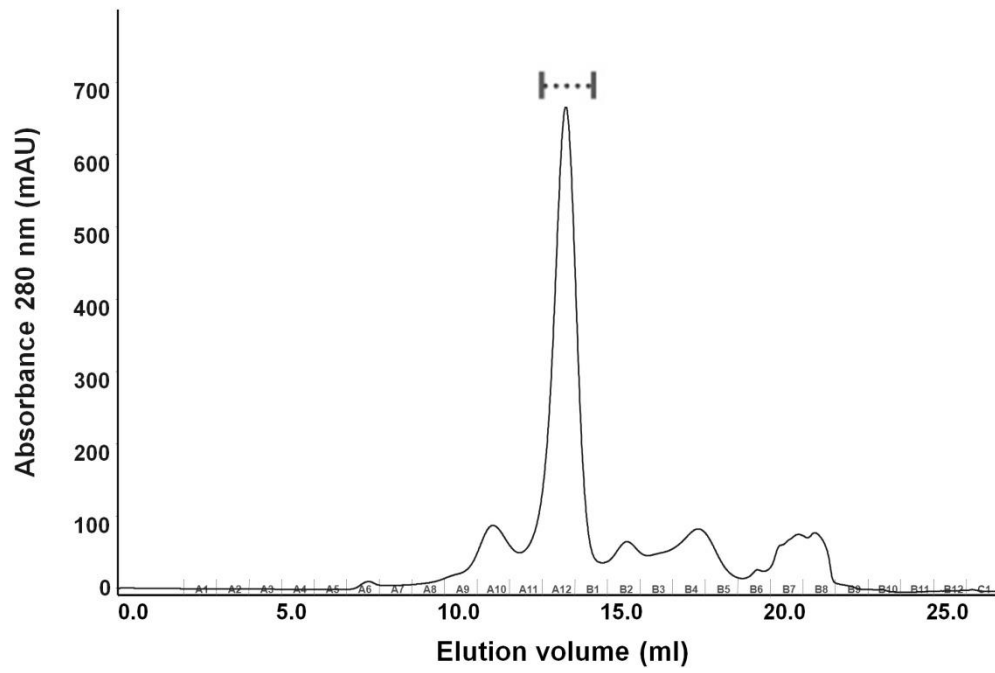


**Figure 15.** Superdex 200 10/300 GL chromatography of VCC-RAGE.

The VCC-RAGE domain construct was eluted as a single peak from the size exclusion chromatography column. Fractions containing VCC-RAGE, indicated by the dotted line, were confirmed by SDS-PAGE.

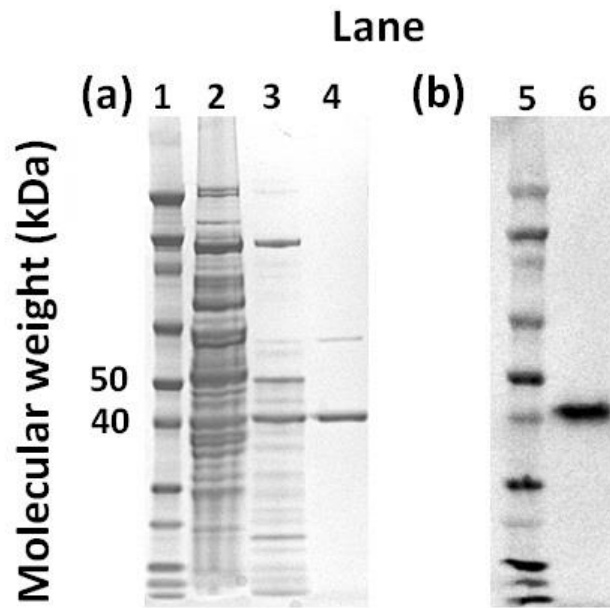


**Figure 16.(a) SDS-PAGE and (b) Western blot of VCC-RAGE.**

In SDS-PAGE (a), a protein ladder marker was loaded into lanes 1 and 5. Lane 2 contains the soluble crude fraction with VCC-RAGE after sonication. Lane 3 contained the VCC-RAGE fraction after heparin chromatography purification. Lane 4 contained the VCC-RAGE fraction after separation with size exclusion chromatography. Lane 6 of the Western Blot (b) shows the total VCC-RAGE obtained after purification.

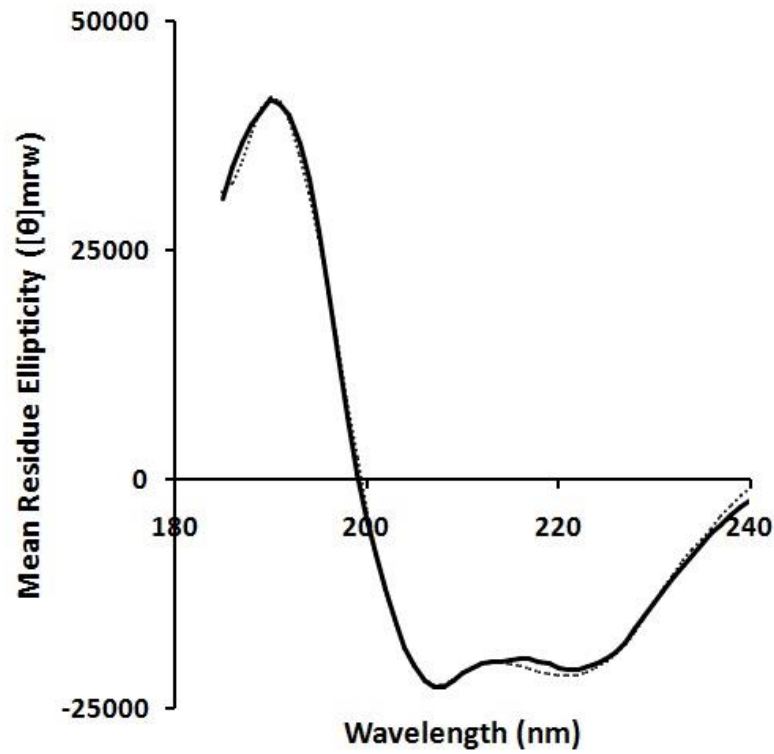


**Figure 17.** Circular dichroism profile of HMGB1.

The percentage of secondary structure of purified recombinant HMGB1 was determined by circular dichroism and analysed with DichroWeb, as explained in the Methods chapter, section 2.12.1. The experimentally determined spectrum, represented by the bold line, appears to match quite well the model fitted by CONTIN, represented by the dotted line. This close fit was indicated by a normalized root-mean-square deviation (NRMSD) value of 0.075. NRMSD take values between 0 and 1, with smaller NRMSD values representing a tighter fit.

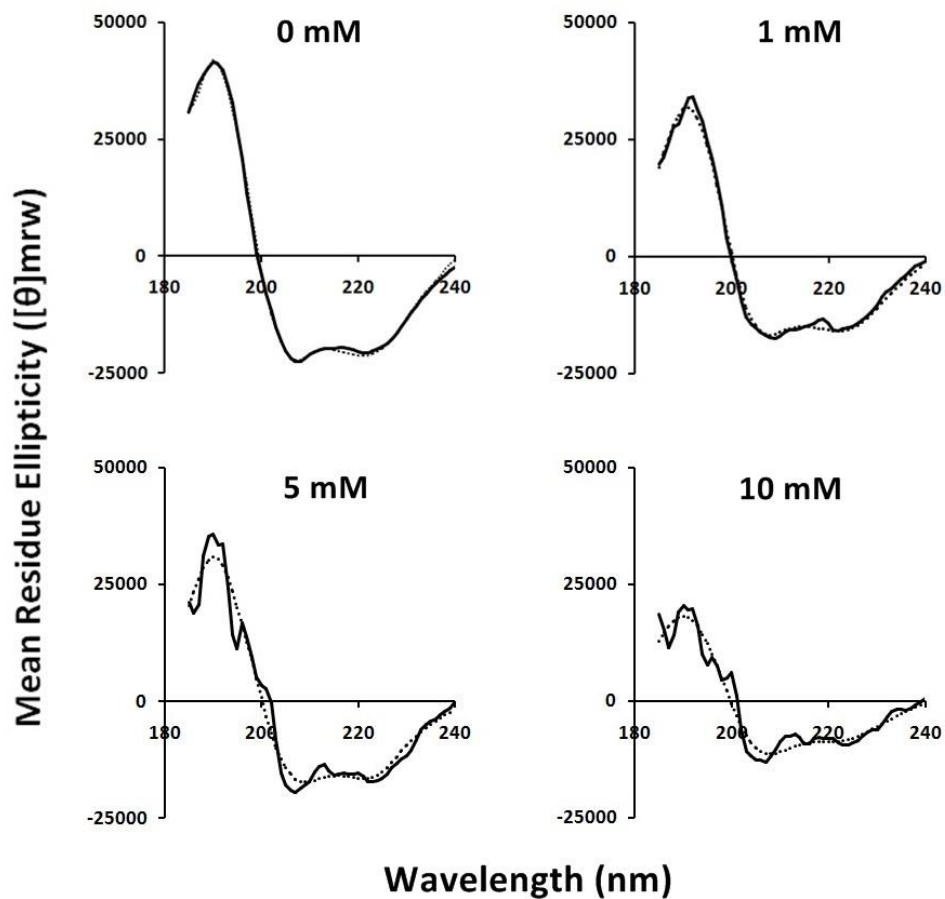


**Figure 18.** CD spectra of HMGB1 treated with  $\beta$ -mercaptoethanol.

Three aliquots of HMGB1 were treated with different concentrations of  $\beta$ -mercaptoethanol, from 1 to 10 mM, as described in the Methods chapter, section 2.12.2, and were compared to untreated HMGB1 at 0 mM  $\beta$ -mercaptoethanol. The experimentally-determined spectrum is represented by the bold line, whereas the CONTIN fit is represented by the dotted line.

It was not possible to determine reliably the percentages of secondary structure upon addition of  $\beta$ -mercaptoethanol due to the noise in the data, however, the plots in Figure 18 show significant decrease of mean residue ellipticity, especially the scales for the peak around 193 nm and the dips around 208 and 222 nm, along with the increase of  $\beta$ -mercaptoethanol concentration. This qualitatively indicated a loss of  $\alpha$ -helical content within the protein structure.

Figure 19 shows that alkylation of the free cysteine residue of HMGB1 with increasing concentration of iodoacetamide appeared to alter the secondary structure of the protein, relative to untreated HMGB1 (0 mM iodoacetamide). Addition of as little as 0.5 mM iodoacetamide resulted in a visible change in the CD profile. It was again not possible to determine reliably the percentages of secondary structure contents due to the noise in the data. But similarly with the CD spectra of different  $\beta$ -mercaptoethanol concentrations, the plots in Figure 19 indicated a clear loss of  $\alpha$ -helical content of the structure. This was shown by a significant decrease of mean residue ellipticity when the concentration of iodoacetamide increased, especially the scales for the peak around 193 nm and the dips around 208 and 222 nm. Compared with the CD spectra of  $\beta$ -mercaptoethanol experiment, the loss of secondary structure was more significant after treatment with iodoacetamide.

### **3.3.2 VCC RAGE secondary structure**

The structure of VCC-RAGE consists of three immunoglobulin(Ig)-like domains, which require correct folding. Although the purified VCC-RAGE construct appears to have a significant portion of unordered structure (43%),  $\alpha$ -helix (24%) is the predominant secondary structure, followed by 20% turns and 13%  $\beta$ -sheet (Figure 20). A normalized root-mean-square deviation (NRMSD) value of 0.098 indicated that the error in fitting the experimental spectrum was small.

### **3.4 Optimization of surface plasmon resonance (SPR)**

In the absence of bovine serum albumin (BSA) in the Biacore running buffer, the interaction between VCC-RAGE and HMGB1 could be clearly and reproducibly observed (Figure 21a) at concentrations of the VCC-RAGE analyte above 10  $\mu$ M. However, no response was observed following dilution of the VCC-RAGE analyte to below 10  $\mu$ M.

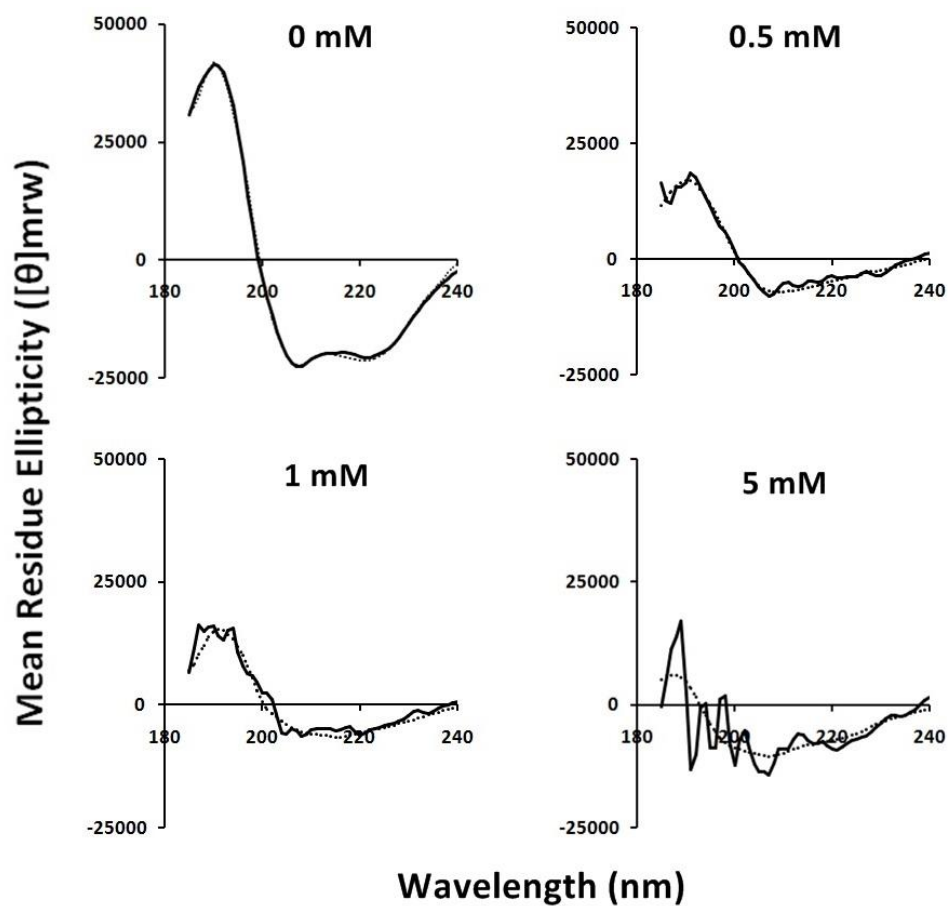


**Figure 19.** CD spectra of HMGB1 treated with iodoacetamide.

HMGB1 aliquots were treated with increasing concentrations of iodoacetamide, from 0.5 to 5 mM, as described in the Methods chapter, section 2.12.2. The bold line and the dotted line represent the experimentally-determined spectrum and the CONTIN fit, respectively.



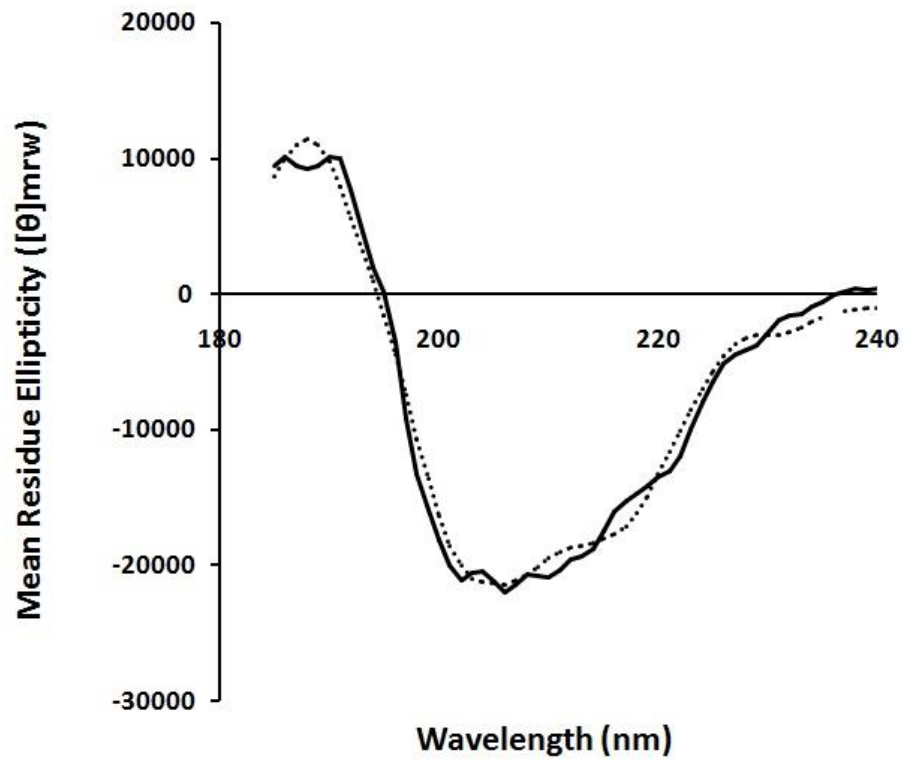


**Figure 20.** CD spectrum of VCC-RAGE.

The percentage of secondary structure of the purified VCC-RAGE construct was determined by CD and analysed with DichroWeb, as outlined in the Methods chapter, section 2.12.1. The experimentally-determined spectrum is represented by the bold line and the CONTIN fit is represented by the dotted line. The tightness of fit was indicated by a normalized root-mean-square deviation (NRMSD) value of 0.098.

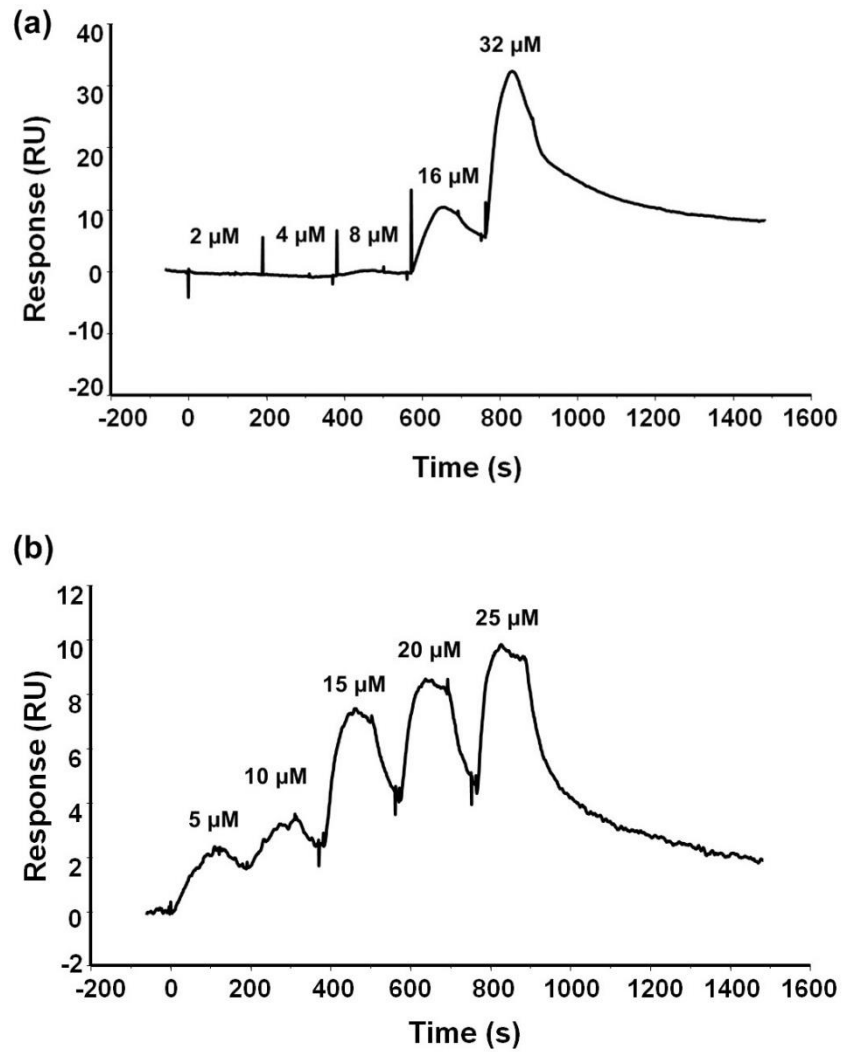


**Figure 21. Optimization of SPR experiments.**

SPR experiments involved injecting different concentrations of VCC-RAGE over the immobilized HMGB1 (see Chapter 2, section 2.13.1. Sensorgram (a) shows the typical profile obtained when using buffer without 0.1% BSA. Sensorgram (b) shows the profiles after using buffer with 0.1% BSA, which helped to retain the signal when low concentrations of VCC-RAGE were used. All the optimization steps were done with the single cycle kinetics (SCK) analysis method (Appendix E, section 6.5).

This observation was highly reproducible. This was not due to the inability of the instrument to detect a low response, as the Biacore T200 can detect the signal down to 0.1 RU. The addition of 0.1% of BSA in the SPR running buffer prevented the apparent loss of signal at concentrations of VCC-RAGE below 10  $\mu$ M (Figure 21b). Whilst the addition of BSA in the running buffer circumvented the loss of SPR signal at lower VCC-RAGE concentrations, visible dips in the sensorgrams were reproducibly observed at the end of the association phases, prior to the dissociation phases (Figure 21b). Such dips would lead to poor data fitting and modelling. Re-purification of the VCC-RAGE and HMGB1 by size exclusion chromatography, immediately prior to immobilization on the sensor chip, was found to be essential to circumvent this problem. As shown in Figure 22, the SPR sensorgrams were highlighted by typical association/dissociation phases, free of dips and spikes, down to nanomolar concentration of VCC-RAGE when the experiment was conducted after the re-purification step<sup>2</sup>.

### 3.5 Binding activity of purified recombinant HMGB1

The biological activity of the HMGB1 immobilized to a CM5 sensor chip was evaluated by assessing its ability to bind either VCC-RAGE (Figure 22) or DNA (Figure 23). VCC-RAGE clearly interacted with the HMGB1 in a concentration dependent manner (Figure 22). A 1:1 Langmuir model did not fit the data particularly well (data not shown), probably because the interaction is more complex than a simple 1:1 interaction, as will be elaborated in section 4.6 of Discussion chapter. A two-state reaction model did provide a better fit with a small residual value, as shown in Figure 22. The affinity of the interaction of VCC-RAGE and HMGB1 was estimated to be 54 nM. The  $K_D$  in all experiments are obtained from the ratio of  $k_d/k_a$  (dissociation rate/association rate), which was automatically calculated by the Biacore T200 software. In this case, the  $k_d$  was 0.035 and the  $k_a$  was  $6.5 \times 10^5$ , resulting in a  $K_D$  value of 54 nM. Plasmid DNA pBluescript II SK(-) also bound HMGB1 with high affinity in a concentration dependent manner, but was well

---

<sup>2</sup> Single cycle kinetics sensorgrams shown in **Error! Reference source not found.** enables convenient optimization steps as they avoid multiple regeneration cycles. The multi cycle kinetics shown in Figure 22 enables a more critical evaluation of the data. Appendix E (section 6.5) further details the theory and background for single cycle and multi cycle kinetics.

fitted using a 1:1 Langmuir model (Figure 23). The affinity of interaction ( $K_D$ ) was estimated to be 3.1 pM.

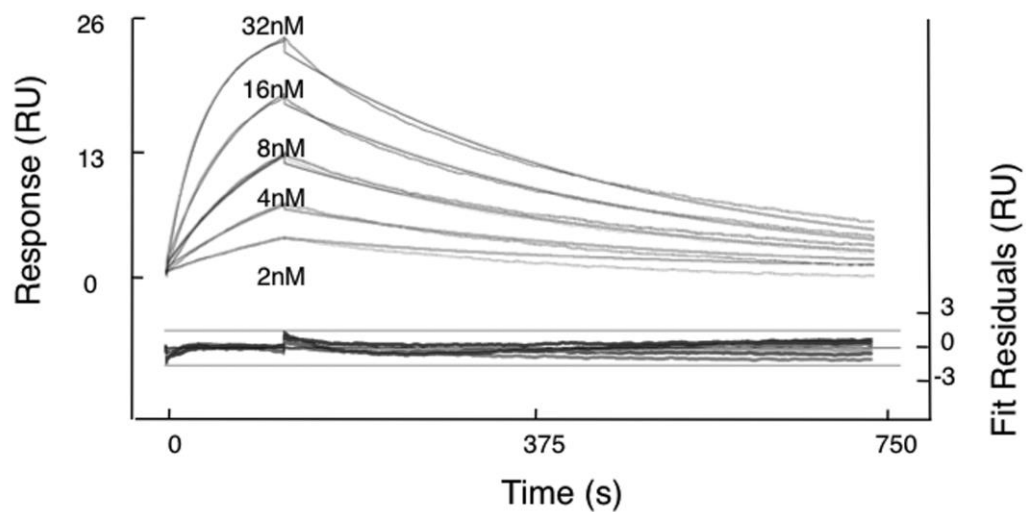


**Figure 22. Multi cycle kinetics (MCK) of the interaction of HMGB1 with VCC-RAGE.**

VCC-RAGE was cycled over HMGB1 on a CM5 chip. The sensorgram was fitted with a two-state reaction model, giving a nanomolar interaction affinity. The assay was carried out as outlined in the Methods chapter, section 2.13.2.

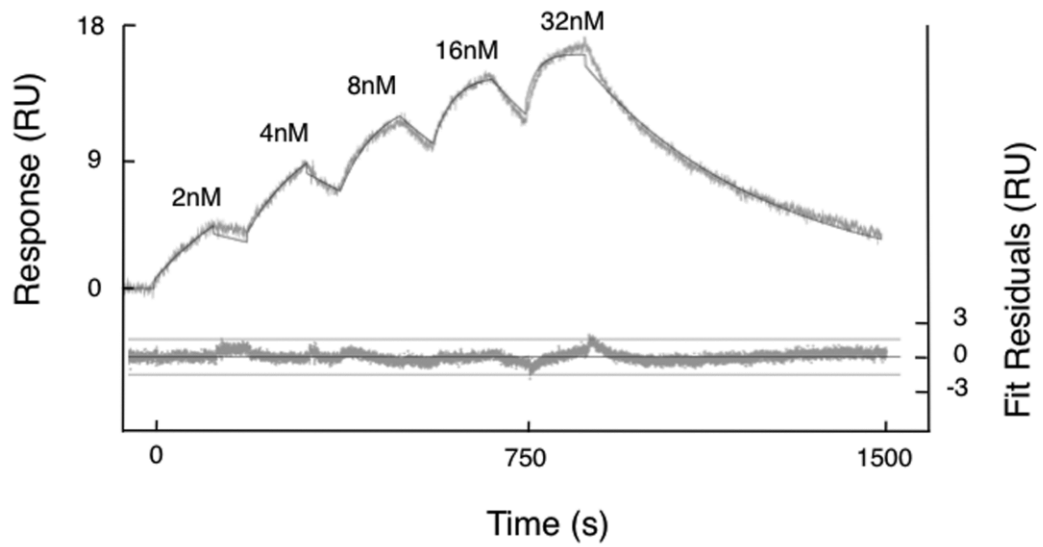


**Figure 23.**Single cycle kinetics (SCK) of the interaction of HMGB1 with pBluescript II SK(-).

The plasmid DNA pBluescript II SK(-) with concentrations from 2 to 32 nM was shown to interact with HMGB1 on the CM5 chip. The sensorgram was fitted with a 1:1 Langmuir model.

### 3.6 The self-association of HMGB1

HMGB1 interacted with itself in a specific manner at the sensor chip surface. The binding constants over a broad range of HMGB1 analyte concentrations were analysed using multi cycle kinetics (Figure 24a) and a steady state affinity approach (Figure 24b). The equilibrium dissociation constant  $K_D$  was estimated to be approximately 2  $\mu\text{M}$ . However, this is not an accurate estimation of the affinity of the interaction. It is evident from the visual inspection of sensorgram Figure 24a, that the fits of the dissociation phases are poor, which will lead to inaccuracy in estimation of the dissociation rate, that subsequently will affect the determination of the affinity constant. Thus, different models were fitted to the data as illustrated in Figure 25 and Figure 26. There were no large differences in the fits between the various models to the association phases (Figure 25), however, the two-state reactions model and the two self-association models seemed to fit the data best across the different concentration range. More complex models than the 1:1 Langmuir model clearly provided better fits to the dissociation phase of the data (Figure 26). Two fitting models were developed and considered in order to better analyse the kinetic constants. The first model is the custom built self-association dimer/tetramer model (Methods chapter, section 2.13.3), and the second is the dimer/trimer/tetramer model, which was developed in collaboration with GE Healthcare in Sweden. Figure 25 and Figure 26 indicates that the dimer/trimer/tetramer and dimer/tetramer models appear to give better fits compared to the other fits. However, it is recommended to choose a fitting model which has fewer fitting parameters to avoid over-fitting of the sensorgrams (Rich and Myszka, 2008), which further supports the choice of the dimer/tetramer model over the dimer/trimer/tetramer model.

The goodness of fit of the dimer/tetramer model was evaluated for HMGB1 across different concentrations and ionic strength. Examination of the parameters describing the goodness of fit, the U-values and  $\text{Chi}^2$  values, showed that the U-values exceeded 25 for most of the Langmuir fits, as highlighted in Figure 27a, to the data generated at different ionic strength and concentration of HMGB1. A U-value greater than 25 suggests that the parameters cannot be independently determined, as previously explained in Methods chapter, section 2.13. The  $\text{Chi}^2$  value was as much as 4-8% for most of the measurements when the 1:1 Langmuir fit was applied to the data (Figure 27b).

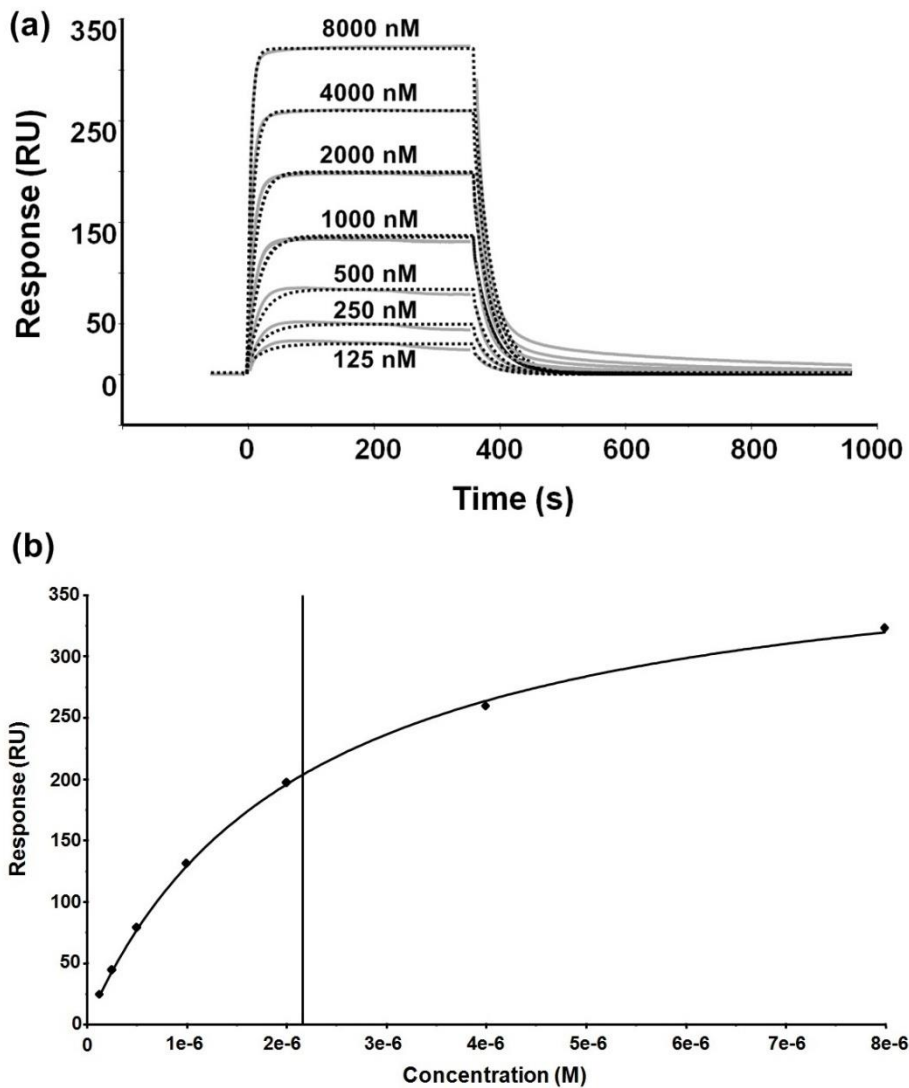


**Figure 24. Self-association of HMGB1 analyzed by (a) multi cycle kinetics and (b) steady state affinity.**

All self-association assays were performed according to the Methods chapter, section 2.13.3. The binding constants between immobilized and analyte HMGB1 for a range of HMGB1 concentrations were characterized by fitting the experimental data of the multi cycle kinetics assay (a) with a 1:1 Langmuir model. The steady state affinity curve (b) was derived from the multi cycle kinetics plot (a). The data points in the steady state curve were the end points of equilibrium phases of the seven sensorgrams in plot (a).



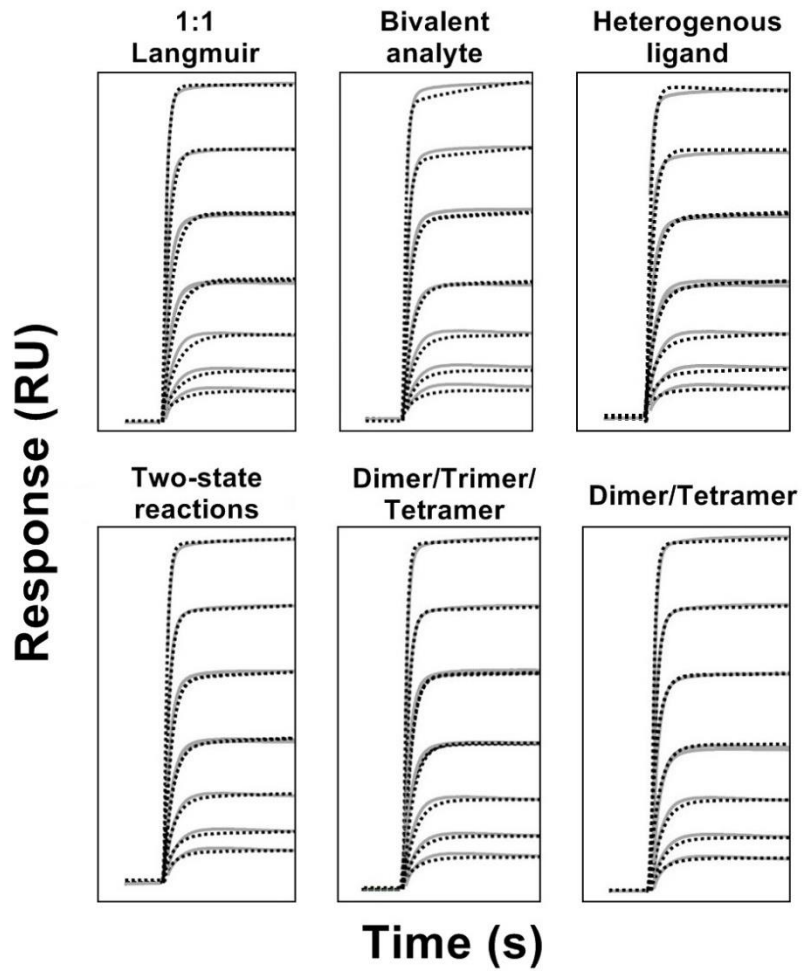


**Figure 25.**The fits of the association phase of sensorgram data using different models.

The experimental sensorgram is represented by the grey lines and each fitting model is represented by dashed lines.

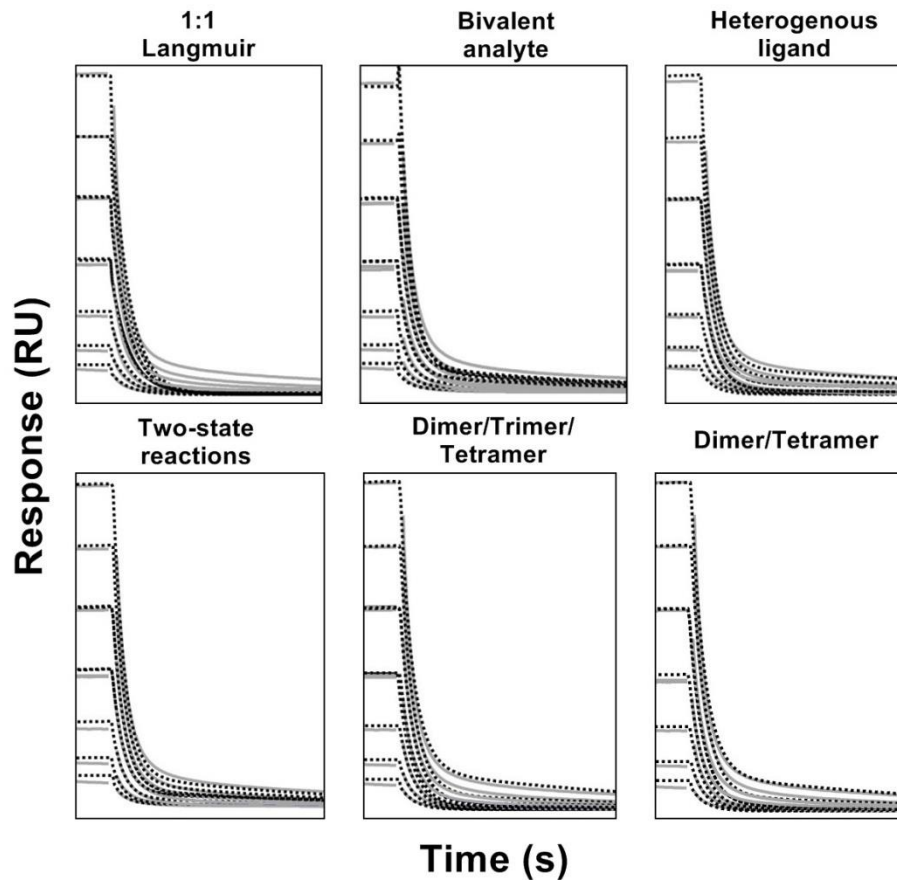


**Figure 26.** The fits of the dissociation phases of sensorgram data using different models.

The experimental sensorgram is represented by the grey lines and each fitting model is represented by dashed lines.

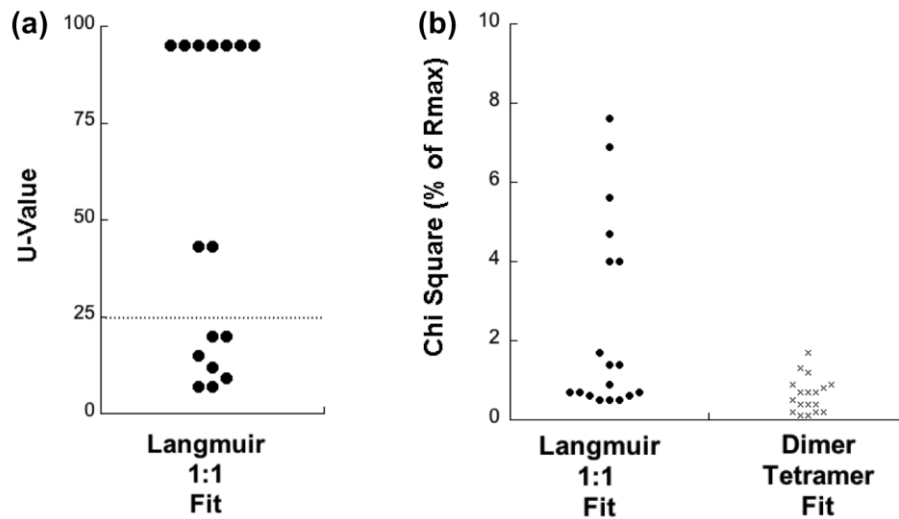


**Figure 27.** U-values and  $\text{Chi}^2$  values of the different kinetic binding models of the self-association of HMGB1.

The points represent the triplicate of 25 nM HMGB1 for all six concentrations of ionic strength (130 to 180 mM). (a) U-values for experimental data fitted with a 1:1 Langmuir model. The dimer/tetramer fit does not give U-values. (b)  $\text{Chi}^2$  values for data fitted with both 1:1 Langmuir and dimer/tetramer models.

The fit is ideal when the value of  $\text{Chi}^2$  is within one percent or so of the maximal response ( $R_{\text{max}}$ ) of the sensorgram. On the other hand, the  $\text{Chi}^2$  values for the dimer/tetramer model fit are in the range of 0-2%, which represents a better fit to the experimental data compared with the 1:1 Langmuir model. Therefore, the dimer/tetramer kinetic binding model was used for fitting and analysis of subsequent data.

The association rate constant  $k_a$  in Figure 28a and dissociation rate constant  $k_d$  in Figure 28b for 1:1 Langmuir fit reside in two apparent groupings, almost four orders of magnitude apart. However, the  $K_D$  values for 1:1 Langmuir fit are grouped in one cluster (Figure 28c), which seems to suggest that the affinity of the self-association of HMGB1 was not significantly affected by the change of ionic strength. This is likely to happen because the U-value from the 1:1 Langmuir fit (Figure 27a) indicated that most of the kinetic rate values (the  $k_a$  and  $k_d$ ) could not be independently determined. This means that the two kinetic constants, which are related to the affinity constant  $K_D$  ( $K_D = k_d/k_a$ ), cannot be resolved individually while it is still possible to specifically determine the  $K_D$ . In addition, the kinetic constants in the upper groupings for the 1:1 Langmuir model fits were difficult to determine as they were outside the limits that can be measured by the 1:1 Langmuir fitting model using a Biacore T200, (data not shown). On the other hand, the  $k_{a1}$  values for the dimer/tetramer model in Figure 28a are grouped in one cluster, whereas the  $k_{a2}$  values are more scattered. Similarly, the  $k_{d1}$  values (Figure 28b) are more clustered than the  $k_{d2}$  values. Consequently, the  $K_{D1}$  values in Figure 28c are less scattered than the  $K_{D2}$  values. This may suggest that the  $k_{a2}$ ,  $k_{d2}$  and  $K_{D2}$ , which represent the tetramer formation of HMGB1, were more influenced by changes in ionic strength, as is detailed further in section 3.6.1.

In conclusion, a 1:1 Langmuir model did not adequately describe the data and therefore, it was then reasonable to use a more complex model that could rationally describe the interaction. As will be discussed in great detail in the Discussion chapter, a dimer/tetramer model was chosen to evaluate all subsequent data, being the next simplest model that rationally may explain the interaction of HMGB1 as analyte with itself as a ligand on the sensor chip surface.

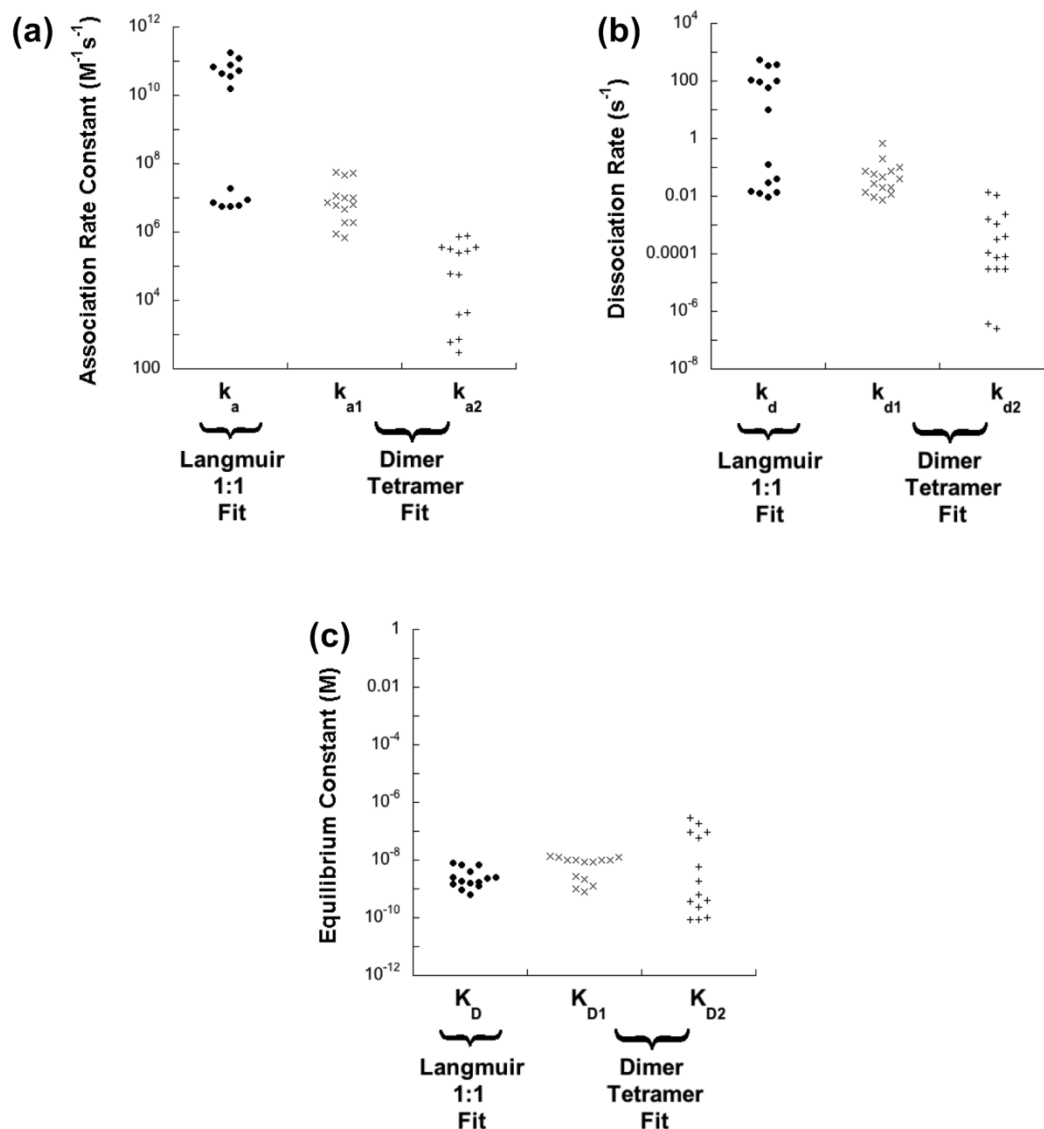


**Figure 28.** Comparison of kinetic constants between the 1:1 Langmuir and the dimer/tetramer kinetic binding models of the self-association of HMGB1.

The data points are the triplicate of 25 nM of HMGB1 for all concentrations of ionic strength (130 -180 mM). The  $k_a$  and  $k_d$  values for the dimer/tetramer model in plots (a) and (b) are given as two sets of values:  $k_{a1}$ ,  $k_{a2}$  and  $k_{d1}$ ,  $k_{d2}$ . The constants  $k_{a1}$  and  $k_{d1}$  represent the dimer formation stage and  $k_{a2}$  and  $k_{d2}$  represent the tetramer formation stage. There was only one  $k_a$  and one  $k_d$  for the 1:1 Langmuir model. The distributions of the  $k_a$  and  $k_d$  for each model determined their respective  $K_D$  values.

### 3.6.1 The effect of ionic strength

SPR sensorgrams of HMGB1 binding to itself on a CM5 sensor chip were collected at a different ionic strength concentrations and fitted with the dimer/tetramer model (Figure 29). The individual rate constants and affinities of dimer and tetramer formation were determined and evaluated in Debye-Hückel plots (Figure 30). These Debye-Hückel plots show that the rate of dimer association ( $k_{a1}$ ) and dissociation ( $k_{d1}$ ) are independent of ionic strength (Figure 30a and c). Consequently, the affinity of monomers to form dimers ( $K_{D1}$ ) is not affected by the changes of ionic strength (Figure 30e). On the other hand, the association rate of tetramers ( $k_{a2}$ ) was strongly dependent on ionic strength (Figure 30b). As might be expected, ionic strength did not greatly influence the rate of dissociation of tetramers ( $k_{d2}$ ) (Figure 30d). As a result, the affinity of dimers to form tetramers ( $K_{D2}$ ) decreases dramatically by about two to three orders of magnitude as the ionic strength is increased from 130 mM to 180 mM (Figure 30f).

The stoichiometry of the self-interaction of HMGB1 was affected by ionic strength. Increasing ionic strength resulted in a decrease in the stoichiometry of the self-association of 25 nM HMGB1 from around 2.2 at 130 mM ionic strength to around 1.4 at 180 mM ionic strength (Figure 31). Increasing ionic strength promoted a greater change in the stoichiometry of the self-association at 3000 nM HMGB1 from around 7.5 at 100 mM ionic strength, which is close to an octamer, to around 2.5 at 200 mM ionic strength, which is close to dimer. At physiological ionic strength (150 mM), a concentration of 25 nM for HMGB1 appears to predominantly lead to the formation of dimers, whereas, interestingly, 3000 nM HMGB1 appears to form tetramers (Figure 31). The rate constants at a concentration of 3000 nM HMGB1 were not analysed as the data were unreliably fitted with the dimer/tetramer model. The unreliability was indicated by the  $\text{Chi}^2$  values which were higher than 300%. This is perhaps not surprising given that the stoichiometry reaches almost eight at low ionic strength.

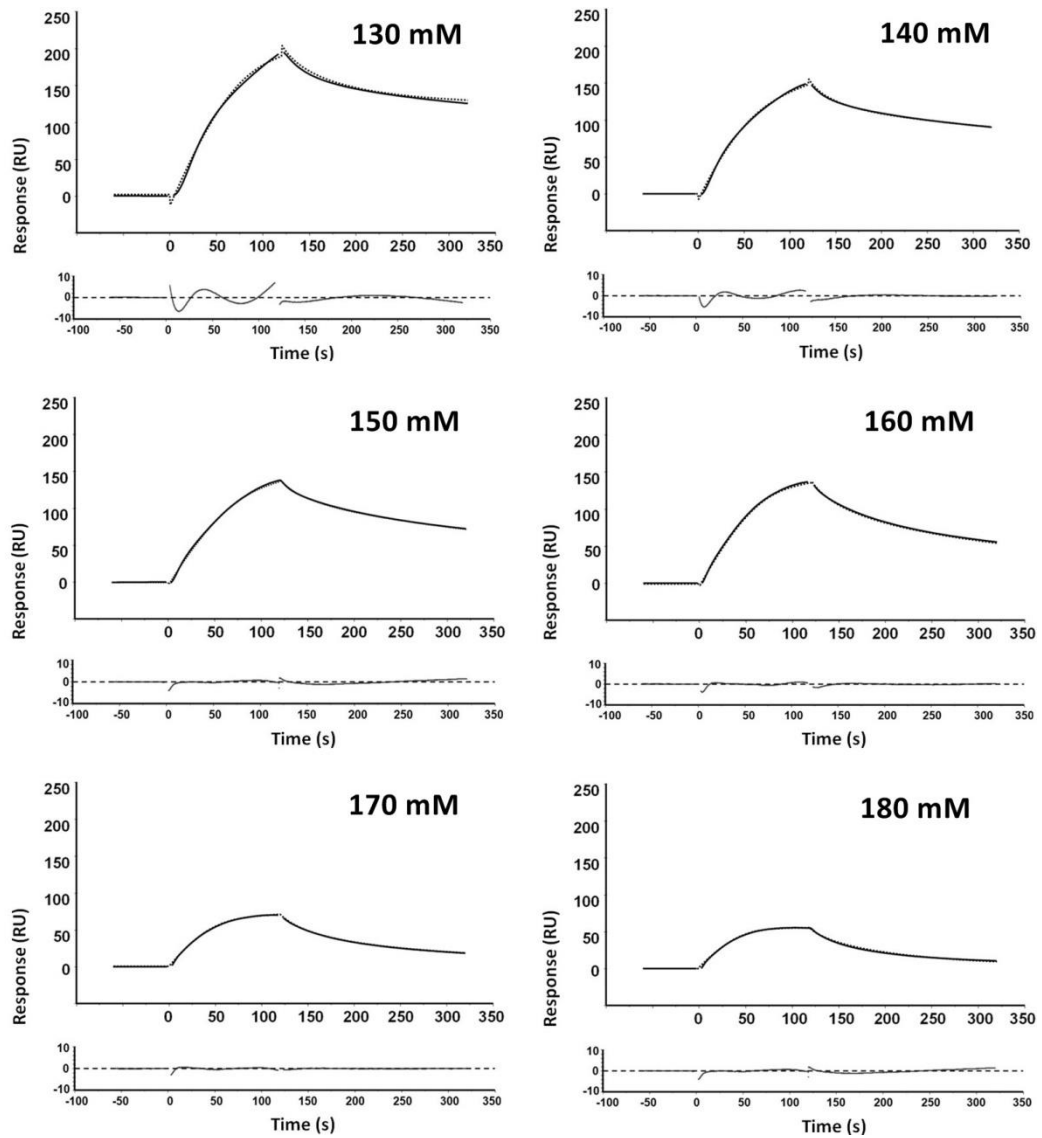


**Figure 29.**Effect of ionic strength on the self-association of HMGB1 fitted with dimer/tetramer model.

The ionic strength concentrations are indicated on the top right of each sensorgram. The black line represents the experimental sensorgram, while the dotted line represents the fit. These diagrams represent one of the experimental triplicates as outlined in the Methods chapter, section 2.14.1. Multi cycle kinetics were conducted using an analyte concentration of 25 nM HMGB1 at different ionic strength (25 nM HMGB1 was chosen to minimize non-specific aggregation of HMGB1 whilst still providing adequate RU signal).

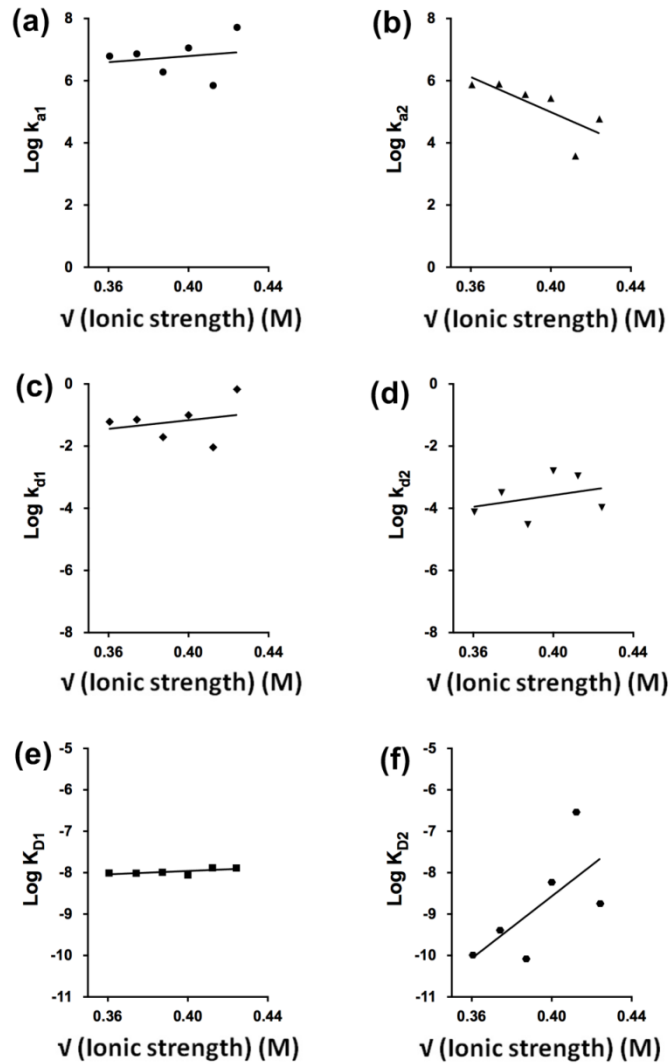


**Figure 30.** Debye-Hückel plots of the self-association of HMGB1.

The values on y-axis are square-root values of ionic strength (M), which means that 0.36 is equal to 130 mM, 0.40 is equal to 160 mM and 0.44 is equal to 194 mM. (a) association rate for dimer formation; (b) association rate for tetramer formation; (c) dissociation rate for dimer formation; (d) dissociation rate for tetramer formation; (e) equilibrium dissociation constant for dimer formation; and (f) equilibrium dissociation constant for tetramer formation. Experiments were performed in triplicate, with ionic strengths ranging from 0.13 to 0.18 M and with 25 nM HMGB1, as described in the Methods chapter, section 2.14.1. The triplicate data were globally fitted with the dimer/tetramer kinetic binding model.



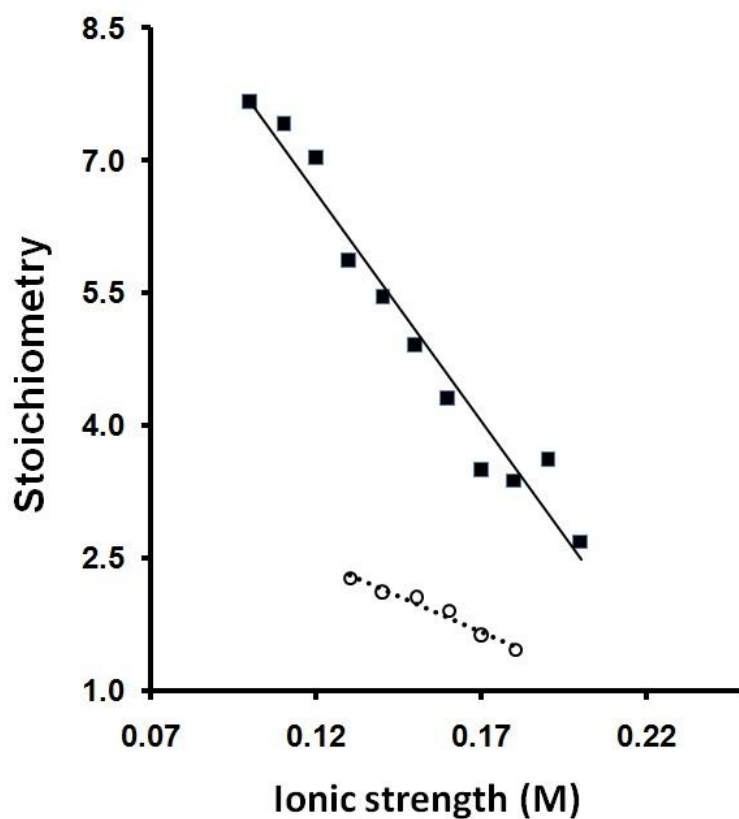


**Figure 31.**Stoichiometry of the self-association of 25 nM and 3000 nM HMGB1 at different ionic strengths.

The self-association of HMGB1 with 25 nM HMGB1 as analyte is shown with a solid line and closed symbols. The self-association of HMGB1 with 3000 nM HMGB1 as analyte is shown with a dotted line and open symbols. The stoichiometry values are represented by response unit (Rmax) values at each ionic strength concentration. The Rmax values were obtained by globally fitting the triplicate sensorgram data with the dimer/tetramer model.

### 3.6.2 Effect of zinc and other divalent metal ions

Divalent metal ions strongly influenced the self-association of different concentration of HMGB1, as illustrated in Figure 32 and Figure 33. In the absence of divalent metal ions, the affinity ( $K_D$ ) of the self-association was  $1.2 \times 10^{-7}$  M. The inclusion of 2 mM of calcium did not alter the affinity ( $K_D = 1.1 \times 10^{-7}$  M), however, the stoichiometry increased in the presence of calcium (Figure 33). Magnesium (1 mM) increased the affinity approximately two-fold ( $K_D = 5.4 \times 10^{-8}$  M) and this was correlated with a significant increase in the stoichiometry of binding (Figure 33). Zinc was by far the most potent metal ion tested. Just 5  $\mu$ M of zinc increased the affinity of self-association by approximately three-fold ( $K_D = 3.6 \times 10^{-8}$  M). Moreover, the inclusion of 5  $\mu$ M zinc promoted the formation of tetramers (rather than dimers in its absence) (Figure 33). It is notable that the inclusion of high concentration of zinc (50  $\mu$ M) resulted in gross oligomerization of HMGB1, which was difficult to fit using the dimer/tetramer model (data not shown).

Given the dramatic effect of zinc on the concentration-dependent self-association of HMGB1 shown in Figure 32 and Figure 33, the effect of ionic strength on the zinc-dependent self-association at 25 nM HMGB1 was evaluated. Interestingly, the association rate of dimers appeared to be influenced by the presence of 5  $\mu$ M zinc, as shown by the Debye-Hückel plot in Figure 34a, which contrasts the influence of ionic strength on dimer formation in the absence of zinc or in the presence of 3 mM EDTA (Figure 34a). The rate of dissociation of dimers appeared to be less influenced by zinc relative to the controls (Figure 34c). Together, this resulted in zinc increasing the affinity of dimer formation about 5 fold at physiological ionic strength (Figure 34e).

The effect of ionic strength on the zinc-dependent self-association of HMGB1 tetramers was more dramatic than dimer formation. As illustrated in Figure 34b, d and f, respectively, ionic strength had a dramatic effect on both the rate of tetramer association, dissociation and affinity of the tetramer. This seemed to enhance the already noted effect of ionic strength on tetramer formation in the absence of zinc (Figure 30b, d and f).

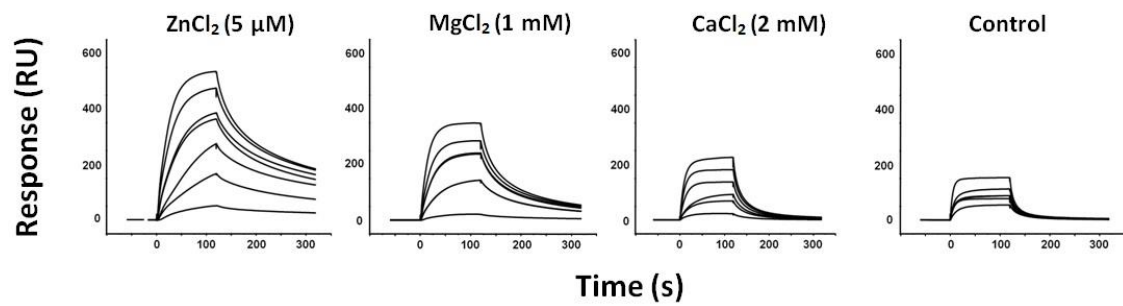


**Figure 32. Influence of divalent metal ions on the self-association of HMGB1.**

The sensorgrams correspond to a different concentration range of analyte HMGB1. Each of the experiments was performed as described in the Methods chapter, section 2.14.2, and the sensorgrams were fitted globally with the dimer/tetramer kinetic binding model.

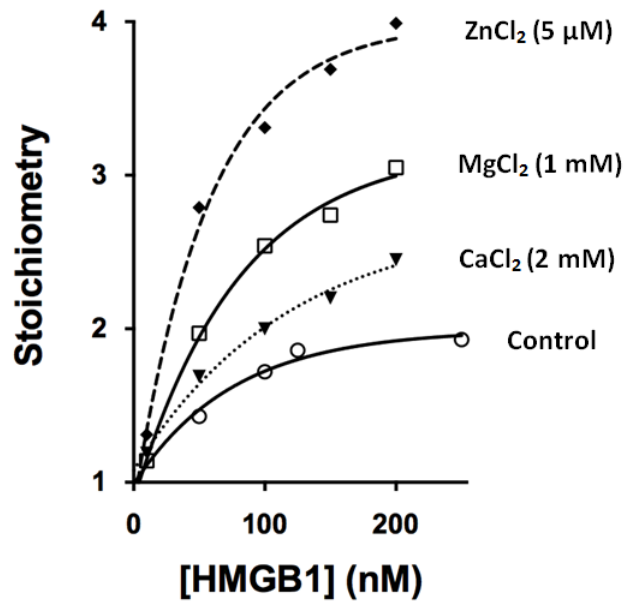


**Figure 33. Stoichiometry of HMGB1 self-association in the presence of divalent metal ions.**

Stoichiometries are based on the response units (RU) values of the different concentration range of HMGB1 as derived from Figure 32.

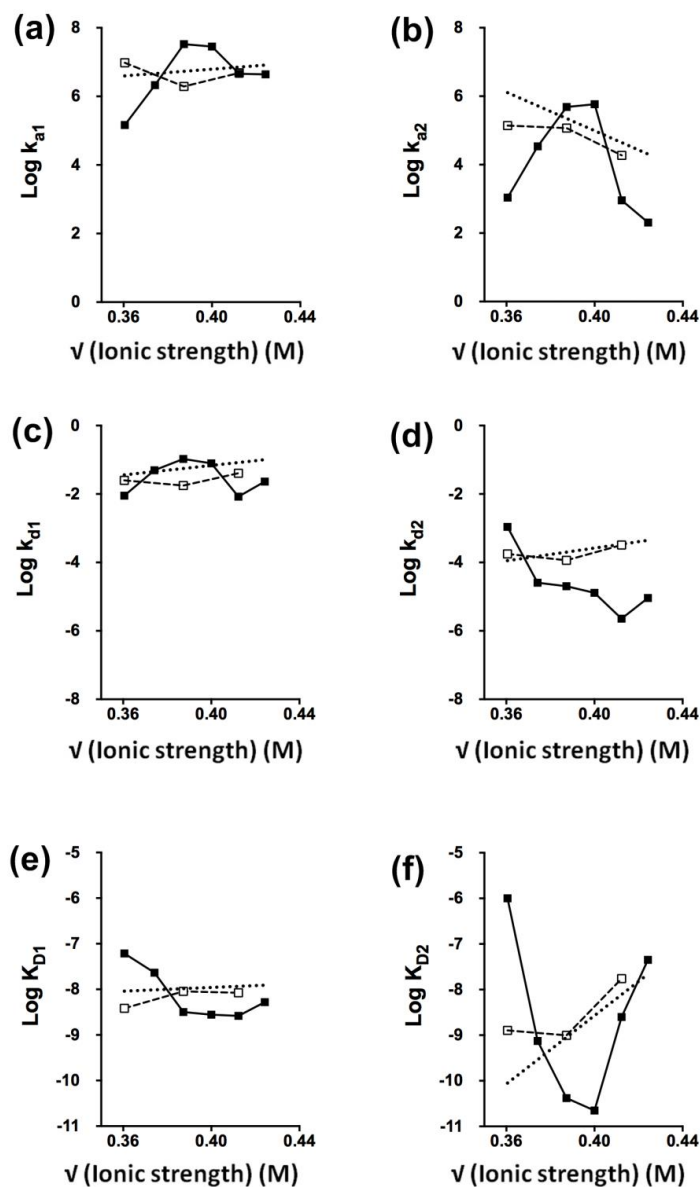


**Figure 34. Debye-Hückel plots of the effect of ionic strength on the zinc-dependent self-association of 25 nM HMGB1.**

The values on y-axis are square-root values of ionic strength (M), which means that 0.36 is equal to 130 mM, 0.40 is equal to 160 mM and 0.44 is equal to 194 mM. (a) dimer association rates, (b) tetramer association rates, (c) dimer dissociation rates, (d) tetramer dissociation rates, (e) dimer equilibrium dissociation constants, and (f) tetramer equilibrium dissociation constants. The control (i.e. HMGB1 in the absence of zinc) is shown with a dotted line without markers, HMGB1 in the presence of zinc and EDTA is shown with a dashed line with open markers, and HMGB1 in the presence of zinc only is shown with a straight line with closed markers. The triplicate data were globally fitted with the dimer/tetramer kinetic binding model.

Interestingly, the peak in the rate of association of tetramers and the affinity describing the tetramer formation approached a maximum near physiological ionic strength (150 mM) (Figure 34f). Indeed, the affinity at this point is almost two orders of magnitude greater than the controls (Figure 34f). EDTA dramatically diminished the effect of zinc in promoting the formation of HMGB1 oligomers, further validating the effect of zinc (Figure 34).

Large changes were observed in the stoichiometry at ionic strengths lower than 140 mM and higher than 160 mM, in the presence of zinc (Figure 35). The stoichiometry at ionic strengths lower than 140 mM decreased from 7 to 2 at 140 mM. At ionic strengths higher than 160 mM, the stoichiometry gradually increases to a value of approximately 3. This may indicate that zinc promotes aggregation at low and high ionic strengths.

### **3.6.3 Effect of the redox environment**

Given that the reducing agent  $\beta$ -mercaptoethanol substantially affects the secondary structure of HMGB1 as shown by the change of CD spectra of the secondary structure of HMGB1 in Figure 18, experiments were conducted to investigate whether the redox state of HMGB1 is important for the self-association properties of HMGB1 (Figure 36). In the absence of any reducing agent (0 mM  $\beta$ -mercaptoethanol for 1 hour), the apparent affinity for tetramer formation was about 100 fold greater than for dimer formation (Figure 36e). However, when HMGB1 was incubated with >1 mM  $\beta$ -mercaptoethanol, it was apparent that there was a dramatic change in affinities for dimer and tetramer formation. The affinity for tetramer decreased by up to three orders of magnitude, whereas the affinity of the dimers increased by about 10 fold (Figure 36e). These remarkable changes appeared to be largely due to an increased rate of association of dimer from monomer, shown by a 50 fold change in Figure 36b, and also a large increase in dissociation rate of tetramer to dimer, shown by a 150 fold change in Figure 36d.

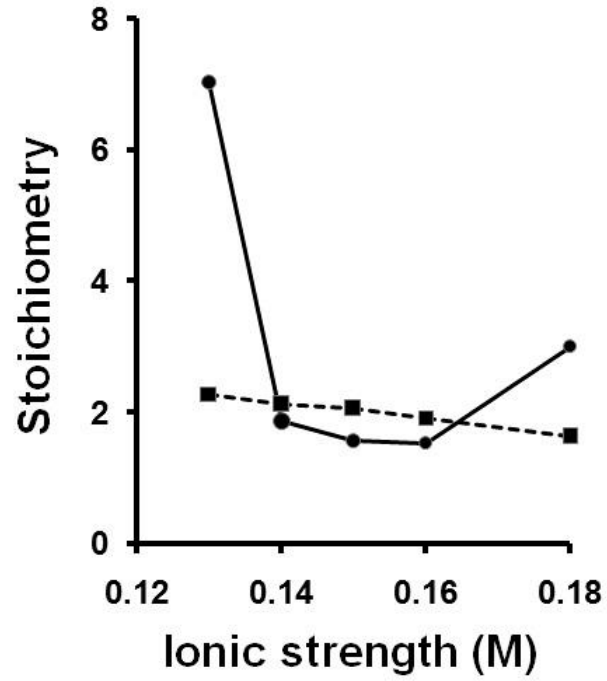


**Figure 35. Stoichiometry of the self-association of 25 nM HMGB1 in the presence of zinc as a function of ionic strength.**

The straight black line shows the self-association under the influence of zinc, whereas the dashed line shows the self-association minus the zinc. The data at 180 mM was the only data point not well fitted, and therefore it was considered to be an outlier.

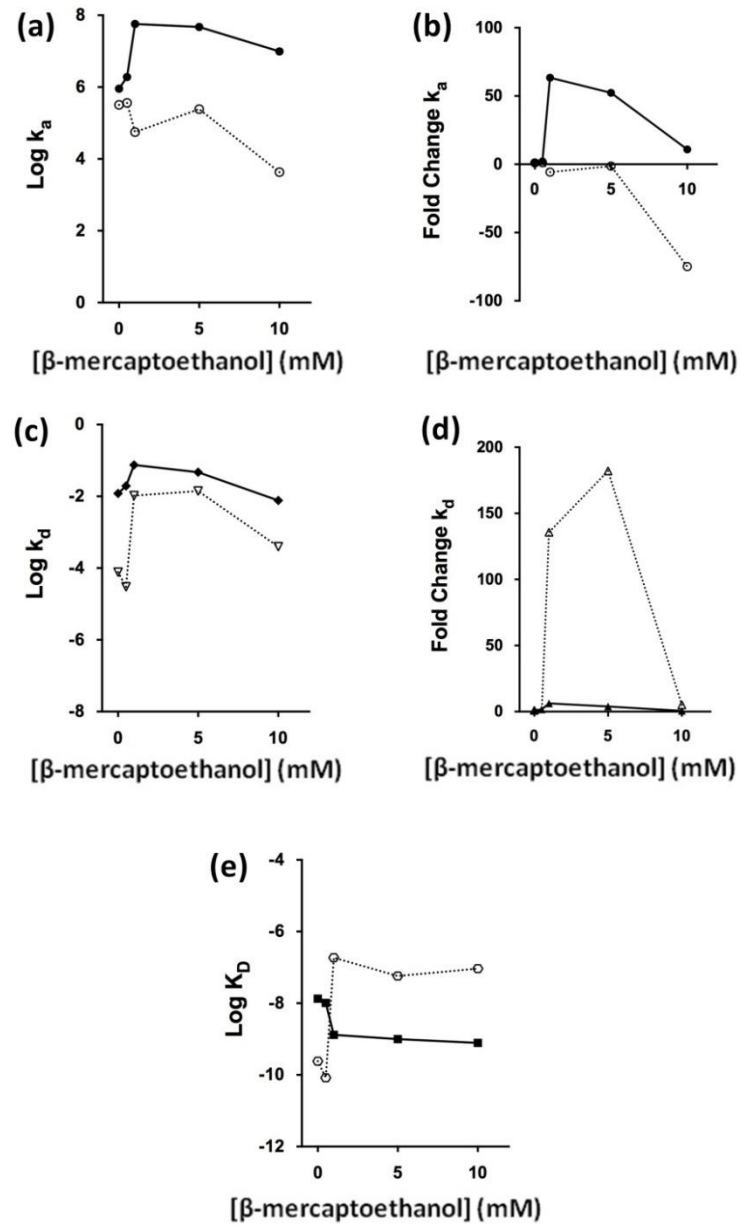


**Figure 36.**The effect of  $\beta$ -mercaptoethanol on the self-association of HMGB1.

(a) Association rates of dimer and tetramer; (c) Dissociation rates of dimer and tetramer; (b) and (d) Fold change of the association and dissociation rates from (a) and (c), respectively; (e) Equilibrium dissociation constant ( $K_D$ ) of dimer and tetramer. Sensorgram data were fitted with the dimer/tetramer kinetic binding model. Straight lines with closed markers are used for the association rate, dissociation rate and dissociation constant for dimer formation:  $k_{a1}$ ,  $k_{d1}$ , and  $K_{D1}$ , respectively. Dotted lines with open markers are used for the association rate, dissociation rate and dissociation constant for tetramer formation:  $k_{a2}$ ,  $k_{d2}$  and  $K_{D2}$ , respectively.



### 3.6.4 Effect of pH

The theoretical pI value of HMGB1 was calculated using ProtParam in the Protein Identification and Analysis Tools on the ExPASy webserver (<http://web.expasy.org/protparam/>) (Lafarga et al., 2014) and determined to be 5.6. This means that at pH 5.6, the net charge of HMGB1 is zero and the protein is least soluble. The protein may tend to aggregate at this point. Figure 37 shows that the highest level of aggregation for HMGB1 occurred at a pH of 4.8 and not 5.7. At a pH of 4.8, the sensorgram shows an almost linear association phase, suggesting that mass transport limitation may occur. The response of more than 400 RU shows that the HMGB1 analyte formed large oligomers. Formation of large oligomers may indicate that the interaction is mass transport limited and, therefore, imposed a limitation on the binding rate between analyte and ligand (Healthcare, 2008a). The mass transport limitation caused difficulties when fitting the sensorgram with the dimer/tetramer kinetic binding model, as indicated by the high projection of RU (4881 RU). Thus, it was not possible to reliably derive the rate constants for the self-association of HMGB1 at pH 4.8. A dramatic decrease in the self-association of HMGB1 was observed at pH 4.0. Indeed, no significant response was detected at pH 4.0. The effect of pH on self-association was fully reversible. The chip used for experiment at pH 4.0 could reproduce the sensorgram observed at pH 7.4.

### 3.7 Thermal shift assay for HMGB1

There are two types of data derived from a thermal shift assay: an amplification curve and a derivative curve. A sigmoidal peak in the amplification curve of the control protein LptA (Figure 38a) and the downward peak of the corresponding derivative curve (Figure 38b) exhibit typical peaks indicative of the limit of protein stability. The peaks demonstrate that the LptA protein denatures and unfolds due to the increasing temperature, resulting in the exposure of its hydrophobic core. Therefore, the fluorescence signal of LptA increases at around 60°C due to the binding of the HEX dye to the exposed hydrophobic surfaces of the denatured protein. This result indicates that the dye and buffer conditions worked well for LptA as an “ideal” control protein. These conditions were used as a starting point to evaluate the thermal stability of HMGB1.

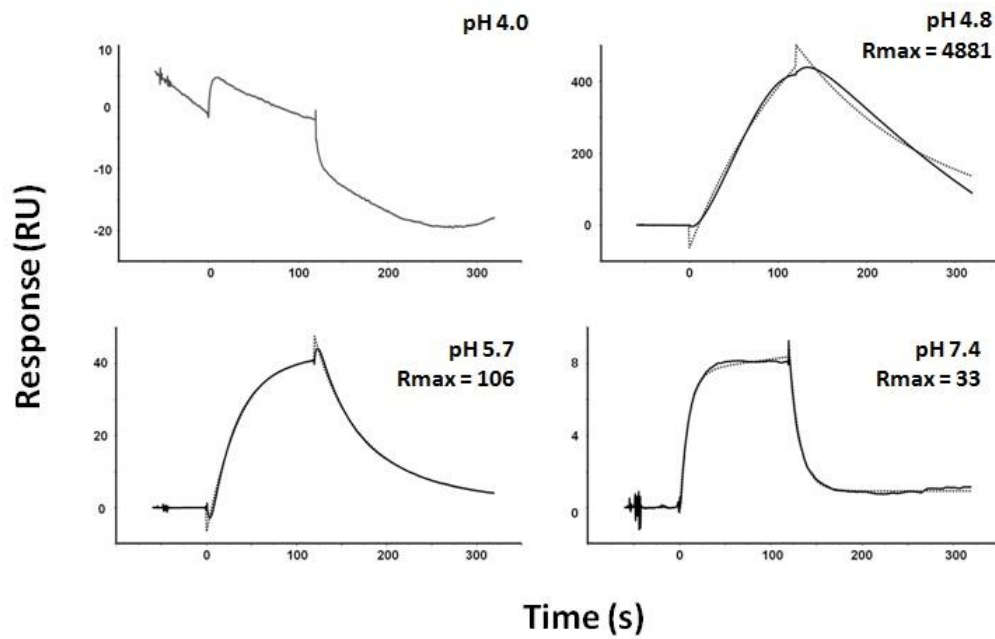


**Figure 37. Effect of pH on the self-association of HMGB1.**

The interaction of 25 nM HMGB1 with the 180 RU of HMGB1 bound to the sensor chip was measured as described in Methods chapter, section 2.14.5. Where possible, the sensorgram was fitted with the dimer/tetramer model.

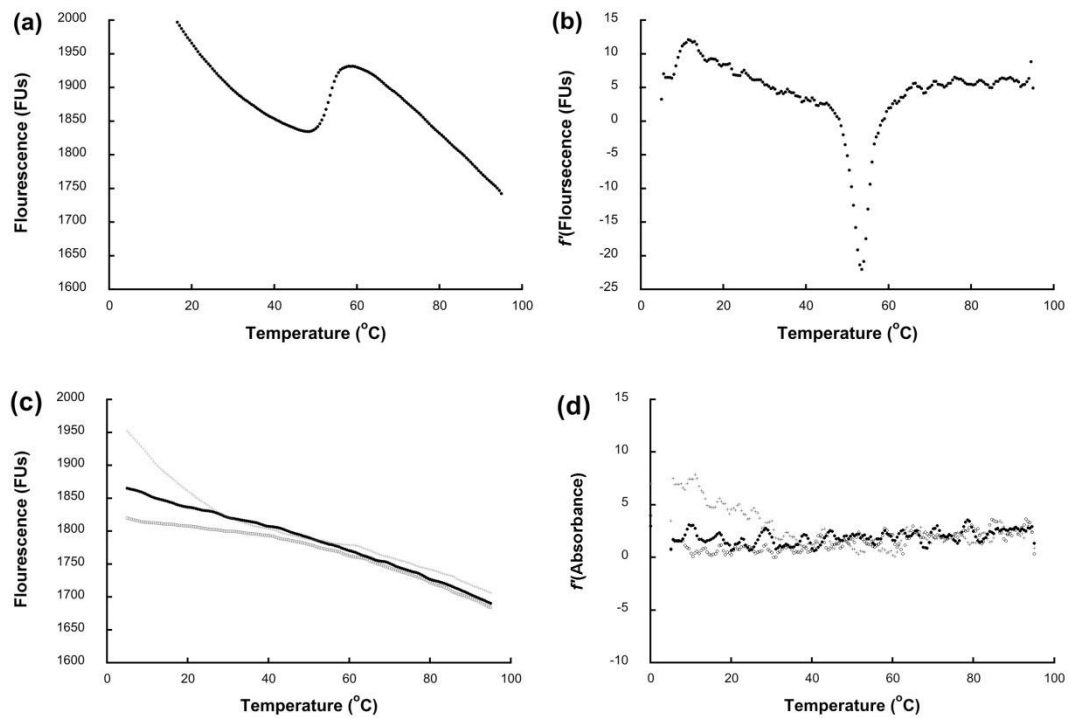


**Figure 38. Thermal shift plots of LptA and HMGB1 controls.**

The LptA protein control is represented by an amplification plot (a), which typically shows a sigmoidal peak as the protein starts to denature, while the derivative plot (b) shows a downward peak corresponding to the highest point of the sigmoidal peak. The HMGB1 controls are shown as three different lines on the amplification plot (c) and derivative plot (d). A concentration of 3.6 mg/ml HMGB1 was used. The negative controls were (1) buffer with 5  $\mu$ M zinc and 0.5 mM  $\beta$ -mercaptoethanol combined with dye but without HMGB1, indicated by a black line; (2) buffer with 5  $\mu$ M zinc and 0.5 mM  $\beta$ -mercaptoethanol without either HMGB1 or dye, indicated by a thick grey line; and (3) buffer with 5  $\mu$ M zinc and 0.5 mM  $\beta$ -mercaptoethanol with HMGB1 but without dye, indicated by a thin, light grey line (done in collaboration with Prof. Alice Vrijlink and Ms. Caroline Snowball from University of Western Australia).

Besides the LptA positive control experiment, three different negative controls were included for HMGB1, involving combinations in the presence and absence of the HEX dye HMGB1,  $\beta$ -mercaptoethanol and zinc. The resulting amplification and derivative curves for these negative controls are shown in Figure 38c and Figure 38d. The amplification plot shows three straight lines with no visible peak, whereas the derivative plot also shows the three lines remaining on the baseline. These results suggest that (1) the dye did not react non-specifically with the components in the buffer, (2) when the buffer was tested alone without either HMGB1 or dye, there was no signal detected, indicating that the buffer contained no interfering agents, and (3) when HMGB1 was added to the buffer without dye, there was no shift in the fluorescence signals.

The plots in Figure 39 characterise different conditions for HMGB1 with variations of the presence or absence of  $\beta$ -mercaptoethanol and/or zinc. The amplification plot in Figure 39a shows that there is no fluorescence response in the presence of 0.5 mM  $\beta$ -mercaptoethanol alone, indicated by an almost flat, decreasing black line which overlaps the grey line for control. This may indicate that HMGB1 had already denatured from the beginning of the gradual temperature increase. The derivative plot in Figure 39b confirms this observation. However, the shift of the fluorescence signal starts to be detected as a higher peak relative to the control for HMGB1 in the presence of 5  $\mu$ M ZnCl<sub>2</sub> (Figure 39c). In Figure 39d, this shift was depicted in more detail as the occurrence of three small peaks in the 20-60°C temperature range. This suggests that HMGB1 gains more stability in the presence of zinc ions. The three small peaks in the derivative plot in Figure 39d are also detected again in Figure 39f which describes the increasing fluorescence signal of HMGB1 after the addition of both zinc and  $\beta$ -mercaptoethanol. The evidence of the shift is supported by the sigmoidal peak visible in the amplification plot (Figure 39e), in which the peak was higher than the control. The presence of both ZnCl<sub>2</sub> and  $\beta$ -mercaptoethanol appears to substantially increase the fluorescence signal, which is shown by the shift of the sigmoidal peak. As explained previously in section 3.6.3, the presence of 0.5 mM  $\beta$ -mercaptoethanol promotes the formation of HMGB1 oligomers. The addition of 5  $\mu$ M ZnCl<sub>2</sub> also promotes the self-association of HMGB1, as shown in section 3.6.2. The results of these thermal shift assays suggest that the combination of thiol and zinc seems to increase the stability of the HMGB1 structure. Furthermore, there were three peaks that were detected on the derivative plots (Figure 39d and f), as indicated by the arrows. The evidence that the presence of these three peaks, which were initially detected in plot Figure 39d, were repeated in Figure 39f may suggest that this occurrence was not due to

background noise. It could represent denaturation of different oligomerization state of HMGB1 that exist as the temperature increases.

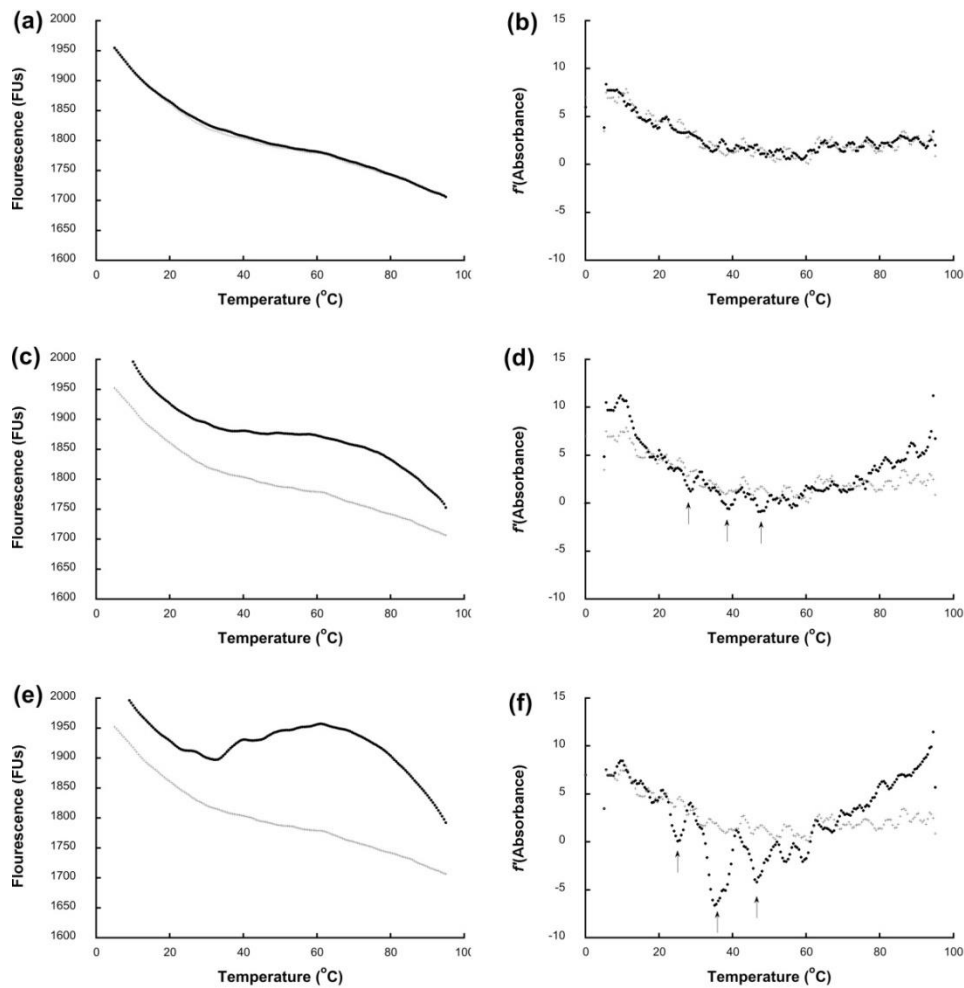


**Figure 39.** Thermal shift plots of HMGB1 with or without ZnCl<sub>2</sub> and β-mercaptoethanol.

Three aliquots of 3.6 mg/ml HMGB1 were treated with three different combinations of 5 μM ZnCl<sub>2</sub> and 0.5 mM β-mercaptoethanol. The top panel shows the amplification plot (a) and derivative plot (b) of the control sample, i.e. HMGB1 in buffer without both ZnCl<sub>2</sub> and β-mercaptoethanol (grey line), and HMGB1 in buffer with 0.5 mM β-mercaptoethanol (black line). The second panel shows the amplification plot (c) and derivative plot (d) of the control sample (grey line) compared with HMGB1 in buffer with zinc (black line). Plot (c) for HMGB1 in the presence of zinc shows a shift in the sigmoidal peak, while plot (d) also shows a corresponding slight shift with the control. Three peaks also appear in the derivative plot (indicated by arrows). The bottom panel has the amplification plot (e) and derivative plot (f) of the control sample (grey line) compared with HMGB1 in buffer with both zinc and β-mercaptoethanol (black line) (done in collaboration with Prof. Alice Vrijlink and Ms. Caroline Snowball from University of Western Australia).

## **4 DISCUSSION**

#### 4.1 Purification of HMGB1

Protein purity of at least 95% is preferred when characterising proteins and their interactions using methods such as SPR, CD or thermal shift assays. This is particularly important for self-association studies, as non-specific aggregates, common in impure protein preparations, are likely to lead to misinterpretation of data. Indeed, early SPR sensorgrams using impure HMGB1 preparations yielded uninterpretable kinetics due to confounding peaks and dips in the data (Figure 21a and b), which can be typical of non-specific protein aggregation (Healthcare, 2008a). The SPR sensorgrams were substantially improved through the purification of HMGB1 and VCC-RAGE proteins to homogeneity (>95%). Both proteins were also repurified by repeating the size exclusion chromatography step when the proteins were stored at -80°C for longer than 3-4 weeks.

It is interesting that the HMGB1 purified in this study appeared predominantly as a single peak following size exclusion chromatography and there was no obvious appearance of multiple peaks, which would have suggested the occurrence of self-association. This may be explained in a number of ways. Firstly, size exclusion chromatography was not performed under conditions demonstrated in our SPR study to favour self-association. Zinc ions were absent and EDTA was also used in all buffers when purifying HMGB1 in this study. The Superdex 200 column used in this step was also selected to provide separation of a wide range of molecular sizes and was not in any way optimised to enable separation of HMGB1 oligomers. Size exclusion chromatography is also not a method of choice for studying interactions involving relatively fast association/dissociation rates, as were readily observed in this study using SPR. Equilibration of species during size exclusion chromatography may thus preclude the “visualisation” of interactions with fast rate constants.

It also has to be appreciated that the size exclusion chromatography performed in this study was done under non-denaturing conditions and that the indicative size of molecules separated were determined against other commonly used protein standards. The size observed (25-30 kDa) for HMGB1 eluting off the Superdex 200 gel appears to be monomeric HMGB1, but this is of course dependent on the conditions of the experiment. HMGB1 does not have the hallmarks of a “typical” protein. It comprises a basic region and a highly acidic tail, making the protein highly charged (Parkkinen et al., 1993). Indeed, it is interesting that Ranatunga et al (Ranatunga et al., 1999) reported that HMGB1 eluted off Sephadex superfine G-75 gel as an apparent 55 kDa (HMGB1 is a 25 kDa protein).



However, under the conditions used for their sedimentation equilibrium studies, the authors concluded that HMGB1 sedimented predominantly as a monomeric protein and they could not explain this apparent discrepancy, although they used 1 mM of reducing agent dithiothreitol which may promote the formation of HMGB1 oligomers (this study used reducing agent  $\beta$ -mercaptoethanol, as explained in section 4.3.3). Thus, whilst size exclusion chromatography can be used to purify proteins, it is probably not useful as a method for determining the self-association behaviour of proteins; especially unique proteins such as HMGB1.

In one study, the affinity of HMGB1 towards DNA was micromolar when HMGB1 was purified using 5% trichloroacetic acid and/or 25% perchloric acid for 2 to 5 hours precipitation step (Wagner et al., 1995). However, it was unclear why the researchers used such extreme acid precipitation method. The low affinity of their HMGB1 is perhaps not surprising given the extensive denaturation that the protein would have undergone. The same authors concluded that HMGB1 purified using non-denaturing conditions has nanomolar affinity to DNA (Wagner et al., 1995).

In the present study, it was first attempted to exclude the acid precipitation step when purifying HMGB1. Despite significant effort and the inclusion of separation methods such as ion-exchange chromatography, in addition to heparin chromatography and size exclusion chromatography, HMGB1 could not be purified to homogeneity in good yield. The expression of HMGB1 with a polyhistidine or other tag to facilitate its purification and immobilisation on SPR sensor chips was considered, but as explained further in section 4.2.1, the inclusion of tags was avoided as they can complicate the data relating to the self-association of HMGB1. Thus, in this study HMGB1 was purified by including the traditional TCA precipitation step, which significantly removed the bulk of contaminant proteins in one high yielding easy step. The percentage of TCA was kept to 2% and care was taken to ensure that this step was completed within 30 min.

Despite the inclusion of the TCA step in our purification protocol, the HMGB1 used in this study was highly active, binding DNA with a picomolar affinity (Figure 23) and VCC-RAGE with nanomolar affinity (Figure 22), which is comparable to the nanomolar affinity reported by another SPR study of the HMGB1-RAGE interaction (Ling et al., 2011). The CD spectra of HMGB1 in the present study are consistent with the preservation of an intact, functional structure. Alpha helices were determined to predominate in the secondary structure of HMGB1, as would be expected based on the known and predicted structures

for HMGB1 boxes (Wang et al., 2013, Rowell et al., 2012), and the spectra were comparable to those reported in another study (Belgrano et al., 2013). It is thus possible to confidently conclude that the HMGB1 used in this study was appropriately folded and fully active.

## **4.2 Characterization of HMGB1 interactions using SPR**

The self-association of HMGB1 is a somewhat controversial topic, being indirectly implicated in some studies (Bonne et al., 1980, Mathis et al., 1980, Alexandrova and Beltchev, 1987, Rauvala and Pihlaskari, 1987, Bianchi et al., 1992, Stros et al., 1994, Teo et al., 1995, Grasser et al., 1998, Marekov et al., 1984), but not others (Weir et al., 1993, Ranatunga et al., 1999). In this study, the self-association of HMGB1 was characterised using an ultra-sensitive, SPR instrument (Biacore T200), which can detect minute changes in refractive index at the sensor chip surface and enables mass changes of less than 100 fg/mm<sup>2</sup> to be measured in real-time. This approach has not been reported previously for the study of the self-association of HMGB1.

### **4.2.1 Immobilization, mass transport and rate constant determination**

In this SPR study, HMGB1 was immobilized by covalently attaching its exposed primary amine groups to the carboxylic end groups activated as *N*-hydroxysuccinimide (NHS) ester of the dextran surface of a CM5 chip (Healthcare, 2008a). This amine coupling method was chosen as it is very reliable and easy to perform. Indeed, this method is used in approximately 90% of SPR applications (Rich and Myszka, 2008). This approach was also taken to minimize the loss of HMGB1 from the sensor chip surface during the various run and regenerations cycles. Whilst the experiments performed in this study were reproduced using multiple sensor chips, sensor chips could be coupled with HMGB1 using this procedure and used over several months without appreciable loss of self-association activity, or DNA and RAGE binding ability. Nonetheless, a distinct disadvantage of the amine coupling method is that the presence of multiple primary amines of a ligand may provide multiple attachment points, leading to heterogenous ligand orientation. In these studies, however, it appears that heterogenous ligand orientation was not a significant contributing factor in sensorgram interpretation, because a heterogenous ligand model did not provide a good fit to the sensorgrams (Figure 25 and Figure 26). Therefore, the amine coupling method was chosen as the method of choice throughout this study.

Other less common functional groups such as free thiols can be utilized for coupling (Healthcare, 2008a); however, this would not have been a sensible choice because of the redox sensitivity of the self-association of HMGB1, which will be discussed later. Homogeneous orientation of immobilized HMGB1 may be possible using a specific antibody to “capture” the protein (Healthcare, 2008a). However, this would require more detailed information on HMGB1 binding sites. In this context, it is necessary to locate the binding sites for self-association, DNA and RAGE, so that the antibody that is chosen does not interfere with these interactions. In addition, a high affinity antibody must be selected that stably captures HMGB1, without an excessive base line drift due to antibody-ligand dissociation over the duration of the experiment. Various protein tags can also be used to capture ligands. For example, polyhistidine tags on proteins can be readily captured on sensor chips modified with nitrilotriacetic acid (NTA), which chelates metal ions such as nickel. However, polyhistidine-tagged HMGB1 was not chosen in this study because it has been reported that these polyhistidine tags can promote protein dimerisation (Wu and Filutowicz, 1999), which could lead to conflicting interpretations of the data.

The choice and conditions of ligand immobilization ultimately influences rate constant determinations. Thus, great care was taken in this study to define the immobilisation conditions (Methods chapter, section 2.13.1) and to ensure that phenomena such as mass transport limitation did not inappropriately bias the interpretation of the data. Excessive ligand coupling to the sensor chip surface limits the binding rate of the analyte to the immobilized ligand (Healthcare, 2010). This mass transport-limited condition is typified by a linear association phase in the sensorgram (Rich and Myszka, 2008). This study utilized sensor chips with no more than 180 Response Unit (RU) of HMGB1 immobilized on a CM5 chip surface, which equates to approximately 20-50 nM of HMGB1 at the surface of the sensor chip. With one exception, no mass transport was detected by the in-built Biacore T200 software, which monitors each sensorgram for data quality and mass transport. Mass transport limitation was only detected when measurements were performed at pH 4.8, as discussed later in section 4.3.4. The results of this study were also highly reproducible at lower coupling levels (50 RU); however, these chips appeared to be much less stable than chips coupled with HMGB1 at higher surface density (data not shown). It is not clear why this appeared to be so and the cost of the chips precluded a more detailed investigation of this preliminary observation. Nevertheless, the chips with 180 RU of HMGB1 immobilised were stable for over six months through repeated cycles of runs and regenerations. To further ensure that the data in this study were not inappropriately biased by mass transport, sensorgrams were collected at a flow rate of 30  $\mu$ l/min

throughout this study. A slow flow rate can induce mass transport limitation phenomenon (Rich and Myszka, 2008). In an experiment utilizing a flow rate of 5  $\mu\text{l}/\text{min}$ , the obtained kinetic constants were still within limit of the specification of Biacore T200; however, the association phases were started by spikes and the transitions between association and dissociation phases were divided by clearly visible dips (data not shown), which may indicate mass transport limitation at a lower flow rate of 5  $\mu\text{l}/\text{min}$ .

#### **4.2.2 Optimization of protein preparation and composition of SPR buffer**

Unless otherwise stated, all experiments in this study were done in the presence of low concentrations of the reducing agent  $\beta$ -mercaptoethanol (0.5 mM) and bovine serum albumin (BSA) (0.1%). The inclusion of these agents was crucial for the reproducibility of these studies, as explained below. Their exclusion from most other studies may well explain the confused literature pertaining to the self-association and other physical properties of HMGB1.

$\beta$ -mercaptoethanol was initially included at a base level of 0.5 mM throughout these studies to maintain the free Cys106 of HMGB1 in its reduced form, while still keeping the disulfide bond between Cys23 and Cys45 intact. Redox condition can dramatically influence the conformation of a protein, the activity of an enzyme, as well as ligand-receptor, protein-protein or protein-DNA interactions (Kemp et al., 2008).

The preliminary experiments in this study provide evidence of the retention of the structural and functional integrity of both purified HMGB1 and the VCC-RAGE protein constructs. However, there were traces of protein aggregation visible during the experiments, identified by an uneven equilibrium phase of the sensorgrams (Figure 21a and b). This suggested that further purification was needed before structural studies of these proteins can be undertaken. Final purification step for each of the HMGB1 and VCC-RAGE protein constructs using size exclusion chromatography immediately after column chromatography purifications improved the sensorgrams, by removing the possible protein aggregates.

BSA was added to prevent the loss of signal due to non-specific binding of the analyte proteins to the CM5 chip. The concentration of BSA used restored the signal of protein-protein interactions in the nanomolar range and did not hamper the interactions (Figure 21b), judging from the reasonable values of the rate constants and affinity of interactions. Further concern was raised due to the fact that zinc is known to bind albumin. It was

thought that the BSA used in the SPR buffers may interact non-specifically with zinc, which is a paramount factor for the self-association of HMGB1, as will be discussed in the following section. However, it is known that under normal physiological conditions, zinc occupies less than 0.2% percent of existing albumin in human serum. Furthermore, the binding capacity of albumin for zinc does not even approach saturation (Foote and Delves, 1984). Thus, it was assumed that there would be no significant loss of zinc from binding to a small fraction of the available BSA.

#### **4.2.3 Development of the binding model best fitting SPR sensorgrams**

Analysis of rate data to determine kinetic constants is always challenging because a suitable fitting model must first be chosen and appropriately justified. The 1:1 Langmuir model is a recommended default fit for most rate data, as it is the simplest model that defines many molecular interactions by assuming that one ligand molecule couples with one analyte molecule (Healthcare, 2010). However, this simplest model did not provide an adequate fit to the sensorgrams in this study as shown in Figure 24, Figure 25 and Figure 26, and as explained in the Results chapter, section 3.6 and section 3.6.1. In particular, the dissociation phase of the sensorgrams was inadequately fitted using the simplest 1:1 Langmuir model (Figure 26). Indeed, the U and  $\chi^2$  values for the fits were unsatisfactory using this model (Figure 27). Thus, it was appropriate to evaluate other fitting models. The bivalent analyte and heterogenous ligand models did not fit the sensorgrams sufficiently (Figure 25 and Figure 26), suggesting that these models do not represent adequately the order of complex formation of HMGB1 oligomers. A different model, such as a two state reaction model, provided better fits to the data. This is perhaps not surprising given that a better fit will invariably follow when additional parameters and degrees of freedom are introduced into the fitting. However, none of these other purpose-built models could be readily rationalised to explain the data in this study, and in particular, to account for the stoichiometry of binding observed in this study. In the presence of zinc at physiological ionic strength, the maximum response in the sensorgrams approached tetramer formation (Figure 33). At higher concentrations of HMGB1, much higher order oligomer formation was also observed, especially at lower ionic strength (Figure 31). As reported in previous studies (Bonne et al., 1980, Duguet and de Recondo, 1978), HMGB1 may form beads comprising up to 20 protein molecules when bound to DNA. Self-association models can readily account for higher order oligomer formation and indeed provided good fits to the data in this study. The U and  $\chi^2$  values

were greatly improved using a dimer/tetramer model as the simplest self-association model, adequately fitting most of the data collected in this study.

### **4.3 Physico-chemical factors affecting the self-association of HMGB1**

#### **4.3.1 Effect of ionic strength**

Given that HMGB1 comprises two homologous N-terminal HMGB1 boxes that mainly consist of basic amino acid residues and a highly unstructured acidic tail of 30 consecutive glutamate and aspartate residues, it is not surprising that the interactions of HMGB1 and its oligomerisation are strongly influenced by ionic strength. Indeed, ionic strength dramatically affected the self-association of HMGB1 (Figure 30). In particular, the formation of tetramers was influenced by ionic strength with a 1000-fold decrease in affinity as the ionic strength was increased from 0.13 to 0.18 M (Figure 30b, d and f). In contrast, dimer formation appeared to be quite independent of ionic strength (Figure 30a, c and e). Given the highly charged nature of HMGB1 and the effect of ionic strength on tetramer formation, it is likely that electrostatic steering plays a key role in encounters between HMGB1 dimers.

The Einstein-Smoluchowski value for the limit of electrostatic steering in protein-protein interaction is predicted to be  $6.6 \times 10^9 \text{ M}^{-1}\text{s}^{-1}$  as the ionic strength of a solution approaches zero (Baerga-Ortiz et al., 2000). The interaction of thrombin and thrombomodulin (TM456) occurs with an association rate constant of  $10^9 \text{ M}^{-1}\text{s}^{-1}$ , which approaches the Einstein-Smoluchowski limit and is the fastest interaction reported to date. This interaction was hypothesized to be caused by the presence of two highly positively charged patches in thrombin, which may strongly attract TM456 (Baerga-Ortiz et al., 2000).

In this study, the Einstein-Smoluchowski values were calculated for both dimer and tetramer formation (from the respective intercepts of  $k_{a1}$  and  $k_{a2}$  of the self-association of HMGB1 at 0 mM ionic strength) to be  $10^5 \text{ M}^{-1}\text{s}^{-1}$  and  $10^{16} \text{ M}^{-1}\text{s}^{-1}$ , respectively. The rate of association for the dimer is within the Smoluchowski limit, whereas the constant for the tetramer far exceeds the limit by seven orders of magnitude. This sharply contrasts the effect of electrostatic steering in tetramer formation relative to dimer formation.

The fact that the rate constant for tetramer formation far exceeds the Smoluchowski limit could be explained in a number of ways. Firstly, there is a possibility that the dimer/tetramer fitting model that was used to fit the experimental results potentially overestimated the kinetic rates. It may well be that the characterization of the self-association of HMGB1 needs a novel fitting model which accommodates a more accurate estimation of the kinetics of higher oligomeric forms than tetrameric HMGB1. Indeed, in this study it was determined that HMGB1 formed higher order oligomers, and this was especially evident from the stoichiometry plot at micromolar concentrations of HMGB1 at low ionic strength (Figure 31). The formation of up to 20mer oligomeric beads of HMGB1 has also been reported previously (Bonne et al., 1980).

Observations regarding the impact of ionic strength on the self-association of HMGB1, and its interaction with DNA and other targets, is supported by several other studies (Duguet and de Recondo, 1978, Mathis et al., 1980, Rauvala et al., 1989, Bianchi et al., 1992, Stros et al., 1994) and is discussed in detail in the Literature Review chapter in section 1.5. For example, the percentage of SV40 DNA binding to HMGB1 decreased by more than five-fold as the ionic strength increased from 0 to 0.1 M, in a manner that is independent of the protein/DNA ratio (Bonne et al., 1980). In a sucrose velocity sedimentation study, HMGB1 apparently behaved as a tetrameric 106,000 Da protein at physiological ionic strength, but as a monomer at ionic strength above 0.2 M (Alexandrova and Beltchev, 1987). It might be speculated though that oligomeric forms of HMGB1 may well be transient or difficult to observe in the absence of DNA, as the oligomers of some DNA-binding proteins only become stable upon binding to their target DNA (Nooren and Thornton, 2003). In this study, molecular encounters at the surface of SPR chips may be under the influence of macromolecular crowding, as the interactions occur within a 2% dextran matrix on a CM5 chip. The influence of macromolecular crowding on the occurrence of the self-association of HMGB1 in SPR system, in absence of DNA, is explored in section 4.5.

It may also well be that various assumptions inherent in the Einstein-Smoluchowski calculation are incorrect. The Einstein-Smoluchowski equation states that the rate of encounter for two spheres in water at a temperature of 300 K, which is approximately equal to 27°C, is independent of the size of the spheres (Baerga-Ortiz et al., 2000). Thus, the calculations may provide an inaccurate estimation of the rate of HMGB1 self-interaction as they disregard the size (mass) of HMGB1. In addition, one of the HMGB1 molecules was fixed to the chip, so it is not diffusing. Furthermore, HMGB1 itself does not

assume a spherical form as it not a globular protein and it lies in an equilibrium of folded and unfolded states (Stott et al., 2010). Therefore, assuming that HMGB1 is a “sphere” to accommodate the Einstein-Smoluchowski assumptions may not be an ideal approach to characterise the association rate constant of self-association.

In conclusion, variations of ionic strength affected the stoichiometry and the kinetics of the self-association of HMGB1, particularly the association rate of tetramer formation, hence influencing the affinity between dimers. It can be speculated that DNA may bind to the dimeric form of HMGB1, as this was the form which appeared more stable, regardless of the value of the ionic strength. The shift between dimer and tetramer forms will be discussed in later sections.

#### **4.3.2 Effect of zinc**

Zinc is an essential component of a number of metalloenzymes which conduct DNA synthesis, and low levels of zinc may diminish the rate of zinc-activated gene transcription of critical mitogenic signals, which subsequently results in impaired cell division (MacDonald, 2000). In fact, a large group of DNA-binding proteins belong to the category of zinc protein based on their primary structure. Zinc proteins possess a well-known motif called ‘zinc finger’, formed by a series of conserved histidine and cysteine residues separated by a variable number of amino acids, which serves as a DNA recognition site (Vallee et al., 1991). The zinc finger motif also serves as a mediator for protein-protein interactions and it undergoes little or no structural rearrangement upon the binding of a partner protein. The interaction mediated by the zinc finger motif is generally of a moderate to low affinity; however, the interaction is highly specific (Gamsjaeger et al., 2007). HMGB1 is a DNA-binding protein; but perhaps surprisingly, it has not been reported previously whether HMGB1 binds zinc. However, as detailed further in the section 4.5, a molecular model of a HMGB1 dimer that involves the formation of a “clasp” zinc binding domain has been developed.

The SPR measurements in this study demonstrate that zinc potently promotes the self-association of HMGB1 (Figure 32). Low micromolar concentrations of zinc had a more prominent effect on self-association compared to millimolar concentrations of  $\text{CaCl}_2$  and  $\text{MgCl}_2$  (Figure 33). The effect of zinc has not been reported previously. In keeping with this observation, the addition of ethylenediaminetetraacetic acid (EDTA), a metal-chelating agent, greatly diminished the effect of zinc ions towards the self-association of HMGB1 (Figure 34). Zinc appears to play a role in both dimer and tetramer formation, although its



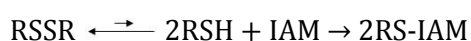
impact was greatest on the affinity of tetramer formation (Figure 34f) than dimer formation (Figure 34e). It is noteworthy that zinc has the greatest impact on promoting dimer and tetramer formation near physiological ionic strength (0.15 M). The stability of HMGB1 in oligomeric form will also be explored further when discussing the thermal shift assay (section 4.5).

Further support for the involvement of zinc was obtained in preliminary isothermal titration calorimetry (ITC) studies (Appendix F, section 6.6). A substantial release of heat was observed when zinc was titrated into a HMGB1 solution. This contrasted the control which showed no release of heat when zinc was titrated into buffer alone (Appendix F, section 6.6). These ITC studies need to be elaborated to enable detailed modelling of the interaction.

Together, these findings indicate that the ideal environment for HMGB1 tetramers involves the combination of physiological ionic strength and the presence of zinc ions.

#### **4.3.3 Effect of the redox environment**

Several experiments in this study demonstrate that the structure of HMGB1 is clearly sensitive to its redox state. Firstly, the CD spectra of HMGB1 changed markedly as HMGB1 was treated with different concentrations of the mild sulphhydryl-reducing agent,  $\beta$ -mercaptoethanol (Figure 18), which is indicative of changes in the secondary structure of the protein as it becomes more reduced. Secondly, the CD spectra of HMGB1 also changed significantly as HMGB1 was alkylated with iodoacetamide (Figure 19). Typically, iodoacetamide alkylates free sulphhydryl groups and the Cys106 residue in HMGB1 would be the expected target. The extent of changes in the CD spectra upon alkylation of HMGB1 was surprising and even more significant than the effect of extensive reduction of HMGB1. This could be because the disulphide bond in HMGB1, between Cys23 and Cys45, might be strained and therefore labile. Indeed, molecular modelling of HMGB1, as discussed in section 4.4, suggests that the disulphide bond of HMGB1 is likely to assume a strained conformation. Sulphydryl alkylating agents could irreversibly split a strained or labile disulphide bond by pushing the oxidised disulphide equilibrium towards the free sulphhydryl species, which could then be alkylated according to the following equation, where IAM is iodoacetamide:



Strained and more labile disulphide bonds are now well recognised for their functional significance in many proteins such as thrombospondin (TSP)-1, transcription factor Yap1 and tubulin (Hogg, 2003, Delaunay et al., 2002, Britto et al., 2005). An alternative explanation is that alkylating agents such as iodoacetamide are not as specific for cysteine residues as reported previously (Lee et al., 2014, Absar et al., 2014). There is some evidence that iodoacetamide might also alkylate other amino acid residues such as histidine, asparagine and phenylalanine (Fruchter and Crestfield, 1967, Woods et al., 2012). However, we do not consider this to be a likely explanation of the findings in this study, especially given the extent of secondary structure change induced by alkylation of HMGB1. HMGB1 is more likely to be unfolded by splitting the disulphide bond in its Box A than by the structural imposition that might be delivered by the more non-specific alkylation of multiple amino acid types.

The SPR experiments undertaken in this study also strongly support the redox sensitivity of HMGB1. Treatment of HMGB1 with the mild reducing agent in  $\beta$ -mercaptoethanol clearly affected its self-association properties (Figure 36). At low concentrations of reducing agent (< 1 mM), the affinity for tetramer formation was substantially higher than for dimer formation. Conversely, the affinity of dimer formation was substantially higher than for tetramer formation as the concentration of reducing agent was increased above 1 mM. This is interesting in view of the fact that the redox potentials inside and outside cells are quite different, and it may relate to the shift between dimer and tetramer forms as explained in the following paragraphs.

The intracellular redox potential is controlled by the thioredoxin and the glutathione (GSH)/glutathione disulfide (GSSG) systems, whereas the extracellular redox potential is regulated by the GSH/GSSG and Cys/CySS systems (Iyer et al., 2009). GSH is the most abundantly available low molecular mass thiol in an animal cell. The overall intracellular GSH concentration is estimated to be 0.5-10 mM, while the extracellular concentration is up to three orders of magnitude lower (Lushchak, 2012). It is estimated that 8 mM of GSH is present in the nucleus (Sahu et al., 2008) where it maintains the reduced state of the sulfhydryl group of the proteins involved in DNA repair, nucleic acid synthesis and standard antioxidant functions (Lushchak, 2012). It is also known that at the plasma, the concentration of Cys is 8-10  $\mu$ M, whereas the concentration of CySS is 40-50  $\mu$ M, which are significantly higher than extracellular GSH/GSSG concentrations (Ghosh and Brewer, 2014).

It is noteworthy that other studies have also suggested that HMGB1 may be present in different oxidation states depending on the different redox potentials found in different compartments of cells (Sahu et al., 2008). The proportion of HMGB1 with an oxidized disulphide bond is as high as 44% in the cytoplasm, whereas above 80% of nuclear HMGB1 is reduced (Sahu et al., 2008). The disulphide bond of extracellular HMGB1 may exist in both reduced and oxidized forms, although the reduced disulphide bond of HMGB1 is thought to be short-lived due to the oxidative environment (Sahu et al., 2008). However, under oxidative stress, GSSG concentration rises to over 500  $\mu$ M, which speeds up the rate of disulphide bond oxidation and most likely causes the accumulation of oxidized disulphide bonds (Sahu et al., 2008). Under reducing conditions, Box A binds with 10 fold higher affinity towards cisplatinated-DNA compared to non-reducing conditions. On the other hand, the binding affinity decreased under oxidizing conditions, leading to speculation that the residues of the disulfide bond interact directly with the cisplatinated-DNA (Park and Lippard, 2011).

It is tempting to speculate that different concentrations of the reducing agent determined the order of oligomerisation of HMGB1. This oligomerization behaviour may be related to the redox potential in physiological cellular conditions. The nuclear GSH concentration, which is slightly higher than the cytoplasmic GSH concentration, is assumed to be roughly equal to  $\beta$ -mercaptoethanol (RSH) concentrations above 1 mM, whereas the cytoplasmic and extracellular GSH concentration is presumed to be similar to RSH concentrations below 1 mM. Thus, nuclear HMGB1 may preferentially form dimers, whereas cytoplasmic and extracellular HMGB1 may preferentially exist as tetramers. The dynamic exchange between dimer and tetramer of HMGB1 may influence its functionality. The predominant form of HMGB1 inside the reducing environment of the nucleus may be the dimeric form. On the other hand, under the more oxidising conditions of the extracellular environment, HMGB1 tetramers may be more potent in binding to RAGE and Toll-like receptors that promote the resulting inflammatory response. It will be interesting in future to evaluate the potency of HMGB1 in binding to and promoting inflammatory pathways under conditions that favour oligomer formation. As discussed in the next section (section 4.6), these future studies should also evaluate the effect of combinations of zinc, ionic strength and various redox conditions which either favour or destabilise HMGB1 self-association.

#### 4.3.4 Effect of pH

The pH of a solution regulates the charges of ionisable residues and hence controls the electrostatic interactions that contribute to protein-protein binding (Jensen, 2008), protein structure, enzyme catalysis and protein function (Di Russo et al., 2012). This study demonstrated that the self-association of HMGB1 is also dramatically influenced by pH. Interestingly, whilst the rate of self-association appeared highest at pH 7.4, the stoichiometry of oligomer formation increased 3-4 fold at pH 5.7, which is near the isoelectric point of HMGB1 ( $pI = 5.6$ ) (Figure 37). This is perhaps not surprising given that a protein is least soluble at its isoelectric point and this condition is likely to favour oligomer formation. However, the size of the oligomers appeared greatest at a lower pH of 4.8, below the isoelectric point of HMGB1, where the protein would carry a net positive charge. The size of the oligomers was about 150-fold greater at pH 4.8 relative to pH 7.4. It is difficult to rationalise this observation at this point in time. It should be noted, however, that at pH 4.8, the sensorgrams appear to be almost linear in the association phase in Figure 37, which is classically indicative of mass transport limitation. This may be an indication of formation of HMGB1 aggregates where the order of the oligomer cannot be clearly specified. Whilst mass transport limitation makes the kinetic rate evaluations at pH 4.8 virtually uninterpretable, the condition is consistent with the formation of large oligomeric complexes that impedes the transfer of the analyte to the ligand attached at the surface of the sensor chip.

Remarkably, absolutely no response was detected when the pH was lowered by less than 1 pH unit from pH 4.8 to pH 4.0 (Figure 37). The self-association of HMGB1 was completely restored when the pH was returned to pH 7.4, which indicates that the protein was not irreversibly denatured. This would be expected given the very acid-stable nature of HMGB1 (section 4.1). The fact that HMGB1 forms higher order oligomers at and above pH 4.8 that are abolished as the pH is lowered to pH 4.0 is suggestive of the involvement of amino acid residues protonated as the pH is lowered from pH 4.8 to pH 4.0. Such a steep pH dependent effect may be indicative of cooperative effects between putative acidic residues involved. There are other examples of proteins whose activity is dramatically affected by small changes in pH. For example, the activity of the potassium channel protein (TASK-3), which exists in dimeric form, is strongly pH-dependent due to cooperative interactions between two His98 and two Glu70 residues from each TASK-3 molecule that modulate the open/closed state of the channel (Gonzalez et al., 2013).

Asp and Glu residues are likely candidates involved in the pH dependence of the self-association of HMGB1 as the value of their pKa within a protein are typically between 3.6 and 4.3, and they play key roles in protein structure (Nelson, 2008). It is tempting to speculate the involvement of the C-terminus tail of HMGB1, which comprises a negatively-charged cluster of 30 residues of either Asp or Glu residues. On the basis of the likely pKa of Asp and Glu, these residues may be more prone to protonation before the pH reaches a value of 4.0. The assumed cooperative pH-dependent protonation of the residues of the acidic tail may explain the sensitivity of HMGB1 towards the change of pH. If the acidic tail is involved in the self-association to some extent, this may also explain why the self-association of HMGB1 persists at pH higher than 5.7 but stops at pH 4.0. A pH of 4.0 could be the point where the acidic C-terminus tail becomes sufficiently neutralized to prevent self-association. It will be of interest to evaluate the self-association of HMGB1 in connection with its acidic tail to confirm this postulate. Another candidate could be Glu26 residue, which is positioned within the zinc-clasp model as postulated in the next section.

#### **4.4 Molecular models of the self-association of HMGB1**

In this study, molecular models explaining zinc binding and tetramer formation of HMGB1 were developed<sup>3</sup>. Firstly, the role of zinc in coordinating the self-association of HMGB1 was investigated. The FEATURE metal scanning server (<http://feature.stanford.edu/metals>) (Ebert and Altman, 2008) was used to detect possible zinc-binding sites in HMGB1. Three residues of Box A in a single HMGB1 molecule, His27, His31 and Glu26, were identified by the server as forming a zinc-binding site. The fourth residue of the zinc-binding motif was proposed to be the free Cys106 from Box B of another HMGB1 molecule. Restrained molecular docking was performed to bring the free Cys106 close to the proposed location of the zinc atom to create a possible dimer structure. In the selected model, the position of the Cys23-Cys45 disulfide bond of Box A of the first HMGB1 was close to the Cys106 side chain of the second HMGB1 molecule, although the disulfide did not interact directly with the zinc ion (Figure 40).

---

<sup>3</sup> *Construction of the molecular models was done in collaboration with Dr. Mark Agostino (Curtin University).*

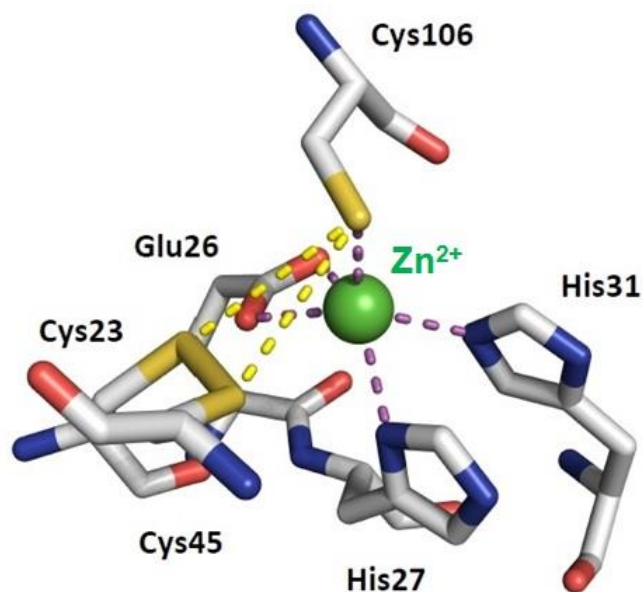


**Figure 40. Zinc clasp model describing the self-association of HMGB1.**

The molecular model of a HMGB1 dimer involves the free thiol group of Cys106 from Box B of one HMGB1 molecule and Glu26, His27 and His31 from Box A of another HMGB1 molecule. These residues coordinate a zinc ion (Anngayasti, Agostino, Mancera and Helmerhorst, Lorne Conference on Protein Structure and Function (2014)).

Disulfide bonds can be classified based on five relevant torsional angles, which can give a number of different combinations of conformational categories (Marques et al., 2010). Molecular dynamics (MD) simulations showed that the disulfide bond of Cys23-Cys45 mainly exists as the low strain  $-RH$ spiral conformation (84%), with the next most frequently observed conformation being the high strain- $RH$ Hook (10%). Examination of the proposed HMGB1 dimer indicated that the structure was moderately stable, as indicated by a persistent low root-mean-squared deviation over time. It also suggested that HMGB1 could undergo a disulfide exchange between Cys23-Cys45 in Box A of one HMGB1 molecule and Cys106 in Box B of another HMGB1 molecule. A tetrameric structure of HMGB1 is proposed, consisting of two dimer subunits joined by another HMGB1 dimer, with the domains oppositely configured to the previous HMGB1 dimer. The HMGB1 molecules in the tetrameric form are linked together by the interbox loops which form small bundles, enabling many other interactions (Figure 41).

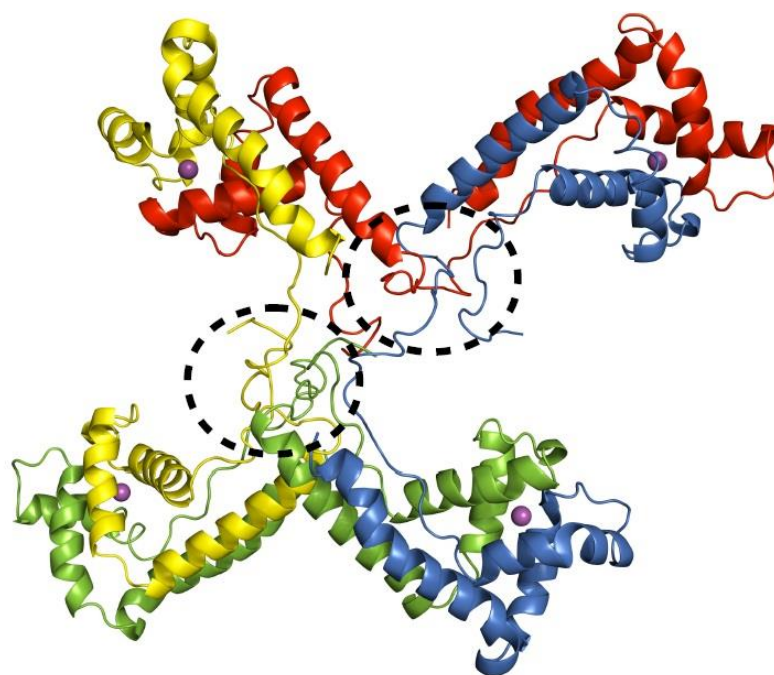


**Figure 41.**A molecular model of HMGB1 tetramer formation.

The tetramer of HMGB1 is built up by four subunits of HMGB1 dimers, each coordinating a zinc ion. The dimer subunits appear to undergo many interactions between the interbox loops, marked by the two circles with dashed line (Anggayasti, Agostino, Mancera and Helmerhorst, Lorne Conference on Protein Structure and Function (2014)).

However, the molecular models were based on the HMGB1 boxes without the acidic tail, whilst it is already suggested in this study that the acidic tail may play a key role in HMGB1 self-association. A more robust model will likely supports the crystallization and NMR study of the full-length HMGB1 structure which to this point in time has been unavailable.

#### **4.5 Macromolecular crowding and the self-association of HMGB1 in solution**

Biochemical reactions *in vivo* take place in a medium where macromolecules account for a significant portion of the volume of the medium. Thus, the medium is in a “crowded” state, and the phenomenon is known as “macromolecular crowding” (Minton, 2001). The addition of macromolecules, i.e. dextran, as a crowding agent to a protein solution has been reported to trigger the formation of the more compact state of the protein to minimize the volume excluded to the inert macromolecules (Snoussi and Halle, 2005). However, the macromolecular crowding phenomenon specifically influences complexes

with many subunits, i.e. oligomers or polymers (Phillip and Schreiber, 2013). It can be speculated that the lack of a macromolecular crowding and other non-optimal conditions *in vitro* may, at least in part, explain why there have been differing reports of the self-association of HMGB1. The CM5 chip utilized in this study consists of 2% dextran, which is known as a macromolecular crowder. It is likely that the dextran matrix helps to provide a suitable substrate for the self-association of HMGB1.

Whilst the dextran matrix on SPR chips may facilitate the self-association of HMGB1 by providing a macromolecularly crowded environment, there is evidence that HMGB1 self-association or oligomerization occur in the absence of macromolecular crowders (Mathis et al., 1980, Marekov et al., 1984, Alexandrova and Beltchev, 1987, Stros et al., 1994). However, the self-association may be more difficult to observe. In particular, the absence of zinc and absence of appropriate redox conditions other previous studies may well explain many of the conflicting reports of HMGB1 self-association.

The thermal shift assays conducted in this study (Figure 38 and Figure 39) gives strong support to the importance of zinc and an appropriate redox environment for the stability of HMGB1. The physico-chemical factors supporting the self-association of HMGB1 provide critical information on the conditions needed for HMGB1 to self-associate.

#### **4.6 Conclusion and future directions**

HMGB1 is classified as a DAMP molecule, and has been shown to promote inflammation, sepsis, vascular pathology, tumour growth and neuro-degeneration. Therefore, HMGB1 is considered an important pharmacological target. It is becoming increasingly evident that ligand self-association, as has been thoroughly investigated in the case of other DAMP molecules such as S100 proteins, could be important for the formation of ligand-receptor complexes and subsequent signal transduction. This process is not well understood for HMGB1 in its extracellular functions. This study utilizes well-established and suitable biochemical and biophysical techniques to show evidence for HMGB1 self-association.

Given the complexity of biological systems, the combinations of the physico-chemical factors that constitute an *in vivo* “physiological environment” is difficult to define and reproduce *in vitro*. Nevertheless, this study has shown that HMGB1 self-association is influenced by the redox environment, pH, ionic strength and the presence of metal cations. In particular, mild reducing conditions, along with physiological pH and ionic



strength, typical of the extracellular environment, seem to favour the formation of tetramers, which may preferentially bind RAGE and TLRs. In contrast, more reducing conditions at physiological pH and ionic strength, typical of the nucleus, favour the formation of dimers. The nucleus recruits GSH during cell proliferation (Markovic et al., 2007).

It might be predicted that the HMGB1 dimer is preferred in the nucleus during cell proliferation to bind to and rearrange DNA. Zinc may also promote the formation of HMGB1 tetramers in the nucleus under specific conditions. Preliminary molecular models were developed to explain the formation of a dimer, assisted by a zinc ion, as well as the formation of tetramers. Macromolecular crowding, which occurs inside and outside cells, is also likely to influence the kinetics of self-association of HMGB1.

Preliminary experiments using isothermal titration calorimetry (ITC) confirmed that HMGB1 interacts with zinc ions in solution (Appendix F, Figure D1 and D2). Binding activity was indicated by a clear release of heat during the titration of HMGB1 with zinc. However, more detailed ITC experiments are needed in future using this technology to enable modelling of the ITC data. This would provide a valuable comparison with the SPR data detailed in this study.

Given that HMGB1 interacts with RAGE and TLR4 in the extracellular environment, most likely in predominantly tetramer form, it will be interesting to determine the affinity of HMGB1 to its receptors under different physico-chemical conditions. It is notable that the redox state of Cys106 of HMGB1 and modulation of zinc levels in different compartments of the cells affects protein-protein interactions, cell proliferation, NF $\kappa$ B translocation and the interaction of HMGB1 with DNA (Mackenzie et al., 2002, Yang et al., 2012, MacDonald, 2000). Further studies are therefore needed to evaluate the influence of zinc and the redox sensitivity of HMGB1 self-association, in regards to its interaction with RAGE and TLR4.

The thermal shift experiments in the present study could help define conditions for the successful crystallisation of HMGB1. In the absence of optimal conditions for the oligomerisation of HMGB1, this task has proved elusive to date. Thermal shift assays support our findings using SPR; 5  $\mu$ M ZnCl<sub>2</sub> and 0.5 mM  $\beta$ -mercaptoethanol at a pH of 7.4, with total ionic strength of 150 mM, stabilizes the oligomeric structure of HMGB1 (Figure 39). However, further thermal shift assay experiments could be performed to optimise these conditions; for example, a pH of 4.8 seemed to further promote HMGB1

oligomerisation. Interestingly, macromolecular crowders such as dextran or polyethylene glycol are often tested to facilitate crystallisation of protein. The influence of macromolecular crowding on the kinetics of HMGB1 self association could be further explored by SPR on chips comprised of different dextran matrices (e.g. CM3 chip) or by comparing results following the inclusion of soluble dextran or polyethylene glycol. Similarly, thermal shift assays could be detailed in the presence and absence of dextran or polyethylene glycol. Some feasible arrangements of HMGB1 molecules in a crystal structure may possibly be predicted based on the proposed molecular models (Figure 40 and Figure 41). However, a more detailed molecular model of full-length HMGB1 is needed because the molecular models, as well as all of the existing NMR structures of HMGB1 (Discussion chapter, Section 4.1), are based on the structures of HMGB1 boxes without its acidic tail. It will be important to investigate how the acidic tail affects the self-association and stability of HMGB1. In addition, other techniques such as analytical ultracentrifugation or NMR spectroscopy might be helpful as a follow up on this study, using the conditions described in this thesis.

HMGB1 formed the highest order of oligomers at pH 4.8. However, the oligomer formation was abolished as the pH was lowered to pH 4.0, which is suggestive of the involvement of amino acid residues protonated as the pH is lowered from pH 4.8 to pH 4.0 (Figure 37). This leads to speculation that the acidic tail may play a crucial role in the self-association of HMGB1. The absence of the acidic tail influences the biological functions of HMGB1, such as DNA supercoiling (Stros et al., 1994) and regulation of the interaction between box A and DNA (Stott et al., 2010). In this study, a preliminary CD experiment was done by treating truncated HMGB1 (HMGB1 without its acidic C-terminus tail) with the reducing agent  $\beta$ -mercaptoethanol and the alkylating agent iodoacetamide (both data are not shown). The absence of the acidic tail appears to enable truncated HMGB1 to be reduced easier than full-length HMGB1. But these studies need to be repeated to confirm this observation. In future, SPR studies should also be directed to compare the self-association of HMGB1 in the presence of absence of its acidic tail under a variety of different physio-chemical conditions.

The self-association of HMGB1 could affect its interaction with RAGE to invoke pro-inflammatory responses. Firstly, it is of importance to address the interaction between RAGE and HMGB1. Although several attempts have been made to characterize the interaction between RAGE and HMGB1, there are doubts as to whether these two proteins interact with each other (Park et al., 2006, Park et al., 2004). However, this study

does suggest that HMGB1 interacts with VCC-RAGE in a highly specific manner and with relatively high affinity  $K_D$  of 54 nM (Figure 22). The binding constant is comparable to results an SPR study using commercially purchased RAGE and HMGB1 (Ling et al., 2011), as outlined in Section 1.2.1. However, it is considerably different from  $\sim 10$  nM affinity obtained in other studies (Hori et al., 1995, Srikrishna et al., 2002). The possible reason of the lower affinity in this study is because VCC-RAGE used here is expressed in *E. coli*, and therefore not glycosylated. The studies by Hori, et al. and Srikrishna, et al. used fully glycosylated RAGE from bovine lung. The de-glycosylation of RAGE lowers its affinity for HMGB1 (Srikrishna et al., 2002). In particular, the N-glycans on the V-domain of RAGE are implicated in binding HMGB1 (Srikrishna et al., 2002); it will be interesting to investigate in the future whether the N-glycans affects the RAGE-HMGB1 interaction under various physico-chemical conditions evaluated in this study. Indeed, preliminary experiments (data not shown) showed that the binding of HMGB1 to VCC-RAGE appears to be highly dependent on ionic strength (0.15-0.35 M), suggesting the presence of strong electrostatic interactions between HMGB1 and VCC-RAGE. However, the sensorgrams were not well fitted by the simple Langmuir 1:1 binding model. These initial studies suggest that the kinetics of the interaction are complex and may be best supported by a more complex fitting model, such as a dimer/tetramer kinetic binding model. This may indicate that the proteins form oligomers prior to or during interaction.

Several studies suggest that RAGE forms oligomers prior to or upon interacting with its ligands (Matsumoto et al., 2008, Dattilo et al., 2007). RAGE has been reported to self-associate through its V and VC domain (Koch, 2010, Zong et al., 2010). The self-association between different VC-RAGE domains was reported to be influenced by the presence of zinc and the increase of pH (Koch, 2010). Interestingly, a RAGE tetramer binds S100A12, which assumes a hexameric form facilitated by six molecules of calcium ions (Xie et al., 2007). As a continuation of this study, it would be interesting to investigate the self-association of the different domains of RAGE (VCC-RAGE, VC-RAGE and V-RAGE) under certain physico-chemical conditions, as well as to characterise its effect on the interaction with HMGB1. It will be interesting to evaluate the interaction of RAGE, either in monomeric or oligomeric form, under the conditions which favour the oligomer formation of HMGB1, since it was found that the tetramer may be the predominant extracellular form of HMGB1. The modulation of zinc ion concentration may be crucial in the interaction between RAGE and HMGB1 since the oligomerisation of both proteins are influenced by zinc. There are only a few studies reporting on the oligomerisation of TLR (Dasu et al., 2010a, Dasu et al., 2010b, Tsan and Gao, 2004), however, it may be of interest

to also investigate whether the interaction of HMGB1 with TLR4 is affected by conditions favouring various oligomeric forms of HMGB1.

The above future studies would progress our understanding of the role of the self-association of HMGB1 on its interaction with DNA and receptors such as RAGE. This may help us better understand the role of HMGB1 in normal and disease states and lead to new opportunities to develop inhibitors of the self-association of HMGB1, which could impede the progress of inflammatory diseases such as cancer, diabetes and Alzheimer's disease.

## 5 REFERENCES

- ABSAR, S., KWON, Y. M. & AHSAN, F. 2014. Bio-responsive delivery of tissue plasminogen activator for localized thrombolysis. *J Control Release*, 177, 42-50.
- ALEXANDROVA, E. A. & BELTCHEV, B. G. 1987. Differences between HMG1 proteins isolated from normal and tumour cells. *Biochim Biophys Acta*, 915, 399-405.
- ALI, M. H. & IMPERIALI, B. 2005. Protein oligomerization: how and why. *Bioorg Med Chem*, 13, 5013-20.
- ARIMA, Y., TODA, M. & IWATA, H. 2011. Surface plasmon resonance in monitoring of complement activation on biomaterials. *Adv Drug Deliv Rev*, 63, 988-99.
- BAERGA-ORTIZ, A., REZAI, A. R. & KOMIVES, E. A. 2000. Electrostatic dependence of the thrombin-thrombomodulin interaction. *J Mol Biol*, 296, 651-8.
- BELGRANO, F. S., DE ABREU DA SILVA, I. C., BASTOS DE OLIVEIRA, F. M., FANTAPPIE, M. R. & MOHANA-BORGES, R. 2013. Role of the acidic tail of high mobility group protein B1 (HMGB1) in protein stability and DNA bending. *PLoS One*, 8, e79572.
- BIANCHI, M. E., FALCIOLA, L., FERRARI, S. & LILLEY, D. M. 1992. The DNA binding site of HMG1 protein is composed of two similar segments (HMG boxes), both of which have counterparts in other eukaryotic regulatory proteins. *EMBO J*, 11, 1055-63.
- BONNE, C., DUGUET, M. & DE RECONDO, A. M. 1980. Single-strand DNA binding protein from rat liver: interactions with supercoiled DNA. *Nucleic Acids Res*, 8, 4955-68.
- BRITTO, P. J., KNIPLING, L., MCPHIE, P. & WOLFF, J. 2005. Thiol-disulphide interchange in tubulin: kinetics and the effect on polymerization. *Biochem J*, 389, 549-58.
- BUSTIN, M. 2001. Revised nomenclature for high mobility group (HMG) chromosomal proteins. *Trends Biochem Sci*, 26, 152-3.
- CHANDLER, D. J. 2015. *Expression, Purification and Characterisation of the Recombinant Soluble Receptor for Advanced Glycosylation End Products (sRAGE)*. Doctor of Philosophy PhD Thesis, Curtin University.
- DASU, M. R., DEVARAJ, S., PARK, S. & JIALAL, I. 2010a. Increased toll-like receptor (TLR) activation and TLR ligands in recently diagnosed type 2 diabetic subjects. *Diabetes Care*, 33, 861-8.
- DASU, M. R., THANGAPPAN, R. K., BOURGETTE, A., DIPIETRO, L. A., ISSEROFF, R. & JIALAL, I. 2010b. TLR2 expression and signaling-dependent inflammation impair wound healing in diabetic mice. *Lab Invest*, 90, 1628-36.
- DATTILO, B. M., FRITZ, G., LECLERC, E., KOOI, C. W., HEIZMANN, C. W. & CHAZIN, W. J. 2007. The extracellular region of the receptor for advanced glycation end products is composed of two independent structural units. *Biochemistry*, 46, 6957-70.
- DELAUNAY, A., PFLIEGER, D., BARRAULT, M. B., VINH, J. & TOLEDANO, M. B. 2002. A thiol peroxidase is an H<sub>2</sub>O<sub>2</sub> receptor and redox-transducer in gene activation. *Cell*, 111, 471-81.

- DEVARAJ, S., DASU, M. R., ROCKWOOD, J., WINTER, W., GRIFFEN, S. C. & JIALAL, I. 2008. Increased toll-like receptor (TLR) 2 and TLR4 expression in monocytes from patients with type 1 diabetes: further evidence of a proinflammatory state. *J Clin Endocrinol Metab*, 93, 578-83.
- DI RUSSO, N. V., ESTRIN, D. A., MARTI, M. A. & ROITBERG, A. E. 2012. pH-Dependent conformational changes in proteins and their effect on experimental pK(a)s: the case of Nitrophorin 4. *PLoS Comput Biol*, 8, e1002761.
- DING, Q. & KELLER, J. N. 2005. Splice variants of the receptor for advanced glycosylation end products (RAGE) in human brain. *Neurosci Lett*, 373, 67-72.
- DUGUET, M. & DE RECONDO, A. M. 1978. A deoxyribonucleic acid unwinding protein isolated from regenerating rat liver. Physical and functional properties. *J Biol Chem*, 253, 1660-6.
- EBERT, J. C. & ALTMAN, R. B. 2008. Robust recognition of zinc binding sites in proteins. *Protein Sci*, 17, 54-65.
- ERICSSON, U. B., HALLBERG, B. M., DETITTA, G. T., DEKKER, N. & NORDLUND, P. 2006. Thermofluor-based high-throughput stability optimization of proteins for structural studies. *Anal Biochem*, 357, 289-98.
- FAGES, C., NOLO, R., HUTTUNEN, H. J., ESKELINEN, E. & RAUVALA, H. 2000. Regulation of cell migration by amphotericin. *J Cell Sci*, 113 ( Pt 4), 611-20.
- FOOTE, J. W. & DELVES, H. T. 1984. Albumin bound and alpha 2-macroglobulin bound zinc concentrations in the sera of healthy adults. *J Clin Pathol*, 37, 1050-4.
- FRUCHTER, R. G. & CRESTFIELD, A. M. 1967. The specific alkylation by iodoacetamide of histidine-12 in the active site of ribonuclease. *J Biol Chem*, 242, 5807-12.
- GAMSJAEGER, R., LIEW, C. K., LOUGHLIN, F. E., CROSSLEY, M. & MACKAY, J. P. 2007. Sticky fingers: zinc-fingers as protein-recognition motifs. *Trends Biochem Sci*, 32, 63-70.
- GARDELLA, S., ANDREI, C., FERRERA, D., LOTTI, L. V., TORRISI, M. R., BIANCHI, M. E. & RUBARTELLI, A. 2002. The nuclear protein HMGB1 is secreted by monocytes via a non-classical, vesicle-mediated secretory pathway. *EMBO Rep*, 3, 995-1001.
- GHOSH, D. & BREWER, G. J. 2014. External cys/cySS redox state modification controls the intracellular redox state and neurodegeneration via Akt in aging and Alzheimer's disease mouse model neurons. *J Alzheimers Dis*, 42, 313-24.
- GONZALEZ, W., ZUNIGA, L., CID, L. P., AREVALO, B., NIEMEYER, M. I. & SEPULVEDA, F. V. 2013. An extracellular ion pathway plays a central role in the cooperative gating of a K(2P) K+ channel by extracellular pH. *J Biol Chem*, 288, 5984-91.
- GOODWIN, G. H., NICOLAS, R. H. & JOHNS, E. W. 1975. An improved large scale fractionation of high mobility group non-histone chromatin proteins. *Biochim Biophys Acta*, 405, 280-91.
- GRASSER, K. D., TEO, S. H., LEE, K. B., BROADHURST, R. W., REES, C., HARDMAN, C. H. & THOMAS, J. O. 1998. DNA-binding properties of the tandem HMG boxes of high-mobility-group protein 1 (HMG1). *Eur J Biochem*, 253, 787-95.

- GREENFIELD, N. J. 2004. Circular dichroism analysis for protein-protein interactions. *Methods Mol Biol*, 261, 55-78.
- GREENFIELD, N. J. 2006. Using circular dichroism spectra to estimate protein secondary structure. *Nat Protoc*, 1, 2876-90.
- HEALTHCARE, G. 2008a. Biacore T200 Sensor Surface Handbook Uppsala, Sweden: General Electric Company.
- HEALTHCARE, G. 2008b. *Biacore Training Courses: Introduction to Biacore T100*, Uppsala, Sweden, General Electric Company.
- HEALTHCARE, G. 2010. Biacore T200 Software Handbook. Uppsala, Sweden: General electric company.
- HEALTHCARE, G. 2012. MicroCal™ iTC200 system User Manual. *MicroCal iTC200 User Manual 29017607 AA*. Uppsala, Sweden: General Electric Company.
- HELMERHORST, E., CHANDLER, D. J., NUSSIO, M. & MAMOTTE, C. D. 2012. Real-time and Label-free Bio-sensing of Molecular Interactions by Surface Plasmon Resonance: A Laboratory Medicine Perspective. *Clin Biochem Rev*, 33, 161-73.
- HOFMANN, M. A., DRURY, S., HUDSON, B. I., GLEASON, M. R., QU, W., LU, Y., LALLA, E., CHITNIS, S., MONTEIRO, J., STICKLAND, M. H., BUCCIARELLI, L. G., MOSER, B., MOXLEY, G., ITESCU, S., GRANT, P. J., GREGERSEN, P. K., STERN, D. M. & SCHMIDT, A. M. 2002. RAGE and arthritis: the G82S polymorphism amplifies the inflammatory response. *Genes Immun*, 3, 123-35.
- HOGG, P. J. 2003. Disulfide bonds as switches for protein function. *Trends Biochem Sci*, 28, 210-4.
- HORI, O., BRETT, J., SLATTERY, T., CAO, R., ZHANG, J., CHEN, J. X., NAGASHIMA, M., LUNDH, E. R., VIJAY, S., NITECKI, D. & ET AL. 1995. The receptor for advanced glycation end products (RAGE) is a cellular binding site for amphoterin. Mediation of neurite outgrowth and co-expression of rage and amphoterin in the developing nervous system. *J Biol Chem*, 270, 25752-61.
- HUDSON, B. I., CARTER, A. M., HARJA, E., KALEA, A. Z., ARRIERO, M., YANG, H., GRANT, P. J. & SCHMIDT, A. M. 2008. Identification, classification, and expression of RAGE gene splice variants. *FASEB J*, 22, 1572-80.
- HUTTUNEN, H. 2002. *Role of RAGE as an Amphoterin Receptor: From Development to Disease*. Dissertation, University of Helsinki.
- HUTTUNEN, H. J., FAGES, C., KUJA-PANULA, J., RIDLEY, A. J. & RAUVALA, H. 2002. Receptor for advanced glycation end products-binding COOH-terminal motif of amphoterin inhibits invasive migration and metastasis. *Cancer Res*, 62, 4805-11.
- HUTTUNEN, H. J., FAGES, C. & RAUVALA, H. 1999. Receptor for advanced glycation end products (RAGE)-mediated neurite outgrowth and activation of NF-kappaB require the cytoplasmic domain of the receptor but different downstream signaling pathways. *J Biol Chem*, 274, 19919-24.



- HUTTUNEN, H. J., KUJA-PANULA, J., SORCI, G., AGNELETTI, A. L., DONATO, R. & RAUVALA, H. 2000. Coregulation of neurite outgrowth and cell survival by amphotericin and S100 proteins through receptor for advanced glycation end products (RAGE) activation. *J Biol Chem*, 275, 40096-105.
- IBRAHIM, Z. A., ARMOUR, C. L., PHIPPS, S. & SUKKAR, M. B. 2013. RAGE and TLRs: relatives, friends or neighbours? *Mol Immunol*, 56, 739-44.
- ISHIHARA, K., TSUTSUMI, K., KAWANE, S., NAKAJIMA, M. & KASAOKA, T. 2003. The receptor for advanced glycation end-products (RAGE) directly binds to ERK by a D-domain-like docking site. *FEBS Lett*, 550, 107-13.
- ITO, T. & MARUYAMA, I. 2011. Thrombomodulin: protectorate God of the vasculature in thrombosis and inflammation. *J Thromb Haemost*, 9 Suppl 1, 168-73.
- IYER, S. S., ACCARDI, C. J., ZIEGLER, T. R., BLANCO, R. A., RITZENTHALER, J. D., ROJAS, M., ROMAN, J. & JONES, D. P. 2009. Cysteine redox potential determines pro-inflammatory IL-1 $\beta$  levels. *PLoS One*, 4, e5017.
- JENSEN, J. H. 2008. Calculating pH and salt dependence of protein-protein binding. *Curr Pharm Biotechnol*, 9, 96-102.
- JIANG, Q., AKASHI, S., MIYAKE, K. & PETTY, H. R. 2000. Lipopolysaccharide induces physical proximity between CD14 and toll-like receptor 4 (TLR4) prior to nuclear translocation of NF-kappa B. *J Immunol*, 165, 3541-4.
- KELLY, S. M., JESS, T. J. & PRICE, N. C. 2005. How to study proteins by circular dichroism. *Biochim Biophys Acta*, 1751, 119-39.
- KEMP, M., GO, Y. M. & JONES, D. P. 2008. Nonequilibrium thermodynamics of thiol/disulfide redox systems: a perspective on redox systems biology. *Free Radic Biol Med*, 44, 921-37.
- KIERDORF, K. & FRITZ, G. 2013. RAGE regulation and signaling in inflammation and beyond. *J Leukoc Biol*, 94, 55-68.
- KIRSTEIN, M., BRETT, J., RADOFF, S., OGAWA, S., STERN, D. & VLASSARA, H. 1990. Advanced protein glycosylation induces transendothelial human monocyte chemotaxis and secretion of platelet-derived growth factor: role in vascular disease of diabetes and aging. *Proc Natl Acad Sci U S A*, 87, 9010-4.
- KOCH, M. C., S.; DATTILO, B. M.; SCHIEFNER, A.; DIEZ, J.; CHAZIN, W. J.; FRITZ, G. 2010. Structural Basis for Ligand Recognition and Activation of RAGE. *Structure Article*, 18, 1342-1352.
- KOKKOLA, R., ANDERSSON, A., MULLINS, G., OSTBERG, T., TREUTIGER, C. J., ARNOLD, B., NAWROTH, P., ANDERSSON, U., HARRIS, R. A. & HARRIS, H. E. 2005. RAGE is the major receptor for the proinflammatory activity of HMGB1 in rodent macrophages. *Scand J Immunol*, 61, 1-9.
- KOOLMAN, J. & ROEHM, K. H. 2005. *Color Atlas of Biochemistry*, Thieme.

- KUJA-PANULA, J., KIILTOMAKI, M., YAMASHIRO, T., ROUHIAINEN, A. & RAUVALA, H. 2003. AMIGO, a transmembrane protein implicated in axon tract development, defines a novel protein family with leucine-rich repeats. *J Cell Biol*, 160, 963-73.
- KUNIYASU, H., OUE, N., WAKIKAWA, A., SHIGEISHI, H., MATSUTANI, N., KURAOKA, K., ITO, R., YOKOZAKI, H. & YASUI, W. 2002. Expression of receptors for advanced glycation end-products (RAGE) is closely associated with the invasive and metastatic activity of gastric cancer. *J Pathol*, 196, 163-70.
- KUNIYASU, H., YANO, S., SASAKI, T., SASAHIRA, T., SONE, S. & OHMORI, H. 2005. Colon cancer cell-derived high mobility group 1/amphoterin induces growth inhibition and apoptosis in macrophages. *Am J Pathol*, 166, 751-60.
- LAFARGA, T., O'CONNOR, P. & HAYES, M. 2014. Identification of novel dipeptidyl peptidase-IV and angiotensin-I-converting enzyme inhibitory peptides from meat proteins using in silico analysis. *Peptides*, 59, 53-62.
- LECLERC, E., FRITZ, G., VETTER, S. W. & HEIZMANN, C. W. 2009. Binding of S100 proteins to RAGE: an update. *Biochim Biophys Acta*, 1793, 993-1007.
- LEE, J. J., HA, S., KIM, H. J., HA, H. J., LEE, H. Y. & LEE, K. J. 2014. Sulfhydryl-specific probe for monitoring protein redox sensitivity. *ACS Chem Biol*, 9, 2883-94.
- LEE, K. B. & THOMAS, J. O. 2000. The effect of the acidic tail on the DNA-binding properties of the HMG1,2 class of proteins: insights from tail switching and tail removal. *J Mol Biol*, 304, 135-49.
- LEVENTHAL, J. S. & SCHROPPEL, B. 2012. Toll-like receptors in transplantation: sensing and reacting to injury. *Kidney Int*, 81, 826-32.
- LING, Y., YANG, Z. Y., YIN, T., LI, L., YUAN, W. W., WU, H. S. & WANG, C. Y. 2011. Heparin changes the conformation of high-mobility group protein 1 and decreases its affinity toward receptor for advanced glycation endproducts in vitro. *Int Immunopharmacol*, 11, 187-93.
- LUAN, Z. G., ZHANG, H., YANG, P. T., MA, X. C., ZHANG, C. & GUO, R. X. 2010. HMGB1 activates nuclear factor-kappaB signaling by RAGE and increases the production of TNF-alpha in human umbilical vein endothelial cells. *Immunobiology*, 215, 956-62.
- LUM, H. K. & LEE, K. L. 2001. The human HMGB1 promoter is modulated by a silencer and an enhancer-containing intron. *Biochim Biophys Acta*, 1520, 79-84.
- LUSHCHAK, V. I. 2012. Glutathione homeostasis and functions: potential targets for medical interventions. *J Amino Acids*, 2012, 736837.
- MACDONALD, R. S. 2000. The role of zinc in growth and cell proliferation. *J Nutr*, 130, 1500S-8S.
- MACKENZIE, G. G., ZAGO, M. P., KEEN, C. L. & OTEIZA, P. I. 2002. Low intracellular zinc impairs the translocation of activated NF-kappa B to the nuclei in human neuroblastoma IMR-32 cells. *J Biol Chem*, 277, 34610-7.

- MAREKOV, L. N., DEMIROV, D. G. & BELTCHEV, B. G. 1984. Isolation of high-mobility-group proteins HMG1 and HMG2 in non denaturing conditions and comparison of their properties with those of acid-extracted proteins. *Biochim Biophys Acta*, 789, 63-8.
- MARKOVIC, J., BORRAS, C., ORTEGA, A., SASTRE, J., VINA, J. & PALLARDO, F. V. 2007. Glutathione is recruited into the nucleus in early phases of cell proliferation. *J Biol Chem*, 282, 20416-24.
- MARQUES, J. R., DA FONSECA, R. R., DRURY, B. & MELO, A. 2010. Conformational characterization of disulfide bonds: a tool for protein classification. *J Theor Biol*, 267, 388-95.
- MATHIS, D. J., KINDELIS, A. & SPADAFORA, C. 1980. HMG proteins (1 + 2) form beaded structures when complexed with closed circular DNA. *Nucleic Acids Res*, 8, 2577-90.
- MATSUMOTO, S., YOSHIDA, T., MURATA, H., HARADA, S., FUJITA, N., NAKAMURA, S., YAMAMOTO, Y., WATANABE, T., YONEKURA, H., YAMAMOTO, H., OHKUBO, T. & KOBAYASHI, Y. 2008. Solution structure of the variable-type domain of the receptor for advanced glycation end products: new insight into AGE-RAGE interaction. *Biochemistry*, 47, 12299-311.
- MCKINSEY, T. A., BROCKMAN, J. A., SCHERER, D. C., AL-MURRANI, S. W., GREEN, P. L. & BALLARD, D. W. 1996. Inactivation of I $\kappa$ B $\beta$  by the tax protein of human T-cell leukemia virus type 1: a potential mechanism for constitutive induction of NF- $\kappa$ B. *Mol Cell Biol*, 16, 2083-90.
- MIGNOTTE, B. & BARAT, M. 1986. Characterization of a *Xenopus laevis* mitochondrial protein with a high affinity for supercoiled DNA. *Nucleic Acids Res*, 14, 5969-80.
- MINTON, A. P. 2001. The influence of macromolecular crowding and macromolecular confinement on biochemical reactions in physiological media. *J Biol Chem*, 276, 10577-80.
- MYSZKA, D. G. 1999. Improving biosensor analysis. *J Mol Recognit*, 12, 279-84.
- NEEPER, M., SCHMIDT, A. M., BRETT, J., YAN, S. D., WANG, F., PAN, Y. C., ELLISTON, K., STERN, D. & SHAW, A. 1992. Cloning and expression of a cell surface receptor for advanced glycosylation end products of proteins. *J Biol Chem*, 267, 14998-5004.
- NELSON, D. L., COX, M.M. 2008. *Lehninger Principles of Biochemistry*, New York, NY 10010, W. H. Freeman.
- NOOREN, I. M. & THORNTON, J. M. 2003. Structural characterisation and functional significance of transient protein-protein interactions. *J Mol Biol*, 325, 991-1018.
- O'SHANNESSY, D. J., BRIGHAM-BURKE, M. & PECK, K. 1992. Immobilization chemistries suitable for use in the BIAcore surface plasmon resonance detector. *Anal Biochem*, 205, 132-6.
- OSAWA, M., YAMAMOTO, Y., MUNESUE, S., MURAKAMI, N., SAKURAI, S., WATANABE, T., YONEKURA, H., UCHIGATA, Y., IWAMOTO, Y. & YAMAMOTO, H. 2007. De-N-

- glycosylation or G82S mutation of RAGE sensitizes its interaction with advanced glycation endproducts. *Biochim Biophys Acta*, 1770, 1468-74.
- OSTENDORP, T., LECLERC, E., GALICHET, A., KOCH, M., DEMLING, N., WEIGLE, B., HEIZMANN, C. W., KRONECK, P. M. & FRITZ, G. 2007. Structural and functional insights into RAGE activation by multimeric S100B. *EMBO J*, 26, 3868-78.
- PARK, J. S., GAMBONI-ROBERTSON, F., HE, Q., SVETKAUSKAITE, D., KIM, J. Y., STRASSHEIM, D., SOHN, J. W., YAMADA, S., MARUYAMA, I., BANERJEE, A., ISHIZAKA, A. & ABRAHAM, E. 2006. High mobility group box 1 protein interacts with multiple Toll-like receptors. *Am J Physiol Cell Physiol*, 290, C917-24.
- PARK, J. S., SVETKAUSKAITE, D., HE, Q., KIM, J. Y., STRASSHEIM, D., ISHIZAKA, A. & ABRAHAM, E. 2004. Involvement of toll-like receptors 2 and 4 in cellular activation by high mobility group box 1 protein. *J Biol Chem*, 279, 7370-7.
- PARK, L., RAMAN, K. G., LEE, K. J., LU, Y., FERRAN, L. J., JR., CHOW, W. S., STERN, D. & SCHMIDT, A. M. 1998. Suppression of accelerated diabetic atherosclerosis by the soluble receptor for advanced glycation endproducts. *Nat Med*, 4, 1025-31.
- PARK, S. & LIPPARD, S. J. 2011. Redox state-dependent interaction of HMGB1 and cisplatin-modified DNA. *Biochemistry*, 50, 2567-74.
- PARKKINEN, J., RAULO, E., MERENMIES, J., NOLO, R., KAJANDER, E. O., BAUMANN, M. & RAUVALA, H. 1993. Amphoterin, the 30-kDa protein in a family of HMG1-type polypeptides. Enhanced expression in transformed cells, leading edge localization, and interactions with plasminogen activation. *J Biol Chem*, 268, 19726-38.
- PHILLIP, Y. & SCHREIBER, G. 2013. Formation of protein complexes in crowded environments--from in vitro to in vivo. *FEBS Lett*, 587, 1046-52.
- PHILLIPS, K. & DE LA PENA, A. H. 2011. The combined use of the ThermoFluor assay and ThermoQ analytical software for the determination of protein stability and buffer optimization as an aid in protein crystallization. *Curr Protoc Mol Biol*, Chapter 10, Unit10 28.
- RABBANI, A., GOODWIN, G. H. & JOHNS, E. W. 1978. Studies on the tissue specificity of the high-mobility-group non-histone chromosomal proteins from calf. *Biochem J*, 173, 497-505.
- RAMASAMY, R., YAN, S. F. & SCHMIDT, A. M. 2009. RAGE: therapeutic target and biomarker of the inflammatory response--the evidence mounts. *J Leukoc Biol*, 86, 505-12.
- RANATUNGA, W., LEBOWITZ, J., AXE, B., PAVLIK, P., KAR, S. R. & SCOVELL, W. M. 1999. Reexamination of the high mobility group-1 protein for self-association and characterization of hydrodynamic properties. *Biochim Biophys Acta*, 1432, 1-12.
- RAUVALA, H. & PIHLASKARI, R. 1987. Isolation and some characteristics of an adhesive factor of brain that enhances neurite outgrowth in central neurons. *J Biol Chem*, 262, 16625-35.

- RAUVALA, H., PIHLASKARI, R., LAITINEN, J. & MERENMIES, J. 1989. Extracellular adhesive molecules in neurite growth. *Biosci Rep*, 9, 1-12.
- RAUVALA, H. & ROUHIAINEN, A. 2009. Physiological and pathophysiological outcomes of the interactions of HMGB1 with cell surface receptors. *Biochim Biophys Acta*, 1799, 164-70.
- READ, C. M., CARY, P. D., CRANE-ROBINSON, C., DRISCOLL, P. C. & NORMAN, D. G. 1993. Solution structure of a DNA-binding domain from HMG1. *Nucleic Acids Res*, 21, 3427-36.
- RICH, R. L. & MYSZKA, D. G. 2008. Survey of the year 2007 commercial optical biosensor literature. *J Mol Recognit*, 21, 355-400.
- ROUHIAINEN, A., KUJA-PANULA, J., WILKMAN, E., PAKKANEN, J., STENFORS, J., TUOMINEN, R. K., LEPANTALO, M., CARPEN, O., PARKKINEN, J. & RAUVALA, H. 2004. Regulation of monocyte migration by amphoterin (HMGB1). *Blood*, 104, 1174-82.
- ROUHIAINEN, A., TUMOVA, S., VALMU, L., KALKKINEN, N. & RAUVALA, H. 2007. Pivotal advance: analysis of proinflammatory activity of highly purified eukaryotic recombinant HMGB1 (amphoterin). *J Leukoc Biol*, 81, 49-58.
- ROWELL, J. P., SIMPSON, K. L., STOTT, K., WATSON, M. & THOMAS, J. O. 2012. HMGB1-facilitated p53 DNA binding occurs via HMG-Box/p53 transactivation domain interaction, regulated by the acidic tail. *Structure*, 20, 2014-24.
- SAHU, D., DEBNATH, P., TAKAYAMA, Y. & IWAHARA, J. 2008. Redox properties of the A-domain of the HMGB1 protein. *FEBS Lett*, 582, 3973-8.
- SCAFFIDI, P., MISTELI, T. & BIANCHI, M. E. 2002. Release of chromatin protein HMGB1 by necrotic cells triggers inflammation. *Nature*, 418, 191-5.
- SCHMIDT, A. M., VIANNA, M., GERLACH, M., BRETT, J., RYAN, J., KAO, J., ESPOSITO, C., HEGARTY, H., HURLEY, W., CLAUSS, M. & ET AL. 1992. Isolation and characterization of two binding proteins for advanced glycosylation end products from bovine lung which are present on the endothelial cell surface. *J Biol Chem*, 267, 14987-97.
- SCHMIDT, A. M., YAN, S. D., YAN, S. F. & STERN, D. M. 2000. The biology of the receptor for advanced glycation end products and its ligands. *Biochim Biophys Acta*, 1498, 99-111.
- SIMS, G. P., ROWE, D. C., RIETDIJK, S. T., HERBST, R. & COYLE, A. J. 2010. HMGB1 and RAGE in inflammation and cancer. *Annu Rev Immunol*, 28, 367-88.
- SNOUSSI, K. & HALLE, B. 2005. Protein self-association induced by macromolecular crowding: a quantitative analysis by magnetic relaxation dispersion. *Biophys J*, 88, 2855-66.
- SORCI, G., RIUZZI, F., GIAMBANCO, I. & DONATO, R. 2013. RAGE in tissue homeostasis, repair and regeneration. *Biochim Biophys Acta*, 1833, 101-9.

- SREERAMA, N. & WOODY, R. W. 2000. Estimation of protein secondary structure from circular dichroism spectra: comparison of CONTIN, SELCON, and CDSSTR methods with an expanded reference set. *Anal Biochem*, 287, 252-60.
- SRIKRISHNA, G., HUTTUNEN, H. J., JOHANSSON, L., WEIGLE, B., YAMAGUCHI, Y., RAUVALA, H. & FREEZE, H. H. 2002. N-Glycans on the receptor for advanced glycation end products influence amphotericin binding and neurite outgrowth. *J Neurochem*, 80, 998-1008.
- STOTT, K., WATSON, M., HOWE, F. S., GROSSMANN, J. G. & THOMAS, J. O. 2010. Tail-mediated collapse of HMGB1 is dynamic and occurs via differential binding of the acidic tail to the A and B domains. *J Mol Biol*, 403, 706-22.
- STROS, M., STOKROVA, J. & THOMAS, J. O. 1994. DNA looping by the HMG-box domains of HMG1 and modulation of DNA binding by the acidic C-terminal domain. *Nucleic Acids Res*, 22, 1044-51.
- SUGAYA, K., FUKAGAWA, T., MATSUMOTO, K., MITA, K., TAKAHASHI, E., ANDO, A., INOKO, H. & IKEMURA, T. 1994. Three genes in the human MHC class III region near the junction with the class II: gene for receptor of advanced glycosylation end products, PBX2 homeobox gene and a notch homolog, human counterpart of mouse mammary tumor gene int-3. *Genomics*, 23, 408-19.
- SUHIR, H. & ETZIONI, A. 2010. The role of Toll-like receptor signaling in human immunodeficiencies. *Clin Rev Allergy Immunol*, 38, 11-9.
- TAGUCHI, A., BLOOD, D. C., DEL TORO, G., CANET, A., LEE, D. C., QU, W., TANJI, N., LU, Y., LALLA, E., FU, C., HOFMANN, M. A., KISLINGER, T., INGRAM, M., LU, A., TANAKA, H., HORI, O., OGAWA, S., STERN, D. M. & SCHMIDT, A. M. 2000. Blockade of RAGE-amphotericin signalling suppresses tumour growth and metastases. *Nature*, 405, 354-60.
- TAKEDA, K., KAISHO, T. & AKIRA, S. 2003. Toll-like receptors. *Annu Rev Immunol*, 21, 335-76.
- TANG, D., BILLIAR, T. R. & LOTZE, M. T. 2012. A Janus tale of two active high mobility group box 1 (HMGB1) redox states. *Mol Med*, 18, 1360-2.
- TANG, D., KANG, R., LIVESEY, K. M., CHEH, C. W., FARKAS, A., LOUGHRAN, P., HOPPE, G., BIANCHI, M. E., TRACEY, K. J., ZEH, H. J., 3RD & LOTZE, M. T. 2010. Endogenous HMGB1 regulates autophagy. *J Cell Biol*, 190, 881-92.
- TEO, S. H., GRASSER, K. D. & THOMAS, J. O. 1995. Differences in the DNA-binding properties of the HMG-box domains of HMG1 and the sex-determining factor SRY. *Eur J Biochem*, 230, 943-50.
- TRAHERNE, J. A. 2008. Human MHC architecture and evolution: implications for disease association studies. *Int J Immunogenet*, 35, 179-92.
- TSAN, M. F. & GAO, B. 2004. Endogenous ligands of Toll-like receptors. *J Leukoc Biol*, 76, 514-9.
- VALLEE, B. L., COLEMAN, J. E. & AULD, D. S. 1991. Zinc fingers, zinc clusters, and zinc twists in DNA-binding protein domains. *Proc Natl Acad Sci U S A*, 88, 999-1003.

- WAGNER, J. P., QUILL, D. M. & PETTIJOHN, D. E. 1995. Increased DNA-bending activity and higher affinity DNA binding of high mobility group protein HMG-1 prepared without acids. *J Biol Chem*, 270, 7394-8.
- WANG, J., TOCHIO, N., TAKEUCHI, A., UEWAKI, J. I., KOBAYASHI, N. & TATE, S. I. 2013. Redox-sensitive structural change in the A-domain of HMGB1 and its implication for the binding to cisplatin modified DNA. *Biochem Biophys Res Commun*.
- WATSON, M., STOTT, K. & THOMAS, J. O. 2007. Mapping intramolecular interactions between domains in HMGB1 using a tail-truncation approach. *J Mol Biol*, 374, 1286-97.
- WEIR, H. M., KRAULIS, P. J., HILL, C. S., RAINE, A. R., LAUE, E. D. & THOMAS, J. O. 1993. Structure of the HMG box motif in the B-domain of HMG1. *EMBO J*, 12, 1311-9.
- WHITMORE, D. L. 2001. *DichroWeb - Online Circular Dichroism Analysis* [Online]. London. Available: <http://dichroweb.cryst.bbk.ac.uk/html/home.shtml>.
- WHITMORE, L. & WALLACE, B. A. 2004. DICHROWEB, an online server for protein secondary structure analyses from circular dichroism spectroscopic data. *Nucleic Acids Res*, 32, W668-73.
- WHITMORE, L. & WALLACE, B. A. 2008. Protein secondary structure analyses from circular dichroism spectroscopy: methods and reference databases. *Biopolymers*, 89, 392-400.
- WILTON, R., YOUSEF, M. A., SAXENA, P., SZPUNAR, M. & STEVENS, F. J. 2006. Expression and purification of recombinant human receptor for advanced glycation endproducts in Escherichia coli. *Protein Expr Purif*, 47, 25-35.
- WOODS, A. G., SOKOLOWSKA, I. & DARIE, C. C. 2012. Identification of consistent alkylation of cysteine-less peptides in a proteomics experiment. *Biochem Biophys Res Commun*, 419, 305-8.
- WU, J. & FILUTOWICZ, M. 1999. Hexahistidine (His6)-tag dependent protein dimerization: a cautionary tale. *Acta Biochim Pol*, 46, 591-9.
- XIE, J., BURZ, D. S., HE, W., BRONSTEIN, I. B., LEDNEV, I. & SHEKHTMAN, A. 2007. Hexameric calgranulin C (S100A12) binds to the receptor for advanced glycation end products (RAGE) using symmetric hydrophobic target-binding patches. *J Biol Chem*, 282, 4218-31.
- XIE, J., REVERDATTO, S., FROLOV, A., HOFFMANN, R., BURZ, D. S. & SHEKHTMAN, A. 2008. Structural basis for pattern recognition by the receptor for advanced glycation end products (RAGE). *J Biol Chem*, 283, 27255-69.
- YAN, S. F., RAMASAMY, R. & SCHMIDT, A. M. 2010. Soluble RAGE: therapy and biomarker in unraveling the RAGE axis in chronic disease and aging. *Biochem Pharmacol*, 79, 1379-86.
- YAN, S. F., YAN, S. D., RAMASAMY, R. & SCHMIDT, A. M. 2009. Tempering the wrath of RAGE: an emerging therapeutic strategy against diabetic complications, neurodegeneration, and inflammation. *Ann Med*, 41, 408-22.

- YANG, H., ANTOINE, D. J., ANDERSSON, U. & TRACEY, K. J. 2013. The many faces of HMGB1: molecular structure-functional activity in inflammation, apoptosis, and chemotaxis. *J Leukoc Biol*, 93, 865-73.
- YANG, H., HREGGVIDSDOTTIR, H. S., PALMBLAD, K., WANG, H., OCHANI, M., LI, J., LU, B., CHAVAN, S., ROSAS-BALLINA, M., AL-ABED, Y., AKIRA, S., BIERHAUS, A., ERLANDSSON-HARRIS, H., ANDERSSON, U. & TRACEY, K. J. 2010. A critical cysteine is required for HMGB1 binding to Toll-like receptor 4 and activation of macrophage cytokine release. *Proc Natl Acad Sci U S A*, 107, 11942-7.
- YANG, H., LUNDBACK, P., OTTOSSON, L., ERLANDSSON-HARRIS, H., VENEREAU, E., BIANCHI, M. E., AL-ABED, Y., ANDERSSON, U., TRACEY, K. J. & ANTOINE, D. J. 2012. Redox modification of cysteine residues regulates the cytokine activity of high mobility group box-1 (HMGB1). *Mol Med*, 18, 250-9.
- YONEKURA, H., YAMAMOTO, Y., SAKURAI, S., PETROVA, R. G., ABEDIN, M. J., LI, H., YASUI, K., TAKEUCHI, M., MAKITA, Z., TAKASAWA, S., OKAMOTO, H., WATANABE, T. & YAMAMOTO, H. 2003. Novel splice variants of the receptor for advanced glycation end-products expressed in human vascular endothelial cells and pericytes, and their putative roles in diabetes-induced vascular injury. *Biochem J*, 370, 1097-109.
- ZHU, S., LI, W., WARD, M. F., SAMA, A. E. & WANG, H. 2010. High mobility group box 1 protein as a potential drug target for infection- and injury-elicited inflammation. *Inflamm Allergy Drug Targets*, 9, 60-72.
- ZONG, H., MADDEN, A., WARD, M., MOONEY, M. H., ELLIOTT, C. T. & STITT, A. W. 2010. Homodimerization is essential for the receptor for advanced glycation end products (RAGE)-mediated signal transduction. *J Biol Chem*, 285, 23137-46.



## **6 APPENDICES**

## 6.1 Appendix A

Figure 3 was adapted with permission from Wang, et al. 2013. Redox-sensitive structural change in the A-domain of HMGB1 and its implication for the binding to cisplatin modified DNA. *Biochem Biophys Res Commun.*, copyright 2013, Elsevier.

02/04/2015 RightsLink - Your Account

Copyright Clearance Center RightsLink®

My Orders My Library My Profile Welcome rain\_1904@hotmail.com Log out Help

My Orders > Orders > All Orders

### License Details

Thank you very much for your order.

This is a License Agreement between Wrești Anggayasti ("You") and Elsevier ("Elsevier"). The license consists of your order details, the terms and conditions provided by Elsevier, and the [payment terms and conditions](#).

[Get the printable license.](#)

License Number	3600581363530
License date	Apr 02, 2015
Order Content Publisher	Elsevier
Order Content Publication	Biochemical and Biophysical Research Communications
Order Content Title	Redox-sensitive structural change in the A-domain of HMGB1 and its implication for the binding to cisplatin modified DNA
Order Content Author	Jing Wang, Naoya Tochio, Aya Takeuchi, Jun-ichi Uewaki, Naohiro Kobayashi, Shin-ichi Tate
Order Content Date	29 November 2013
Licensed content volume number	441
Licensed content issue number	4
Number of pages	6
Type of Use	reuse in a thesis/dissertation
Portion	figures/tables/illustrations
Number of figures/tables/illustrations	1
Format	both print and electronic
Are you the author of this Elsevier article?	No
Will you be translating?	No
Original figure numbers	Figure 1A
Title of your thesis/dissertation	The Self Association of High Mobility Group Box 1 (HMGB1): Implications for Interaction with Receptor for Advanced Glycation End-products (RAGE) and DNA
Expected completion date	Apr 2015
Estimated size (number of pages)	150
Elsevier VAT number	GB 494 6272 12
Price	0.00 USD
VAT/Local Sales Tax	0.00 USD / 0.00 GBP
Total	<b>0.00 USD</b>

[← Back](#)

Copyright © 2015 Copyright Clearance Center, Inc. All Rights Reserved. Privacy statement . Comments? We would like to hear from you. E-mail us at [customercare@copyright.com](mailto:customercare@copyright.com)


<https://s100.copyright.com/MyAccount/viewLicenseDetails?ref=504d6db4-92e9-45b9-b1c4-44cd7362fa58>

1/1

## 6.2 Appendix B

Figure 4 was adapted with permission from Lee, K. B. & Thomas, J. O. 2000. The effect of the acidic tail on the DNA-binding properties of the HMG1,2 class of proteins: insights from tail switching and tail removal. *J Mol Biol*, 304, 135-49., copyright 2000, Elsevier.

02/04/2015 RightsLink - Your Account

 **RightsLink®**

[My Orders](#) [My Library](#) [My Profile](#) [Welcome rain\\_1904@hotmail.com](#) [Log out](#) | [Help](#)

[My Orders](#) > [Orders](#) > [All Orders](#)

### License Details

Thank you very much for your order.

This is a License Agreement between Wrești Anggastli ("You") and Elsevier ("Elsevier"). The license consists of your order details, the terms and conditions provided by Elsevier, and the [payment terms and conditions](#).

[Get the printable license.](#)

License Number	3600590206036
License date	Apr 02, 2015
Order Content Publisher	Elsevier
Order Content Publication	Journal of Molecular Biology
Order Content Title	The effect of the acidic tail on the DNA-binding properties of the HMG1,2 class of proteins: insights from tail switching and tail removal <sup>1</sup> Edited by T. Richmond
Order Content Author	None
Order Content Date	24 November 2000
Licensed content volume number	304
Licensed content issue number	2
Number of pages	15
Type of Use	reuse in a thesis/dissertation
Portion	figures/tables/illustrations
Number of figures/tables/illustrations	1
Format	both print and electronic
Are you the author of this Elsevier article?	No
Will you be translating?	No
Original figure numbers	Figure 4
Title of your thesis/dissertation	The Self Association of High Mobility Group Box 1 (HMGB1): Implications for Interaction with Receptor for Advanced Glycation End-products (RAGE) and DNA
Expected completion date	Apr 2015
Estimated size (number of pages)	150
Elsevier VAT number	GB 494 6272 12
Price	0.00 USD
VAT/Local Sales Tax	0.00 USD / 0.00 GBP
Total	<b>0.00 USD</b>

[← Back](#)

Copyright © 2015 Copyright Clearance Center, Inc. All Rights Reserved. [Privacy statement](#) . Comments? We would like to hear from you. E-mail us at [customer@copyright.com](mailto:customer@copyright.com)

### 6.3 Appendix C

Figure 6 was adapted with permission from Matsumoto, S., et al. 2008. Solution structure of the variable-type domain of the receptor for advanced glycation end products: new insight into AGE-RAGE interaction. *Biochemistry*, 47, 12299-311., copyright 2008, American Chemical Society.

**Copyright Clearance Center** RightsLink®

**ACS Publications** Most Trusted. Most Cited. Most Read.

**Title:** Solution Structure of the Variable-Type Domain of the Receptor for Advanced Glycation End Products: New Insight into AGE-RAGE Interaction<sup>†,‡</sup>

**Author:** Shigeyuki Matsumoto, Takuya Yoshida, Hiroko Murata, et al

**Publication:** *Biochemistry*

**Publisher:** American Chemical Society

**Date:** Nov 1, 2008

Copyright © 2008, American Chemical Society

Logged in as:  
Wresti Anggayasti

**LOGOUT**

Home Account Info Help Live Ch

#### PERMISSION/LICENSE IS GRANTED FOR YOUR ORDER AT NO CHARGE

This type of permission/license, instead of the standard Terms & Conditions, is sent to you because no fee is being charged for your order. Please note the following:

- Permission is granted for your request in both print and electronic formats, and translations.
- If figures and/or tables were requested, they may be adapted or used in part.
- Please print this page for your records and send a copy of it to your publisher/graduate school.
- Appropriate credit for the requested material should be given as follows: "Reprinted (adapted) with permission from (COMPLETE REFERENCE CITATION). Copyright (YEAR) American Chemical Society." Insert appropriate information in place of the capitalized words.
- One-time permission is granted only for the use specified in your request. No additional uses are granted (such as derivative works or other editions). For any other uses, please submit a new request.

If credit is given to another source for the material you requested, permission must be obtained from that source.

**BACK**

**CLOSE WINDOW**

Copyright © 2015 Copyright Clearance Center, Inc. All Rights Reserved. [Privacy statement](#). [Terms and Conditions](#).  
Comments? We would like to hear from you. E-mail us at [customer@copyright.com](mailto:customer@copyright.com)

## 6.4 Appendix D

### Circular Dichroism

CD is a structural technique that provides a preliminary assessment of the secondary structure content of a protein and is also useful to determine if a protein has folded correctly. The quantitative evaluation of the secondary structure of a protein is an important prerequisite for more extensive structural and biochemical studies, such as X-ray crystallography and nuclear magnetic resonance (NMR). CD measurements are carried out with a plane polarized light consisting of two circularly polarized light components of equal magnitude: one rotates counter-clockwise and the other one rotates clockwise (Greenfield, 2006). The term 'circular dichroism', which refers to the difference in absorbance between clockwise and counter-clockwise components, is generally reported as the mean residue ellipticity (MRE) in  $\text{degrees}\cdot\text{cm}^2\cdot\text{dmol}^{-1}$  (Whitmore, 2001, Greenfield, 2004). The absorbing components in a protein are the chromophores, which absorb certain wavelengths of far-UV light and reflect others when they are located in a regular, folded conformation. The chromophores include peptide bonds which absorb wavelength below 240 nm, aromatic amino acid side chains which absorb wavelengths between 260-320 nm and disulphide bonds which absorb about 260 nm (Kelly et al., 2005). Each secondary structure element also has its own signature CD spectra. For example,  $\alpha$ -helices show a dip at approximately 222 and 208 nm and peak at about 193 nm (Greenfield, 2006).

Various fitting models can be used to predict the secondary structure of a protein from CD spectra. For example, ridge regression (CONTIN), singular value decomposition (VARSLC and SELCON) and neural network programs (K2D) (Whitmore and Wallace, 2008). CONTIN gives a linear combination of the spectra of a large database of reference proteins with known conformations. Only reference proteins with similar spectral characteristics with the sample protein were used to give a best fit for the sample (Sreerama and Woody, 2000). CONTIN was used for this study as it consistently provided the best fits to the data. A normalized root mean square deviation (NRMSD) value is used to determine the reliability of the CD profile fitting. This "goodness of fit" parameter ranges from 0, for a perfect fit, to 1, which indicates that the experimental spectra do not fit at all with the fitting model. Generally an NRMSD value above 0.25 is regarded as an error in the analysis procedure (Kelly et al., 2005). The secondary structure components of the protein can be

evaluated using the online analysis tool DichroWeb (Whitmore, 2001, Whitmore and Wallace, 2004).

A number of experimental conditions have to be fulfilled in order to obtain a reliable CD spectrum. Firstly, the concentration of the sample should not be too high; otherwise the spectropolarimeter detector may get saturated, which leads to an increase in its sensitivity to compensate for the loss of signal strength. In other words, the readings will be unreliable because the detector will be unable to record the transmission radiation. The saturation rate can be measured by observing the high tension (HT) voltage. The detector is saturated when the HT voltage increases above 600 Volt (Greenfield, 2004, Kelly et al., 2005). Secondly, the protein has to be at least 95% pure without precipitates and should be free from interfering agents, such as nucleic acids and oligonucleotide fragments, as well as protective agents and buffer ions. Appropriate buffer ions are Tris, phosphate and borate. A high concentration of imidazole or Cl<sup>-</sup> ions (100-500 mM) will absorb strongly below 200 nm and are thus incompatible with CD. The reducing agent dithiothreitol (DTT) absorbs quite strongly below 220 nm (Greenfield, 2006). Therefore the use of Cl<sup>-</sup> ions was avoided and DTT was substituted with  $\beta$ -mercaptoethanol.

## 6.5 Appendix E

### Surface plasmon resonance

Surface Plasmon Resonance (SPR) is a real time, label-free, direct optical sensing technique based on total internal reflectance. SPR helps to obtain comprehensive analysis of interaction specificity by examining the extent of binding between different pairs of molecules. It also gives details of binding kinetics and affinity, observed by examining binding behaviour. In addition, SPR can also be used to determine the concentration of a specific molecule in a sample by measuring the response from the sample (O'Shannessy et al., 1992, Myszka, 1999). SPR can investigate protein-protein, DNA-DNA or protein-DNA interactions (Arima et al., 2011).

All SPR assays in this study were done using a Biacore T200 (GE Healthcare), a state-of-the-art instrument, and the methods were written with Biacore T200 control software version 1.0. The Biacore T200 has high sensitivity, being able to detect concentration changes down to approximately 1 pg/mm<sup>2</sup>. Furthermore, it is able to measure compound interactions at the extremes of kinetic behaviour.

There are two terms for interactants in Biacore T200: the 'analyte', the molecule in buffer, which passes over the sensor chip surface; and the 'ligand', the immobilized molecule on the sensor chip surface. The term 'ligand' here does not always imply that the surface-attached molecule is a ligand for a cellular receptor. The ligand can be immobilized to the sensor chip surface by several methods, however, in this study, the ligands were immobilized with the direct immobilization, in which the ligand is directly placed on the chip surface by covalent or electrostatic interaction (Healthcare, 2008b).

The term 'surface plasmon' is defined as a longitudinal charge density wave transmitted parallel to the interface of a metal surface and a dielectric layer. The metal surface is necessary because it exhibits free electron behaviour and the metal used in a Biacore chip is gold (Arima et al., 2011). The Biacore CM5 chip is coated with a thin layer polymer of 100-nm thick carboxylated dextran matrix. Dextran is a water-soluble polymer that carries thiol groups which interact with the gold surface through gold-sulfur bonds. This results in a negatively charged hydrophilic chip surface above pH 3.5 which theoretically will prevent non-specific protein binding (O'Shannessy et al., 1992).

An experiment is performed by injecting a defined concentration of analyte through the flow channel. The analyte passes the sensor chip surface, in a constant flow of running

buffer (called the 'flow buffer' in these methods), and forms an analyte-ligand complex, as illustrated in Figure A (Helmerhorst et al., 2012).

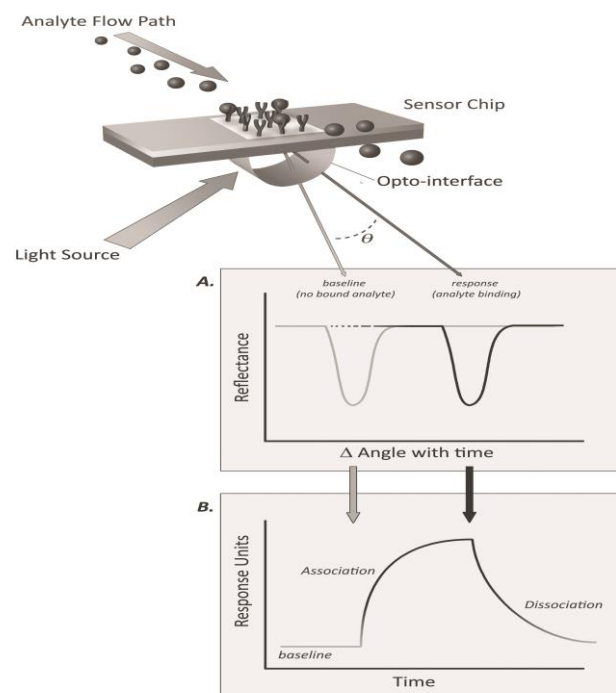


**Figure A. Schematic description of the SPR technique.**

The binding between analyte and ligand causes a change in the reflection angle (A), which is directly plotted as a sensorgram of Response Units (RU) as a function of time (B) (Helmerhorst et al., 2012).

When polarized light is directed to the metal surface of the sensor chip and hits the analyte-ligand complex, the angle of the reflected light is altered because of the electric field intensity. The reflected light excites the plasmons in the metal film of the chip, and the response is detected and quantitated by an optical detection unit. This response is proportional to the bound mass, expressed as response units (RU). The real-time progress of the interaction is shown in a plot of the response against time called a sensorgram. After analyte injection has finished, the buffer flows to enable the dissociation of the analyte from the ligand (O'Shannessy et al., 1992).

There are two types of run setup for kinetics analysis in the Biacore T200 system, namely single cycle kinetics (SCK) and multi cycle kinetics (MCK), as shown in Figure B. The single cycle kinetics analysis consists of at least five cycles, i.e. passing a single concentration of the analyte to the chip. One single cycle kinetics run involves sequentially passing



increasing concentrations of analyte over the chip, with only one regeneration step after the highest concentration of analyte. Multi cycle kinetics involves a regeneration step after each concentration of analyte. Single cycle kinetics is faster and minimises the exposure of the immobilized ligand to the harsh regeneration conditions. However, multi cycle kinetics better characterizes the binding activities of the interacting molecules because it is possible to individually fit single concentration cycle with a particular model. It also provides a better defined association and dissociation phase for each cycle, and enables users to obtain more reliable constants through model fitting.

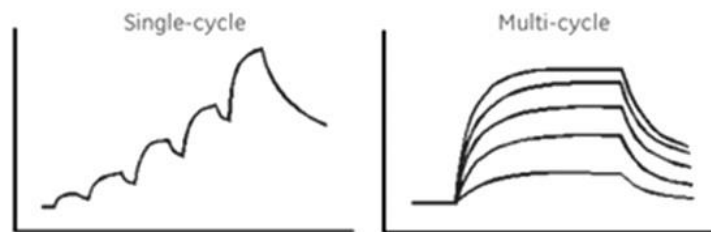


**Figure B. Sensorgrams of single cycle kinetics and multi cycle kinetics analysis.**

## 6.6 Appendix F

### Isothermal titration calorimetry

Isothermal titration calorimetry (ITC) is a technique that measures the heat change resulting from the interaction between molecules (Healthcare, 2012). The heat can be absorbed or released as a result of the rearrangement of noncovalent bonds when the binding partners go from a free state to an interacting state. The heat change is monitored by measuring the power needed to maintain a zero temperature difference between the reference and sample cells in the ITC instrument. The reference cell is usually filled with the buffer, while the sample cell contains one of the binding partners in solution and a stirring syringe, contains has the other binding partner (Healthcare, 2012). The ITC assay of self-association of HMGB1 was performed on a MicroCal iTC<sub>200</sub> calorimeter (GE Healthcare). The experimental programs and all results were written and analysed with software Origin version 7.0.

In an ITC experiment, the binding partner in the syringe is injected into the sample cell in small aliquots, typically 2-3  $\mu\text{l}$  in about 20 injections, until the concentration reaches two- or three-fold higher than the molecule in the sample cell. An experimental titration curve of heat against time is plotted, as depicted in the plot on the right side of Figure C. The plot on the right side of Figure C describes the fit of a 1:1 Langmuir binding model to the titration curve and gives the affinity constant ( $K_D$ ), stoichiometry ( $n$ ) and the interaction enthalpy ( $\Delta H$ ). A simple 1:1 binding experiment measures the enthalpy directly as the heat of 100% binding. The stoichiometry is taken as the midpoint of the titration curve between 100%-0% bindings (Healthcare, 2012).

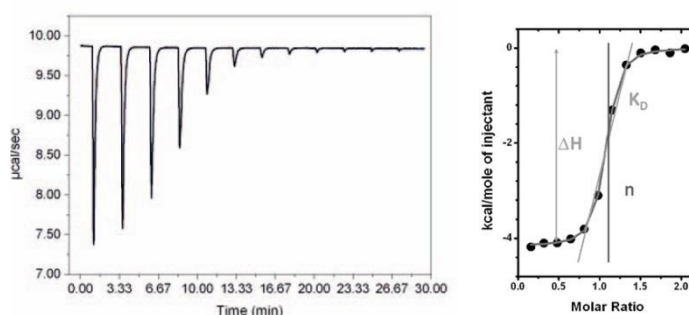


**Figure C.** Titration and fitting curves in ITC.

The first injection of the titration curve depicts the largest heat of nearly 100% binding, and the value gradually gets smaller towards the end of the experiment. This represents the power that is

needed to keep the same temperature between reference and sample cells over time, and is characteristic of an exothermic reaction. The 1:1 Langmuir binding model of the titration curve shows the affinity constant ( $K_D$ ), stoichiometry ( $n$ ) and the interaction enthalpy ( $\Delta H$ ) of the binding interaction (Healthcare, 2012).

Prior to the experiments, samples were first dialyzed against the respective buffer to ensure that the components and pH of the sample and experimental buffers were identical. All experiments were done at 25°C, using a volume of 200  $\mu\text{l}$  in the sample cell. The sample was sequentially titrated with 19 injections from the syringe where the first injection was 0.4  $\mu\text{l}$  and 18 subsequent injections were 2  $\mu\text{l}$  each. The total volume placed in the syringe was 60  $\mu\text{l}$  and this was to ensure sufficient titrant for the entire experiment. The titration curve was fitted with 1:1 Langmuir model to give the constants, as described above.

#### **Method: titration of HMGB1 with zinc ion**

To determine the potential interaction between zinc ion and HMGB1, 10  $\mu\text{M}$  HMGB1 in the sample cell was titrated with 100  $\mu\text{M}$   $\text{ZnCl}_2$ . In the control experiment, only buffer (no HMGB1) in the sample cell was titrated with 100  $\mu\text{M}$   $\text{ZnCl}_2$ . The buffer for both sample and titrant consisted of 10 mM HEPES, pH 7.4 containing 135 mM NaCl, 0.5 mM  $\beta$ -mercaptoethanol, and 0.05% Tween 20. This buffer was also used to dialyze the HMGB1 sample before commencing the experiment.

#### **Results**

The spikes in the control experiment were constant and small, with only about 0.02-0.04  $\mu\text{cal}/\text{sec}$ , indicative of baseline titration Figure D(1). Meanwhile, titration of HMGB1 with zinc resulted in a clear and reproducible pattern of heat release (-0.06 to -0.16  $\mu\text{cal}/\text{sec}$ ), as shown in Figure D(2). Heat exchange occurs within the initial three injections when the total concentration of zinc in the HMGB1 solution would be about 2  $\mu\text{M}$ . These results

suggest a specific interaction between zinc and HMGB1. A greater number of data points will be needed in future for kinetic and thermodynamic analysis<sup>4</sup>.

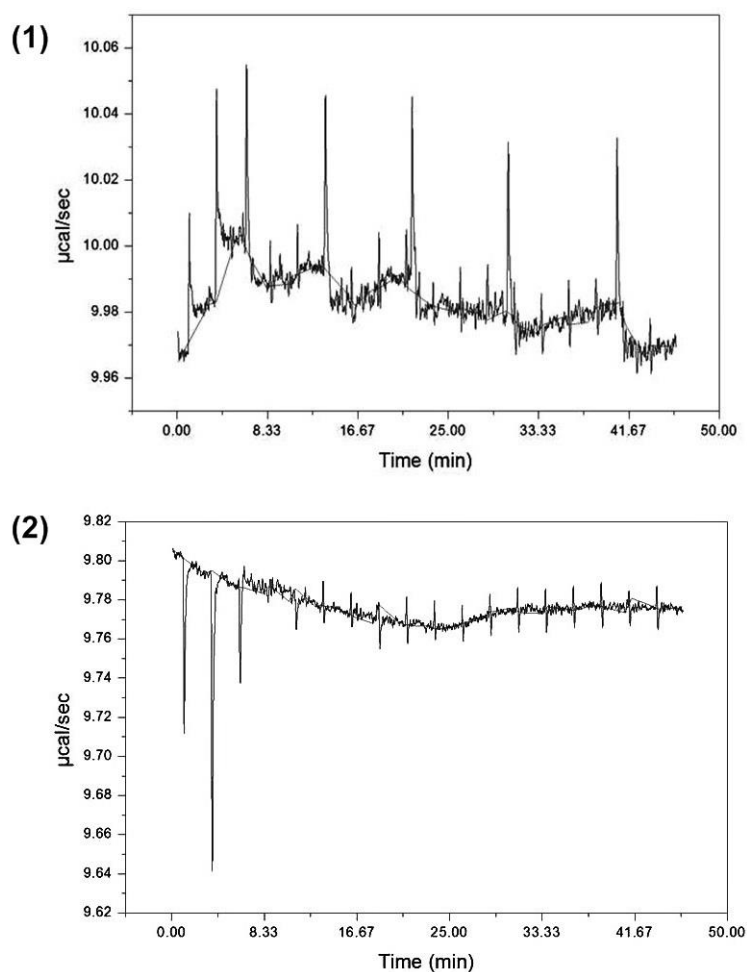


**Figure D. ITC analysis of HMGB1 titration with zinc.**

(1) control experiment where zinc was injected to a blank cell, (b) zinc titration to 10  $\mu\text{M}$  HMGB1.

---

<sup>4</sup> The instrument used for ITC studies was kindly provided by GE Healthcare. Unfortunately, the instrument was only available for short period of time and it was not possible to optimize conditions to observe the heat shift associated with the dissociation of HMGB1 in solution as it is diluted into buffer. Additional studies are clearly required to fully characterise the self-association of HMGB1 using ITC.